

**Management of pathological calcification using phosphorylated apatite-specific
peptide sequences**

by

Janani Ramaswamy

A dissertation submitted in partial fulfillment
of the requirements for the degree of
Doctor of Philosophy
(Biomedical Engineering)
in the University of Michigan
2016

Doctoral committee:

Professor David H. Kohn, Chair
Associate Professor Nan E. Hatch
Senior Lecturer Rupak M. Rajachar, Michigan Technological University
Professor Jan P. Stegemann

© Janani Ramaswamy



All rights reserved

2016

To Vikram, for “being my only constant”

Acknowledgements

First, I thank my advisor Dave Kohn for being a source of constant encouragement and positivity, even at the darkest of times. Your firm belief in my abilities helped me keep sight of the big picture always, and I am indebted to you for molding me into a confident and an independent thinker. I also want to thank my committee members Nan Hatch, Rupak Rajachar and Jan Stegemann for their guidance and mentorship throughout my graduate school experience.

I could not have done any of the work described in this dissertation without the help and support of my collaborators. To Hwa Kyung Nam, Jin Liu, Nan Hatch and Yuji Mishina – thank you so very much for your infinite patience with training me and answering my streams of never-ending questions! You have never turned me down irrespective of what I have asked of you, and I am so lucky to have known and worked with such wonderful people like you. I also want to thank Haichun Pan and Satoru Hayano for their assistance with animal experiments. I am grateful to Dr. Marc McKee, McGill University and Dr. Jose Millan, Sanford Burnham Institute for sharing their expertise as part of our collaborative efforts.

I want to thank the members of the Kohn lab – Harsha Ramaraju, Erin McNerny, Linh Lo, Sharon Miller, Genevieve Romanowicz, Joe Gardinier, Nianli Zhang, Michael Friedman, Nadder Sahar and Kyungsup Shin. Your companionship made lab a fun place to be, and you have endured every aspect of grad school with me, including exhilarating

highs and soul-crushing lows. Thank you for lending a patient ear when I wanted to brainstorm or vent, for sharing immeasurable amounts of delicious baked goods and ice cream, for slacking off at Pinball Pete's, and for being the best support system every grad student needs!

Thank you to Liz Rodriguiz, Maria Steele, Kumud Danak, Wanda Snyder and Deb Keedy for their ceaseless efforts to make our lives smoother in the department. I would also like to acknowledge my funding sources – the National Institutes of Health, Rackham Graduate School and the Biomedical Engineering Department, University of Michigan.

I've been lucky to have made a large number of friends during my stay here at Michigan. To each and every one of you – you helped keep my sanity somewhat in place, and have been my family away from home. Thank you for the happy laughter-filled memories that we have created over the years. Much appreciation also goes out to my very dear friends all across the world, for always checking on me and helping me move forward when I seemed to be stuck in a rut.

I am indebted to my parents and family for providing me with so many opportunities to succeed in life. Thank you for encouraging me to come all the way to Michigan in pursuit of my aspirations, and for being so incredibly understanding of the ups and downs involved with living 8000 miles away from home. And finally, thank you to my husband Vikram, for being my anchor no matter what life threw at us. I could have never come this far without your unwavering faith in me, and this accomplishment is as much yours as it is mine.

Table of Contents

Dedication	ii
Acknowledgements	iii
List of Figures.....	ix
List of Tables	xi
Abstract.....	xii
Chapter 1 Introduction.....	1
1.1.1 Pathological calcification.....	1
1.1.2 Vascular calcification.....	1
1.1.3 Fibrodysplasia ossificans progressiva (FOP).....	2
1.1.4 Craniosynostosis	3
1.2 Bone mineralization regulation	5
1.3 Inhibition of pathological calcification	6
1.4 Hypotheses and aims	8
1.5 Summary and organization of dissertation.....	10
1.6 References	12
Chapter 2 Phosphorylation-dependent mineral-type specificity for apatite-binding peptide sequences	16
2.1 Introduction	16
2.2 Materials and Methods	19
2.2.1 Preparation of biomimetic films and apatite disks.....	19
2.2.2 Peptide synthesis.....	20
2.2.3 Synthetic peptide adsorption assay	21

2.2.4	Cell culture.....	22
2.2.5	Quantification of mineralization.....	23
2.2.6	Assay for cell proliferation.....	23
2.2.7	Binding of fluorescently labelled peptides to osteoblast culture mineral ...	23
2.2.8	Computational modeling and energy calculations.....	23
2.2.9	Statistics.....	24
2.3	Results.....	25
2.3.1	Effect of phosphorylation on peptide adsorption to synthetic apatite-based substrates.....	25
2.3.2	Effect of VTK and pVTK on osteoblast-mediated mineralization.....	25
2.3.3	Effects of amino acid sequence scrambling on adsorption to synthetic apatite-based substrates.....	26
2.3.4	Effect of scrambled pVTK on osteoblast-mediated mineralization.....	27
2.3.5	Binding of peptides to mature osteoblast culture mineral.....	27
2.3.6	Computational modelling.....	28
2.4	Discussion.....	29
2.5	Conclusions.....	33
2.6	References.....	43
	Chapter 3 Inhibition of osteoblast mineralization by phosphorylated phage-derived apatite-specific peptide.....	47
3.1	Introduction.....	47
3.2	Materials and Methods.....	51
3.2.1	Peptide synthesis.....	51
3.2.2	Cell culture and overview of experimental design.....	51
3.2.3	Enpp1 and TNAP enzyme activity assays.....	52
3.2.4	Detection and quantification of mineralization.....	53
3.2.5	Picrosirius Red collagen staining.....	53
3.2.6	Western Blots.....	54

3.2.7	Quantitative Real Time PCR	54
3.2.8	Cell internalization of peptide.....	55
3.2.9	Statistics	55
3.3	Results	56
3.3.1	Effect of pVTK on mineralization and collagen matrix synthesis.....	56
3.3.2	Effect of pVTK on different stages of cell differentiation.....	56
3.3.3	Effect of pVTK on Enpp1 and TNAP.....	57
3.3.4	Effect of pVTK on osteogenic gene expression	57
3.3.5	Effect of pVTK on time course of osteogenic expression	57
3.3.6	Effect of pVTK addition to mineralized cell layers.....	58
3.3.7	Cell internalization of peptide.....	59
3.3.8	Effect of pVTK on calcium chelation.....	59
3.4	Discussion	60
3.5	Conclusions	65
3.6	References	77
Chapter 4 Evaluation of animal models of pathological calcification.....		80
4.1	Vascular calcification.....	80
4.1.1	Materials and methods	81
4.1.2	Results.....	83
4.2	Heterotopic ossification in fibrodysplasia ossificans progressiva.....	84
4.2.1	Materials and methods	85
4.2.2	Results.....	87
4.3	Craniosynostosis.....	88
4.3.1	Materials and methods	89
4.3.2	Results.....	90
4.4	Conclusions	91
4.5	References	104

Chapter 5 <i>In vivo</i> delivery of peptide in a mouse model of craniosynostosis	107
5.1 Introduction	107
5.2 Materials and Methods	108
5.2.1 Animals	108
5.2.2 Subcutaneous calvarial injections	108
5.2.3 Micro-computed Tomography (μ CT)	109
5.2.4 Digital caliper measurements	109
5.2.5 Categorization of phenotype severity	110
5.2.6 Histology	110
5.2.7 Primary osteoblast cell culture	110
5.2.8 von Kossa staining	111
5.2.9 Statistics	111
5.3 Results	111
5.3.1 Effect of pVTK on body weight	111
5.3.2 Effect of pVTK on AF suture fusion	112
5.3.3 Effect of pVTK on craniofacial morphology	112
5.3.4 Effect of pVTK on bone volume and tissue mineral density	113
5.3.5 Effect of pVTK on primary osteoblast culture	113
5.4 Discussion	114
5.5 Conclusions	117
5.6 References	127
Chapter 6 Summary and Future Work	128
6.1 Effect of peptide phosphorylation on apatite binding and mineralization	128
6.2 Mechanisms of mineralization inhibition <i>in vitro</i>	129
6.3 Animal model characterization and <i>in vivo</i> delivery of peptide	131
6.4 Future work	132
6.5 References	136

List of Figures

Figure 1.1: Three dimensional rendering of a mouse skull scanned using micro-computed tomography depicting the major cranial sutures	11
Figure 2.1: Adsorption of VTK and phosphorylated VTK (pVTK) peptides on bone-like mineral (BLM), hydroxyapatite (HA), 5.6% carbonated apatite (CA5), 10.5% carbonated apatite (CA10) and tissue culture polystyrene (TCPS).....	37
Figure 2.2: Mineralizing MC3T3-E1 osteoblast cultures were incubated with VTK and pVTK at the indicated concentrations for 12 days followed by mineral quantification by (A) calcium content determination expressed as a percentage of untreated control cultures, and (B) von Kossa (silver nitrate) staining for mineral.....	38
Figure 2.3: Adsorption of fluorescently-labelled VTK, phosphorylated VTK (pVTK), scrambled VTK (VTK-scram) and scrambled phosphorylated VTK (pVTK-scram) on bone-like mineral (BLM), hydroxyapatite (HA) and tissue culture polystyrene (TCPS). 39	
Figure 2.4: Effect of scrambling pVTK on inhibition of osteoblast culture mineralization	40
Figure 2.5: Binding of peptides to osteoblast culture mineral	41
Figure 2.6: Molecular modeling of peptide binding to the {100} crystallographic face of hydroxyapatite.....	42
Figure 3.1: Effect of pVTK on mineralization and collagen deposition.....	67
Figure 3.2: Effect of pVTK on different stages of cell culture	68
Figure 3.3: Effect of pVTK on Enpp1 and TNAP	69
Figure 3.4: Effect of pVTK on osteogenic differentiation.....	70
Figure 3.5: Effect of pVTK on time course of gene expression	71
Figure 3.6: Effect of pVTK on Runx2 and OPN protein expression.....	72
Figure 3.7: Effect of pVTK on progression of mineralization.....	73
Figure 3.8: Internalization of FITC-tagged pVTK	74
Figure 3.9: Effect of pVTK on media calcium chelation.....	75
Figure 3.10: Schematic summarizing the effect of pVTK on osteoblastic markers	76

Figure 4.1: Aortas from 23 week old Enpp1 knockout mice were sectioned and stained with von Kossa (counter stained with fast nuclear red) to detect arterial calcification	93
Figure 4.2: Aortas from 23 week old Enpp1 knockout mice were sectioned and stained with Alizarin Red to detect arterial calcification	94
Figure 4.3: Mineral formation by vascular smooth muscle cells (VSMCs) cultured with 2mM Pi for 4 weeks and stained by von Kossa	95
Figure 4.4: Schematics demonstrating scoring for range of motion (ROM) and X-ray analysis of heterotopic ossification (HO)	97
Figure 4.5: μ CT images of legs dissected from HO-induced mice treated with PBS (left leg, L) and peptide (right leg, R).....	99
Figure 4.6: μ CT images of legs dissected from HO-induced mice treated with PBS (left leg, L; right leg, R was untreated).....	101
Figure 4.7: Whole mount Alizarin Red staining of calvaria harvested from 1-2 day old (P1-2) C57BL6 Crouzon mice (left panels) and calvaria cultured <i>ex vivo</i> for 1 (middle panels) and 2 weeks (right panels).....	102
Figure 4.8: Calvaria of <i>ex vivo</i> cultured C57BL6 Crouzon mice were sectioned and stained with von Kossa (counterstained with Toluidine blue) to visualize coronal sutures (red arrows).....	103
Figure 5.1: Schematic depicting locations on mouse skull where craniofacial measurements were acquired using digital calipers.....	118
Figure 5.2: Categorization of P10 mutants based on phenotype severity as observed in μ CT 3D rendered images of skulls	119
Figure 5.3: Body weights	120
Figure 5.4: Histological assessment of anterior-frontal (AF) suture fusion	121
Figure 5.5: Digital caliper measurements of nasal (N), frontal (F) and parietal (P) bone lengths and skull widths at the eye and lambdoid sutures	122
Figure 5.6: Digital caliper measurements of categorized mutant nasal (N), frontal (F) and parietal (P) bone lengths and skull widths at the eye and lambdoid sutures.....	123
Figure 5.7: μ CT measurements of bone volume (BV) and tissue mineral density (TMD) around the anterior-frontal (AF) suture in pooled mutants (MT)	124
Figure 5.8: μ CT measurements of bone volume (BV) and tissue mineral density (TMD) around the anterior-frontal (AF) suture in categorized mutants	125
Figure 5.9: Pre-osteoblasts isolated from mutant mice were cultured in growth medium (GM), osteogenic medium (OM) or osteogenic medium supplemented with 300 μ m of pVTK peptide (Pep) for 20 days.....	126

List of Tables

Table 2.1: Amino acid sequences and isoelectric point (pI) of the peptides used in this study.....	35
Table 2.2: Peptide-hydroxyapatite adsorption energies calculated from RosettaSurface computational modeling.....	36
Table 4.1: Summary of experiments conducted to test for vascular smooth muscle cell (VSMC) calcification in culture.....	96
Table 4.2: Range of motion (ROM) and X-ray scoring of mice induced with HO and treated with PBS (left leg) and peptide (right leg).....	98
Table 4.3: Range of motion (ROM) and X-ray scoring of mice induced with HO and treated with either PBS or peptide (left leg), leaving the right leg untreated. Median and total scores were higher in right legs than left legs.....	100

Abstract

Pathological calcification is the abnormal deposition of minerals in soft tissues or the premature or excessive calcification of normally mineralizing tissues, and is associated with several conditions such as coronary heart disease, craniosynostosis and fibrodysplasia ossificans progressiva. Treatments are limited in their ability to prevent pathological calcification, thus necessitating the development of alternative therapeutic strategies. The work presented in this dissertation involves the use of a newly discovered phosphopeptide in testing inhibition of mineralization *in vitro* and treatment of pathological calcification *in vivo*. The global hypothesis was that phosphorylated apatite-specific peptide, pVTK (VTKHLNQLpSQpSY), will inhibit mineralization by physico-chemical and/or cellular pathways involving the TNAP-Enpp1-Ank axis. Further, it was hypothesized that pVTK will prevent premature hypermineralization, suture fusion and abnormal craniofacial morphology in mouse models of craniosynostosis.

Phosphorylation of serine residues resulted in increased pVTK binding to carbonated apatites, as well as dose-dependent inhibition of osteoblast mineralization. Peptide phosphorylation was more important than amino acid sequence order for binding to synthetic apatite substrates, whereas regulation of osteoblast culture mineralization was determined by both serine phosphorylation and sequence order. pVTK was internalized by osteoblasts and following treatment for 10-12 days, downregulation of inhibitors of mineralization (Enpp1, osteopontin and Ank) and upregulation of promoters of

mineralization (TNAP, Runx2 and bone sialoprotein) was observed. It was further demonstrated that mineral inhibition was not due to disruption of collagen matrix production or calcium chelation with negatively charged pVTK.

Several murine models of pathological calcification were evaluated as potential candidates to demonstrate peptide-mediated inhibition of calcification. pVTK was delivered to prematurely mineralizing anterior-frontal cranial sutures in a BMP-linked mouse model of craniosynostosis. Treatment with pVTK caused a partial correction of craniofacial defects, but did not inhibit primary osteoblast mineralization *in vitro* or premature suture fusion *in vivo*. Additionally, pVTK caused a decrease in bone quality, indicating negative effects of peptide on bone growth or turnover.

Further *in vitro* and *in vivo* evaluation of the mechanisms underlying pVTK-mediated inhibition of mineralization will enable the development of a novel class of peptide-based drugs, capable of preventing pathological calcification of tissues and biosprosthetic heart valve implants.

Chapter 1

Introduction

1.1.1 Pathological calcification

Pathological calcification refers to the deposition of minerals in soft tissues that normally do not mineralize, or the premature or excessive calcification of normally mineralizing tissues. Pathological calcification is observed in several diseases such as coronary heart disease, fibrodysplasia ossificans progressiva (FOP), osteoarthritis and craniosynostosis. A brief description of some of these conditions and their current modes of treatment is presented below.

1.1.2 Vascular calcification

Coronary heart disease (CHD) refers to the obstruction of blood vessels usually due to deposition of fatty plaques (atherosclerosis) and can cause angina and heart attacks. CHD was responsible for approximately 1 in every 6 deaths (406,351 deaths total) in the United States in 2007 and it is expected that ~785,000 Americans will have a new coronary attack each year [1]. Coronary artery calcification is a strong predictor of CHD and mortality from cardiovascular disease [2]. Other major types of vascular calcification (pathological mineralization of vascular tissues such as arteries and heart valves) include

medial arterial calcification and valvular aortic stenosis. Medial calcification of arteries (Monckeberg's sclerosis) is associated with type 2 diabetes and chronic kidney disease (CKD). Stiffening of blood vessels (resulting in loss of elastance) increases blood pressure and cardiac work, promoting heart failure.

Treatments to prevent cardiovascular calcification are limited and often have adverse effects on bone metabolism. Bisphosphonates (traditionally used to treat osteoporosis) can physico-chemically inhibit vascular calcification. However, their use is limited by adverse effects on bone health when administered at doses high enough to inhibit vascular calcification. Also, bisphosphonates rely on renal clearance for elimination from the body and, as a consequence, accumulate in the kidneys of CKD patients. 3-hydroxy-3-methylglutaryl coenzyme A reductase inhibitors or statins are used to treat atherosclerosis by reduction of cholesterol levels and also inhibit vascular calcification. *In vitro* mineralization of human aortic smooth muscle cells can be inhibited by statins [3]; however, clinical trials have not clearly demonstrated that statins lower vascular calcification.

1.1.3 Fibrodysplasia ossificans progressiva (FOP)

Heterotopic ossification (HO) refers to ectopic bone formation in extra-skeletal sites and soft tissues. One example of HO is the rare genetic disorder fibrodysplasia ossificans progressiva (FOP) arising from a mutation in the Activin A receptor type I (ACVR1) gene which encodes BMP receptor type 1 [4]. FOP affects ~ 1 in 2 million people and is characterized by spontaneous calcification of muscles, tendons, ligaments and joints, as

well as malformations of the toes [5]. An inflammatory component is also critical in the formation of ectopic bone [6]. FOP cumulatively progresses with age, and most affected patients are immobile and dependent on a wheelchair by the time they reach their twenties. There is no treatment currently available for FOP. Surgical removal of HO lesions induces new outbreaks of ectopic bone formation and therefore must be avoided. Flare-ups of FOP can also occur due to injuries from falls, intramuscular vaccinations, injections for routine dental care or influenza. While no cure exists for FOP, clinical management of symptoms is achieved using anti-inflammatory agents like NSAIDs and corticosteroids, analgesics and short-term use of muscle relaxants [7,8].

1.1.4 Craniosynostosis

Craniosynostosis is a condition affecting ~ 1 in 2500 live births, in which premature fusion of cranial sutures occurs. These sutures are fibrous structures present between the bones of the skull, allowing for deformation and expansion of the skull during childbirth and subsequent growth and development. The major cranial sutures are analogous in humans and rodents, and include the metopic/frontal, coronal, sagittal and lambdoid sutures (Figure 1.1). In humans with normal skull development, the metopic suture fuses within the first two years after birth, while the remaining three major sutures fuse later in adulthood (thirties). In mice, all sutures remain patent throughout the life span, with the exception of the posterior frontal suture, which fuses by 30 – 45 days post-birth [9].

In patients affected with craniosynostosis, the skull is unable to expand normally due to the premature fusion and mineralization of one or more sutures, and can cause

craniofacial deformities, blindness, increased intracranial pressure, abnormal brain development and in severe cases, even death [10–12]. The majority of craniosynostosis cases occur in an isolated manner, but around 15% are observed in conjunction with genetic mutations. Crouzon, Pfeiffer and Apert syndrome patients have mutations in fibroblast growth factor (FGF) receptors; transcription factors such as TWIST and MSX2 are affected in Saetre-Chotzen and Boston type craniosynostosis respectively [10,13–15]. While these syndromic conditions are associated with altered signaling arising from genetic mutations, the causes and molecular mechanisms leading to suture fusion still remain unclear.

The only way to treat craniosynostosis is via surgical procedures, such as cranial vault remodeling, open strip craniectomy and endoscopic strip craniectomy followed by postoperative molding helmet use. The specific surgical approach is dependent on patient age and clinical diagnosis of the complexity of suture fusion (single vs. multiple sutures fused), as well as the risk of future resynostosis necessitating multiple surgeries.

Hence, there is a strong clinical need to develop alternative treatment strategies to prevent pathological calcification seen in cardiovascular disease, FOP and craniosynostosis. In order to create novel therapeutics against pathological calcification, it is important to first gain a firm understanding of the mechanisms involved in the regulation of physiological mineralization.

1.2 Bone mineralization regulation

Bone mineralization is a complex process and involves the interplay between several positive and negative regulators of mineralization. One of the important determinants of mineralization is the ratio of inorganic phosphate (Pi) to extracellular inorganic pyrophosphate (PPi). PPi is a natural inhibitor of mineralization (at micromolar concentrations) and is formed as a by-product of several metabolic reactions. The concentration of extracellular PPi is regulated mainly by the action of three molecules: tissue non-specific alkaline phosphatase (TNAP), ectonucleotide pyrophosphatase/phosphodiesterase 1 (Enpp1) and ankylosis protein (Ank). Enpp1 and Ank increase the concentration of extracellular PPi – Enpp1 cleaves ATP to release PPi and Ank transports PPi from within the cell to the outside, thereby inhibiting mineralization [16,17]. TNAP decreases PPi levels by cleaving PPi to generate Pi thus promoting calcification [18,19]. The action of these three molecules maintains the PPi/Pi ratio, which has a direct consequence on apatitic mineralization – high PPi/Pi ratios inhibit, while low PPi/Pi ratios promote mineralization. Several other transporter and extracellular matrix proteins are also involved in the regulation of mineralization. Pit-1, a sodium-dependent Pi transporter moves Pi into the cell, which is required to initiate mineralization [20–22]. Bone sialoprotein (BSP) and osteopontin (OPN) promote and inhibit mineralization respectively [23,24]. Runx2 is a nuclear transcription factor that promotes bone formation [25]. The interplay between these different promoter and inhibitors molecules also maintains normal bone mineralization and prevents abnormal calcification in soft tissues.

The presence of osteochondrogenic markers in pathological mineral deposits and the role of these markers in the progression of pathological calcification indicate similarities in mechanisms between normal bone mineralization and abnormal calcification of soft tissues. Some examples are: transdifferentiation of vascular smooth muscle cells into osteochondrogenic phenotypes in response to environmental factors [26], widespread soft tissue calcification (of blood vessels, kidneys and joints) in *Enpp1* knockout mice [27], and aberrant FGF and bone morphogenetic protein (BMP) signaling in craniosynostosis patients and mice [13,28]. Hence, a better understanding of physiologic mineralization and the effect of anti-calcification drugs on mechanisms of mineralization will provide useful information for targeting and treating pathological calcification.

1.3 Inhibition of pathological calcification

Treatment options for vascular calcification, FOP and craniosynostosis are limited or even non-existent. Novel non-invasive therapies can significantly alter clinical treatment regimens and improve the standard of care for affected patients. Small molecule drugs and engineered cytokines, genes or peptides have the potential to be developed into new treatments for pathological calcification.

Cardiovascular calcification

Sodium thiosulfate (STS) used to treat calcific uremic arteriopathy (CUA) can attenuate the progression of vascular calcification in hemodialysis patients without affecting

vertebral bone density; however the mechanism of action is unclear [29]. Calcium-free phosphate binders such as sevelamer manage hyperphosphatemia (high circulating phosphorus levels) by reducing phosphate absorption and significantly slowing coronary and aortic calcification in dialysis patients [30]. Calcimimetics which reduce serum calcium levels (e.g. cinacalcet) have been developed more recently and may be useful in slowing the progression of vascular calcification [31]. High-throughput screening of chemical libraries has been employed to identify small molecule inhibitors of TNAP – these compounds were effective in reducing mineralization of vascular smooth muscle cells (VSMCs) isolated from *Enpp1* knockouts [32,33].

Fibrodysplasia ossificans progressiva (FOP)

Advances in the understanding of mutations underlying FOP have led to the identification and testing of a few potential drugs in mouse models. A nuclear retinoic acid receptor γ agonist was able to prevent HO in mice with FOP, with minimal side effects and rebound effects once treatment was stopped [34]. Several small molecule inhibitors of BMP type I receptors that were capable of inhibiting HO in a mouse model of FOP have also been developed [35,36]. An engineered version of the BMP-antagonist Noggin molecule, mutein, was able to block HO formation in a BMP4-induced model of FOP [37].

Craniosynostosis

Tissue engineered sutures have been made from collagen and gelatin seeded with autologous fibroblasts and BMP-2, and remained patent when implanted into rabbits [38]. Organ cultures of calvaria have been useful in studying and understanding suture biology, as well as the effect of treatments on suture patency [39]. Delivery of biomolecules such as TGF β 3, Noggin and anti-TGF β 2 antibodies has prevented suture fusion and postoperative resynostosis in animal models of craniosynostosis [39–41].

In our lab, we have used a combinatorial phage display process to identify the peptide VTKHLNQISQSY (VTK) which binds with specific affinity to apatite [42]. VTK peptide has no acidic amino acids, contrary to known naturally occurring ECM protein domains and previously designed apatite-binding peptides, and therefore is unlikely to have been identified without phage panning. Phosphorylation of the two serine residues on VTK (VTKHLNQI(pS)Q(pS)Y) resulted in a 10-fold increase in binding to apatite. Additionally, phosphopeptide pVTK caused dose-dependent inhibition of osteoblast mineralization *in vitro*, and this inhibition was regulated by peptide sequence and charge distribution (see Chapter 2). Understanding how the phosphorylated peptide interacts with cells to inhibit mineralization could enable the development of novel peptides for the treatment of pathological calcification.

1.4 Hypotheses and aims

There is a clinical need to develop new drug treatments for pathological calcification. The work in this dissertation involves the development and testing of a new anti-calcification

peptide, pVTK, by studying mechanisms of mineralization inhibition *in vitro* and delivering peptide to prevent craniosynostosis *in vivo*.

Global hypothesis: Phosphorylated apatite-specific peptide sequence pVTK will inhibit mineralization by physico-chemical and/or cellular pathways involving the TNAP-Enpp1-Ank axis. pVTK will also prevent premature hypermineralization, suture fusion and abnormal craniofacial morphology in mouse models of craniosynostosis.

Hypothesis 1: pVTK inhibits mineralization via alteration of the Enpp1-TNAP-Ank axis

Aim 1: Identify mechanisms of pVTK-mediated inhibition of mineralization *in vitro* using MC3T3 pre-osteoblasts. Assays were performed at the gene and protein-levels to test the effect of peptide treatment on mineralization, collagen deposition, Enpp1 and TNAP enzyme activity, and osteogenic differentiation in MC3T3 cells. The effect of peptide administration on mineralization at various stages of osteogenic differentiation, and the ability to inhibit progression of mineralization after the initiation of mineralization were also investigated.

Hypothesis 2: pVTK inhibits premature mineralization, suture fusion and abnormal craniofacial morphology observed in craniosynostosis

Aim 2: A conditional transgenic mouse model of craniosynostosis was used to test the efficacy of peptide in inhibiting suture fusion. Characterization of this craniosynostosis

model was conducted, by analyzing craniofacial bone lengths, as well as bone volume and tissue mineral density. Additionally, pVTK peptide was locally delivered to the AF suture, and skulls were analyzed for changes in craniofacial morphology, suture fusion and bone quality.

1.5 Summary and organization of dissertation

In Chapter 2, inhibition of mineralization of MC3T3 pre-osteoblast cells by phosphorylated peptide is demonstrated, along with effects of charge distribution on apatite binding and formation. Chapter 3 extends the work from Chapter 2, identifying *in vitro* cellular and physico-chemical mechanisms of mineralization inhibition using MC3T3 cell cultures (Aim 1). Chapter 4 discusses different murine models of pathological calcification that were studied to identify a suitable model with a reproducible phenotype to test effects of peptide treatment *in vivo*. Chapter 5 addresses Aim 2, wherein a conditional transgenic mouse model of craniosynostosis was characterized and treated with peptide to prevent premature hypermineralization of cranial sutures. Chapter 6 summarizes the key findings and discusses future directions for the work presented in this dissertation.

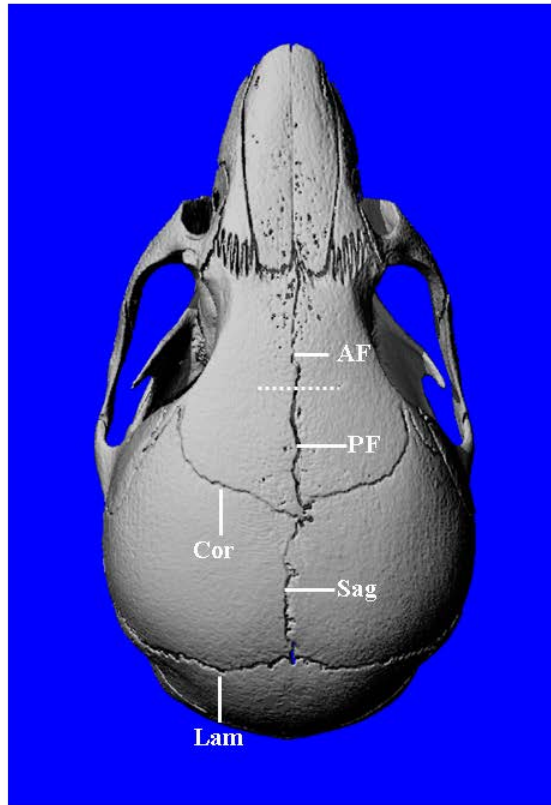


Figure 1.1: Three dimensional rendering of a mouse skull scanned using micro-computed tomography depicting the major cranial sutures: AF - anterior-frontal; PF - posterior-frontal; Cor – coronal; Sag – sagittal; Lam – lambdoid.

1.6 References

- [1] Roger VL, Go AS, Lloyd-Jones DM, Adams RJ, Berry JD, Brown TM, et al. Heart disease and stroke statistics--2011 update: a report from the American Heart Association. *Circulation* 2011;123:e18–209.
- [2] Vliegenthart R, Oudkerk M, Hofman A, Oei H-HS, van Dijck W, van Rooij FJ a, et al. Coronary calcification improves cardiovascular risk prediction in the elderly. *Circulation* 2005;112:572–7.
- [3] Son B, Kozaki K, Iijima K, Eto M, Kojima T, Ota H, et al. Statins Protect Human Aortic Smooth Muscle Cells from Inorganic Phosphate-Induced Calcification by Restoring Gas6-Axl Survival Pathway. *Circ Res* 2006;98:1024–31.
- [4] Shore EM, Xu M, Feldman GJ, Fenstermacher DA, Cho T-J, Choi IH, et al. A recurrent mutation in the BMP type I receptor ACVR1 causes inherited and sporadic fibrodysplasia ossificans progressiva. *Nat Genet* 2006;38:525–7.
- [5] Kaplan FS, Le Merrer M, Glaser DL, Pignolo RJ, Goldsby RE, Kitterman JA, et al. Fibrodysplasia ossificans progressiva. *Best Pract Res Clin Rheumatol* 2008;22:191–205.
- [6] Kaplan FS, Shore EM, Gupta R, Billings PC, Glaser DL, Pignolo RJ, et al. Immunological Features of Fibrodysplasia Ossificans Progressiva and the Dysregulated BMP4 Pathway. *Clin Rev Bone Miner Metab* 2005;3:189–94.
- [7] Pignolo RJ, Shore EM, Kaplan FS. Fibrodysplasia ossificans progressiva: clinical and genetic aspects. *Orphanet J Rare Dis* 2011;6:80.
- [8] Glaser DL, Kaplan FS. Treatment Considerations for the Management of Fibrodysplasia Ossificans Progressiva. *Clin Rev Bone Miner Metab* 2005;3:243–50.
- [9] Bradley JP, Levine JP, Roth D a, McCarthy JG, Longaker MT. Studies in cranial suture biology: IV. Temporal sequence of posterior frontal cranial suture fusion in the mouse. *Plast Reconstr Surg* 1996;98:1039–45.
- [10] Renier D, Lajeunie E, Arnaud E, Marchac D. Management of craniosynostoses. *Child's Nerv Syst* 2000;16:645–58.
- [11] Goldin JH, Wake MJC, Stavrou P, Sgouros S, Willshaw HE, Hockley a. D. Visual failure caused by raised intracranial pressure in craniosynostosis. *Child's Nerv Syst* 1997;13:64–7.

- [12] Shah PS, Siriwardena K, Taylor G, Steele L, Ray P, Blaser S, et al. Sudden infant death in a patient with FGFR3 P250R mutation. *Am J Med Genet A* 2006;140:2794–6.
- [13] Hatch NE. FGF Signaling in Craniofacial Biological Control and Pathological Craniofacial Development. *Crit Rev Eukaryot Gene Expr* 2010;20:295–311.
- [14] Jabs EW, Müller U, Li X, Ma L, Luo W, Haworth IS, et al. A mutation in the homeodomain of the human MSX2 gene in a family affected with autosomal dominant craniosynostosis. *Cell* 1993;75:443–50.
- [15] El Ghouzzi V, Le Merrer M, Perrin-Schmitt F, Lajeunie E, Benit P, Renier D, et al. Mutations of the TWIST gene in the Saethre-Chotzen syndrome. *Nat Genet* 1997;15:42–6.
- [16] Terkeltaub R, Rosenbach M, Fong F, Goding J. Causal link between nucleotide pyrophosphohydrolase overactivity and increased intracellular inorganic pyrophosphate generation demonstrated by transfection of cultured fibroblasts and osteoblasts with plasma cell membrane glycoprotein-1. *Arthritis Rheum* 1994;37:934–41.
- [17] Ho AM. Role of the Mouse ank Gene in Control of Tissue Calcification and Arthritis. *Science* (80-) 2000;289:265–70.
- [18] Moss DW, Eaton RH, Smith JK, Whitby LG. Association of Inorganic-Pyrophosphatase Activity with Human Alkaline Phosphatase Preparations. *Biochem J* 1967;102:53–7.
- [19] Hesse L, Johnson KA, Anderson HC, Narisawa S, Sali A, Goding JW. Tissue-nonspecific alkaline phosphatase and plasma cell membrane glycoprotein-1 are central antagonistic regulators of bone mineralization. *Proc Natl Acad Sci* 2002;99:9445–9.
- [20] Beck GR. Inorganic phosphate as a signaling molecule in osteoblast differentiation. *J Cell Biochem* 2003;90:234–43.
- [21] Beck G. Inorganic phosphate regulates multiple genes during osteoblast differentiation, including Nrf2. *Exp Cell Res* 2003;288:288–300.
- [22] Beck GR, Zerler B, Moran E. Phosphate is a specific signal for induction of osteopontin gene expression. *Proc Natl Acad Sci U S A* 2000;97:8352–7.
- [23] Hunter GK, Goldberg HA. Nucleation of hydroxyapatite by bone sialoprotein. *Proc Natl Acad Sci* 1993;90:8562–5.

- [24] Boskey a L, Maresca M, Ullrich W, Doty SB, Butler WT, Prince CW. Osteopontin-hydroxyapatite interactions in vitro: inhibition of hydroxyapatite formation and growth in a gelatin-gel. *Bone Miner* 1993;22:147–59.
- [25] Byers BA, García AJ. Exogenous Runx2 expression enhances in vitro osteoblastic differentiation and mineralization in primary bone marrow stromal cells. *Tissue Eng* 2004;10:1623–32.
- [26] Steitz SA, Speer MY, Curinga G, Yang H-Y, Haynes P, Aebbersold R, et al. Smooth Muscle Cell Phenotypic Transition Associated With Calcification: Upregulation of Cbfa1 and Downregulation of Smooth Muscle Lineage Markers. *Circ Res* 2001;89:1147–54.
- [27] Mackenzie NCW, Zhu D, Milne EM, van 't Hof R, Martin A, Quarles DL, et al. Altered Bone Development and an Increase in FGF-23 Expression in Enpp1 Mice. *PLoS One* 2012;7:e32177.
- [28] Komatsu Y, Yu PB, Kamiya N, Pan H, Fukuda T, Scott GJ, et al. Augmentation of Smad-dependent BMP signaling in neural crest cells causes craniosynostosis in mice. *J Bone Miner Res* 2013;28:1422–33.
- [29] Mathews JS, Fuentes L, Podaralla P, Cabellon A, Zheng S, Bierhals A, et al. Effects of Sodium Thiosulfate on Vascular Calcification in End-Stage Renal Disease: A Pilot Study of Feasibility, Safety and Efficacy. *Am J Nephrol* 2011;33:131–8.
- [30] Chertow GM, Burke SK, Raggi P. Sevelamer attenuates the progression of coronary and aortic calcification in hemodialysis patients. *Kidney Int* 2002;62:245–52.
- [31] Raggi P, Chertow GM, Torres PU, Csiky B, Naso A, Nossuli K, et al. The ADVANCE study: a randomized study to evaluate the effects of cinacalcet plus low-dose vitamin D on vascular calcification in patients on hemodialysis. *Nephrology Dial Transplant* 2011;26:1327–39.
- [32] Narisawa S, Harmey D, Yadav MC, O'Neill CW, Hoylaerts MF, Millan JL. Novel Inhibitors of Alkaline Phosphatase Suppress Vascular Smooth Muscle Cell Calcification. *J Bone Miner Res* 2007;22:1700–10.
- [33] Sergienko E, Su Y, Chan X, Brown B, Hurder A, Narisawa S, et al. Identification and characterization of novel tissue-nonspecific alkaline phosphatase inhibitors with diverse modes of action. *J Biomol Screen* 2009;14:824–37.
- [34] Shimono K, Tung W, Macolino C, Chi AH-T, Didizian JH, Mundy C, et al. Potent inhibition of heterotopic ossification by nuclear retinoic acid receptor- γ agonists. *Nat Med* 2011;17:454–60.

- [35] Mohedas AH, Xing X, Armstrong KA, Bullock AN, Cuny GD, Yu PB. Development of an ALK2-Biased BMP Type I Receptor Kinase Inhibitor. *ACS Chem Biol* 2013;8:1291–302.
- [36] Yu PB, Deng DY, Lai CS, Hong CC, Cuny GD, Buxsein ML, et al. BMP type I receptor inhibition reduces heterotopic ossification. *Nat Med* 2008;14:1363–9.
- [37] Glaser DL, Economides AN, Wang L, Liu X, Kimble RD, Fandl JP, et al. In vivo somatic cell gene transfer of an engineered Noggin mutein prevents BMP4-induced heterotopic ossification. *J Bone Joint Surg Am* 2003;85-A:2332–42.
- [38] Hong L, Mao JJ. Tissue-engineered Rabbit Cranial Suture from Autologous Fibroblasts and BMP2. *J Dent Res* 2004;83:751–6.
- [39] Amr M. Moursi, Winnard PL, Doug Fryer, Mark P. Mooney. Delivery of Transforming Growth Factor- β 2-Perturbing Antibody in a Collagen Vehicle Inhibits Cranial Suture Fusion in Calvarial Organ Culture 2009.
- [40] Opperman LA, Moursi AM, Sayne JR, Wintergerst AM. Transforming growth factor-beta 3(Tgf-beta3) in a collagen gel delays fusion of the rat posterior interfrontal suture in vivo. *Anat Rec* 2002;267:120–30.
- [41] Cooper GM, Curry C, Barbano TE, Burrows AM, Vecchione L, Caccamese JF, et al. Noggin inhibits postoperative resynostosis in craniosynostotic rabbits. *J Bone Miner Res* 2007;22:1046–54.
- [42] Segvich SJ, Smith HC, Kohn DH. The adsorption of preferential binding peptides to apatite-based materials. *Biomaterials* 2009;30:1287–98.

Chapter 2

Phosphorylation-dependent mineral-type specificity for apatite-binding peptide sequences¹

2.1 Introduction

Biomimetic materials used in the repair of traumatic or pathologic bone and tooth defects endeavor to guide the regeneration of mineralized tissues by providing molecular cues to the damaged tissue. The inherent complexity of skeletal and dental tissues requires not only that biomaterials must elicit specific cellular responses that lead to extracellular matrix formation, but that the tissue formed must be both spatially and temporally controlled, and mineralizable. *In vivo*, highly coordinated temporospatial control is usually provided by biological molecules and cell-to-cell communication, and therefore the incorporation of surface or soluble signals in the design of biomaterials is a logical approach to influence tissue development [1,2]. A central tenet of biomimetic material design for connective tissues is that replicating key aspects of natural extracellular matrices will enable materials to achieve a greater level of control over cell function, and allow better integration into host tissues.

¹ Published as Addison WN, Miller SJ, Ramaswamy J, Mansouri A, Kohn DH, McKee MD; Biomaterials 2010; 31: 9422 - 9430

The choice and design of biologic molecules potentially useful in any given physiologic milieu depends on factors that include the chemistry of the implantable material itself, and the type of defect in a target tissue. Current scaffolding/implant materials commonly used in orthopedic and dental applications such as metals, calcium-phosphate ceramics and polymers each present different surface chemistries, topographies and stiffness, and each have their inherent limitations and applications. Although mineral particles can be used directly to fill bone and tooth defects and enhance the osseointegration of implants [3], induction of bone formation generally requires additional modification by biologic molecules [4]. However, processing and design steps used to fabricate implantable materials often can be detrimental to incorporation of organic, biologic molecules into the implants, an example being the commonly used high sintering temperatures used in the processing of implantable ceramics and composites. The biomimetic precipitation of bone-like mineral (BLM) is an alternative process that occurs at physiologic temperatures (37°C) not destructive to any incorporated biologic components [5]. Biomimetically produced BLM in turn can provide a scaffold for the adsorption/incorporation or co-precipitation of biologic molecules, such that biomolecular functions are retained and induction of osteogenesis can occur [6–8].

Modification of implantable surfaces with bioactive peptides is one approach to designing biomimetic materials. However, unlike polymeric materials, the surface of hydroxyapatite mineral is not easily modified by surface treatments that form functional hydroxyl-, amino, or carboxyl- groups commonly used in implant design, resulting in a need for peptide sequences that preferentially adhere to this material surface. Furthermore, compared to full-length proteins, relatively smaller bioactive peptides are

cheaper and faster to produce, easier to purify, and do not require processing from animal sources. Traditional design methods use peptide sequences adapted from mineral-binding proteins such as osteopontin, bone sialoprotein and statherin [9–11]. Mineral-binding sequences in these proteins are rich in acidic residues (aspartate, glutamate and phosphoserines) resulting in a net negative charge that promotes binding to positively charged calcium at apatite crystal faces [12,13]. These proteins, and peptides derived from them, often lack mineral-type specificity – a notable example being osteopontin which binds to and influences the growth of hydroxyapatite [14], calcium oxalate [15] and calcite [16]. Design of mineral-type specificity is considered advantageous in the design of tissue-specific implantable materials, as these may result in better tissue integration and function. New design methods may also be applicable to the development of material-specific peptides to be used as molecular probes/sensors to identify mineral phases in pathologic crystal deposits, or even as targeting tags for delivery of drugs [17] or tissue-specific molecules.

Previously, we have used phage display to identify a 12-mer peptide sequence – VTKHLNQISQSY (herein called VTK) from a combinatorial library of 10^9 phages – that preferentially adsorbs to bone-like mineral and hydroxyapatite [18]. Phage display technology involves expressing a library of peptide sequences on the protein coat of a bacteriophage, and then panning for sequences that adhere to a ligand or substrate of interest [19]. Phage display has been used to identify peptide sequences that bind to proteins, DNA, cells, polymers, and even inorganic materials such as silver and titanium [19–22]. One limitation of phage display is the inability to include post-translational modifications within the peptides being expressed on the phage protein coat. Post-

translational phosphorylation of serine, threonine and tyrosine residues are particularly important in proteins and peptides involved in the regulation of biomineralization [23]. Phosphorylation of serine residues is common in proteins involved in biomineralization, and VTK contains two serine residues that could potentially be phosphorylated. Phosphorylation could provide a means to further improve peptide adsorption, modulate material specificity and modify cellular responses to the peptides.

In this study, we determined critical design parameters controlling peptide affinity to synthetic and biologically secreted apatites by investigating the effects of phosphorylation and amino acid sequence scrambling on peptide-mineral binding, and, in a functional assay, on their ability to inhibit osteoblast cell culture mineralization. We have also explored the mechanism of mineral-binding of these peptides by RosettaSurface computational simulations for peptide structure prediction at the surface of mineral. Collectively, these studies provide insight on the role of peptide charge, charge distribution, composition and amino acid sequence in the design of functional biomaterials.

2.2 Materials and Methods

2.2.1 Preparation of biomimetic films and apatite disks

A 5% (w/v) 85:15 polylactic-co-glycolic acid (PLGA, Alkermes)-chloroform solution was cast on 12-mm diameter glass slides and dried overnight. The PLGA films were etched in 0.5M NaOH for 7 min., rinsed in ddH₂O, and soaked in modified simulated body fluid (141 mM NaCl, 4.0 mM KCl, 0.5 mM MgSO₄, 1.0 mM MgCl₂, 4.2 mM

NaHCO₃, 5.0 mM CaCl₂·2H₂O, and 2.0 mM KH₂PO₄) at pH 6.8 for 5 days at 37°C [8] to enable self-assembly of a carbonated apatite layer onto the PLGA substrate. The modified simulated body fluid was changed daily to maintain supersaturation and thermodynamic conditions conducive to heterogeneous nucleation of mineral. Hydroxyapatite (HA) disks (10 mm in diameter × 4 mm thick) were pressed from powder (Plasma Biototal Ltd.) at 1 metric ton for 1 min. and sintered at 1350 °C for 1 h.

Carbonated apatite disks were made from 5.6% (CA5) and 10.5% (CA10) carbonated apatite powders (a generous gift from Dr. Mary Tecklenburg [Central Michigan University]). Carbonated apatite disks (8–10 mm in diameter × 2–4 mm thick) were pressed from powders at 0.5 metric ton for 1 min and sintered at 1350 °C for 1 h (heating rate of 10 °C/min). HA and carbonated disks were sonicated in 10 mM HCl, then in ddH₂O. All sintered disks (CA5, CA10, and HA) were autoclaved prior to use. Macroscopic dimensions of all disks were measured with calipers. The morphology, composition, crystallinity and surface area of the materials have been characterized using scanning electron microscopy, Fourier Transform Infrared Spectroscopy, X-ray diffraction, and Brunauer-Emmett Teller (BET) methods, respectively, and were previously reported [18].

2.2.2 Peptide synthesis

A peptide sequence – VTKHLNQISQSY (VTK) – with high and preferential affinity to apatite-based materials was previously discovered from phage display [18,24]. To investigate the role of residue charge, charge distribution and sequence as design parameters in controlling peptide affinity to synthetic and biologic apatite,

phosphorylated (VTKHLNQiSpSY) and scrambled (IYQSKHTLSNQV; IYQpSKHTLpSNQV) variants of the VTK peptide were also studied. Scrambled sequences were obtained using a random number generator. All peptides were fabricated on a Rainin Symphony Synthesizer by Fmoc solid-phase chemistry according to standard peptide synthesis procedures and characterized as having >86% purity by high-performance liquid chromatography (University of Michigan Protein Core). Phosphorylations at specific serine residues in the peptide sequence were achieved using preformed, protected phosphoserine amino acids. Peptides were labelled on resin before cleavage using 5-(and-6)-carboxyfluorescein succinimidyl ester (Molecular Probes C-1311) (University of Michigan Protein Core). The peptides used in this study, and some of their properties, are summarized in Table 2.1. Isoelectric points were calculated using Scansite [25] and the Compute pI/Mw tool on the ExPASy proteomics server [26].

2.2.3 Synthetic peptide adsorption assay

For each peptide, an UV absorbance value vs. absorbance wavelength graph was generated from 200 to 300 nm (BioRad Smartspec 3000). UV absorbance maxima for VTK was at 225 nm. From these graphs, the wavelength resulting in the highest UV absorbance for each peptide was used to generate standard curves (peptide concentration vs. UV absorbance) and estimations of peptide concentrations. Standard curves consisting of the concentrations 0, 1, 5, 10, 25, 50, 75, 100, 250, 500, 750, and 1000 µg/mL were developed for each peptide tested. From duplicate readings per concentration, the error introduced from the detection technique was ~5%. A modified standard curve consisting of values below 100 µg/mL was used for each peptide to calculate the unknown peptide amount that adsorbed onto each material tested. Amino

acid analysis was performed to verify peptide concentration for standard curves created with UV absorbance at 205 nm and 225 nm wavelengths. Peptides were reconstituted in ddH₂O and diluted to ~500 µg/mL in 50 mM Trizma buffer, pH 7.5. BLM films, HA, CA5 and CA10 disks, and blank TCPS wells were soaked in ddH₂O overnight at 4 °C (n = 5-6 per material) in 24-well polystyrene tissue culture dishes. Prior to introducing 1 mL of the peptide or buffer solutions for negative controls, plates were allowed to warm to room temperature and then the overnight solution was removed. Plates were agitated on a Titer Plate Shaker at ~80 rpm for 3 h at room temperature. The films and disks were rinsed with ddH₂O and then soaked in a 10 mM HCl solution for 18 h at room temperature on the same shaker. To determine the amount of peptide adsorbed, aliquots of the HCl solution were read on an UV spectrophotometer.

2.2.4 Cell culture

MC3T3-E1 (subclone 14) murine calvarial osteoblasts [27] (courtesy of Dr. R. Franceschi, University of Michigan, Ann Arbor, MI, USA) were maintained in modified α -minimum essential media (Invitrogen) supplemented with 10% FBS (Hyclone) and 1% penicillin-streptomycin (Invitrogen) at 37°C in a humidified atmosphere of 5% CO₂. All experiments were carried out at a plating density of 50,000 cells/cm². Cell differentiation and matrix mineralization were initiated 24 h after plating by replacing the medium with fresh medium supplemented with 50 µg/ml ascorbic acid (Sigma) and 10 mM β -glycerophosphate (Sigma). Medium, with or without peptide (see above), was changed every 48 h over a 12-day time period.

2.2.5 Quantification of mineralization

After 12 days of culture, mineral was visualized by von Kossa staining using 5% silver nitrate solution (Sigma). For quantification of mineralization by measuring calcium deposited within the cell/matrix layer, cultures were decalcified with 0.5 N HCl, and calcium in the supernatant was determined spectrophotometrically (absorbance at 595 nm) from duplicate readings per well using a calcium assay kit (Diagnostic Chemicals).

2.2.6 Assay for cell proliferation

Cell proliferation and viability in the presence of peptide was measured using the MTT assay [28]. Briefly, cells were incubated with 0.5 $\mu\text{g}/\mu\text{L}$ MTT (3-[4,5-dimethylthiazol-2-yl]-2,5-diphenyl tetrazolium bromide) (Sigma) in medium for 3 h, solubilized with DMSO and absorbance measured at 562 nm.

2.2.7 Binding of fluorescently labelled peptides to osteoblast culture mineral

Maximally mineralized day 12 osteoblast cultures were incubated with 150 μM of fluorescently-labelled peptide in culture medium for 1 h at room temperature. After washing three times with phosphate-buffered saline, cultures were incubated with 30 μM calcein blue (Sigma) for 1 h, dried and visualized a Leica DM IL inverted fluorescent microscope (Leica).

2.2.8 Computational modeling and energy calculations

All simulations were performed using the RosettaSurface Monte Carlo plus minimization structure prediction program [29]. Each execution of the program folds a peptide from a fully extended conformation and results in an energy-minimized solution- and adsorbed-

state structure. Large structural ensembles of 10^5 candidate solution- and adsorbed-state conformers were generated from which only the 100 lowest-energy structures, from each state, were chosen for further analysis. Fully extended peptide structures were constructed with PyMOL (DeLano Scientific). Hydroxyapatite crystal surface with $P2_1/b$ space group, lattice parameters of $a = 9.42$, $b = 2a$, $c = 6.88$ and $\gamma = 120^\circ$, and positive Ca^{2+} termination on the $\{100\}$ crystallographic face was constructed with CrystalMaker (CrystalMaker Software Ltd.). The $\{100\}$ face is a highly stable hydroxyapatite surface to which several mineralization-related proteins are known to bind [30,31].

2.2.9 Statistics

Data is presented as mean values \pm one standard deviation. ANOVA on RANKS with Dunn's post-hoc comparisons (SigmaStat) were used to determine effect of peptide sequence on adsorption to each substrate. Effects of phosphorylation (differences between VTK and pVTK; VTK-scram and pVTK-scram) and scrambling (differences between VTK and VTK-scram; pVTK and pVTK-scram) were also determined from the Dunn's test. Independent samples t-tests were used to determine differences between VTK and pVTK on each material and differences in peptide adsorption between BLM and HA. *In vitro* quantification of mineralization and proliferation were assessed with Student's t-tests for effects of phosphorylation and scrambling (GraphPad Software).

2.3 Results

2.3.1 Effect of phosphorylation on peptide adsorption to synthetic apatite-based substrates

Adsorption of VTKHLNQISQSY (VTK) and VTK phosphorylated at Ser-9 and Ser-11 (pVTK) to four apatite-based minerals and to tissue culture polystyrene (TCPS) was measured using a synthetic peptide adsorption assay. VTK and pVTK did not adsorb to TCPS (Figure 2.1), demonstrating specificity for the apatite-based materials. Phosphorylation of VTK peptide led to a 10-fold increase in peptide adsorption to BLM ($p < 0.001$). Significant increases in peptide adsorption to the carbonated disks – CA5 and CA10 ($p < 0.001$ for both CA5 and CA10) – were also observed for pVTK relative to VTK. Binding of VTK to HA was not significantly enhanced by phosphorylation. There were no significant differences in the amount of VTK adsorbed to the different apatite surfaces. However, when phosphorylated, VTK adsorption to bone-like mineral was significantly greater than to the other apatites. These data suggest that phosphorylation of amino acids on peptide sequences provides a means to control adsorption on carbonated apatite surfaces in a material-specific manner, and to increase peptide concentrations on a biomaterial surface.

2.3.2 Effect of VTK and pVTK on osteoblast-mediated mineralization

The MC3T3-E1 osteoblast cell line is a well-established cell culture model widely used as an *in vitro* model of osteogenesis [27,32]. MC3T3-E1 cells secrete and assemble a collagenous extracellular matrix that subsequently mineralizes over a 12-day period. To

examine the effect of VTK and pVTK on osteoblast-mediated mineralization, cultures were treated with VTK and pVTK for 12 days and the mineral formed was quantified by a biochemical assay for calcium (Figure 2.2A) and was visualized by von Kossa staining (Figure 2.2B). pVTK dose-dependently inhibited mineralization with maximum inhibition occurring at concentrations $> 200 \mu\text{M}$. VTK had no effect on mineralization at comparable doses. Cell proliferation, as measured by the MTT assay, was reduced during days 6 and 9 of culture, but was normal after 12 days of treatment with both peptides (Figure 2.2C); thus, the peptides did not appear to be cytotoxic to the osteoblasts, and inhibition of mineralization is not attributable to toxicity.

2.3.3 Effects of amino acid sequence scrambling on adsorption to synthetic apatite-based substrates

To determine the role of amino acid composition versus amino acid sequence order, and therefore the role of net charge versus local charge distribution, scrambled variants of VTK and pVTK were synthesized and their adsorption onto apatite-based substrates measured. Scrambling of the peptide sequence does not alter the net charge, but does alter the local charge distribution on the peptide, especially in the case of pVTK where the two phosphoserine residues are located at the N-terminus at positions 9 and 11. Scrambling VTK resulted in a significant increase in adsorption to BLM vs. HA, suggesting increased enhancement of binding specificity towards BLM (Figure 2.3). Scrambling of pVTK had no significant effect on binding to BLM nor HA. Adsorption of scrambled pVTK was still greater than VTK or scrambled VTK, although not

statistically significant. These data suggest that not only are specific residues important for binding, but that residue order may be configured to further increase binding affinity. Furthermore, the enhanced BLM binding caused by phosphorylation appears to override any further impact of a more beneficial charge distribution.

2.3.4 Effect of scrambled pVTK on osteoblast-mediated mineralization

pVTK-scam inhibited mineralization in osteoblast cultures with significantly less potency than pVTK (Figure 2.4). Whereas pVTK exhibited a concentration dependent inhibition and at 200 μ M completely inhibited mineralization, 200 μ M pVTK-scam had a significantly lesser effect on mineral inhibition. This suggests that peptide sequence order is critical for *in vitro* regulation of mineralization.

2.3.5 Binding of peptides to mature osteoblast culture mineral

To determine whether the increased mineralization inhibitory potency of pVTK over pVTK-scam also occurred with osteoblast mineral, mature mineralized osteoblast cultures were incubated with fluorescently-labelled peptide for 1 h, washed and visualized by immunofluorescence microscopy. Mineral was labelled with calcein blue. pVTK co-localized with the mineral, indicating strong binding whereas no fluorescence was observed for VTK, VTK-scam and pVTK-scam (Figure 2.5).

2.3.6 Computational modelling

Computational modelling has been beneficial in the understanding of protein/peptide interactions with calcium oxalate, calcite and hydroxyapatite crystal surfaces [15,29,33,34]. The RosettaSurface protocol in particular is capable of structure predictions that are consistent with experimentally measured distances made by solid-state NMR [29]. To understand the peptide-apatite binding observations made in this study, we used molecular modeling to calculate binding energies of VTK, pVTK, pVTK-scam and VTK-scam peptides to the {100} face of hydroxyapatite. The phosphorylated peptides pVTK and pVTK-scam had significantly higher ($p < 0.001$) binding energies than the nonphosphorylated peptides (Table 2.2). Between pVTK and pVTK-scam however, there was no significant difference in the binding energies, suggesting that scrambling the peptide sequence did not alter binding energies. VTK and VTK-scam also had binding energies that were not significantly different. Structural prediction reveals that for pVTK and pVTK-scam the residues contributing most to the peptide-crystal surface interaction (shortest mean distance from crystal surface) were the pSer residues (Figure 2.6B and D). Despite VTK and VTK-scam having similar binding energies, the residues involved in the binding were different. For VTK, binding was mostly through the basic Lys-3 and the polar residues Gln-10 and Tyr-12, whereas for VTK-scam binding occurred via the basic Lys-5 residue (Figure 2.6A and C). Figure 2.6E and F show representative structures of VTK and pVTK, respectively. Lys-3 and Tyr-12 on VTK peptide form electrostatic interactions with the crystal surface (Figure 2.6E). The phospho-serine residues of pVTK co-ordinate with rows of calcium atoms in

the crystal surface while the side-chain hydroxyl of tyrosine also interacts with the crystal surface (Figure 2.6F).

2.4 Discussion

Phage display provides an alternative design strategy for the identification of material-specific peptides for use in functional biomaterials. Using a phage display library expressing 10^9 different peptide sequences, a 12-mer peptide – VTKHLNQLSQSY – was identified to have specificity toward apatite substrates. The affinity of a peptide for a material surface is determined by the physico-chemical properties of the individual amino acids. We therefore hypothesized that residue order and charge are design parameters that could potentially refine peptide affinity and substrate specificity. Using scrambled and phosphorylated variants of VTK, we examined the mechanisms of peptide binding to apatite-based biomaterials and the *in vitro* effects of the peptides on osteoblast-mediated mineralization. The study identifies phosphorylation as a design method to further modulate material binding specificity. In summary, our results show that 1) phosphorylation increases peptide specificity for bone-like mineral and to a lesser extent carbonated apatite, 2) phosphorylation is required for osteoblast mineral binding and inhibition, 3) amino acid sequence order and not simply net composition/charge play an important role in both apatite-substrate binding and in osteoblast culture mineralization inhibition, and 4) binding of peptides to osteoblast culture mineral depends on both peptide composition and peptide sequence.

Binding of VTK to apatite may appear somewhat surprising considering that VTK is positively charged and lacks any acidic amino acid residues. In nature, proteins and peptides associated with mineral are often (if not typically) acidic and negatively charged [12]. Phage display therefore provides a method to identify alternative sequences to those identified by protein sequence searching of naturally occurring proteins. Hydroxyapatite consists of both cations and anions, so there is the potential for both acidic and basic residues to bind to this mineral. Materials with high surface areas can present crystal edges as opposed to crystal faces. Crystal edges could provide an alternative charge distribution compared to crystal faces, further explaining the binding of the positive charged peptide to bone-like mineral. Basic residues are important for binding of the salivary protein statherin [35] and human lysozyme to hydroxyapatite [36]. Indeed, our computational modeling of VTK and VTK-scam binding to hydroxyapatite (Figure 2.6) indicated the use of a variety of amino acids including the basic residue lysine and polar amino acids such as glutamine and tyrosine.

Post-translational modification of proteins, for example phosphorylation of serine, threonine or tyrosine residues, is an *in vivo* mechanism to regulate protein function [23]. We hypothesized that phosphorylation of mineral-binding peptide sequences previously identified by phage display would increase not only affinity, but specificity as well. Phosphate residues lower the isoelectric point of the molecule thereby increasing its net negative charge to favor interaction with calcium within the hydroxyapatite crystal lattice. Phosphorylation of VTK resulted in increased adsorption to bone-like mineral, and 5% and 10% carbonated apatite, but not to non-carbonated HA (Figure 2.1). Furthermore, the increased affinity of pVTK for BLM was 10-fold higher than that for

CA5 and CA10. Bone apatite differs from synthetic hydroxyapatite in that some 7% of phosphates are substituted by carbonate [37]. Furthermore, carbonate substitutions in bone and BLM are mostly Type-B (phosphate group) substitutions, whereas in the sintered hydroxyapatites CA5 and CA10, the substitutions are Type-A (for hydroxyl groups) [38]. These differences in carbonate composition would presumably alter the surface charge distribution thereby influencing peptide affinity. Increased binding to bone-like mineral could also be related to the increased surface area of BLM compared to other apatites [18]. Phosphate modifications have implications for the tailored control of peptide binding to apatite-based materials, and phosphoserine residues in particular appear to be important in peptide interaction with carbonated apatite surfaces.

Peptide phosphorylation is also a mechanism to control *in vitro* osteoblast mineralization. In this study, we observed that phosphorylation is necessary for inhibition of osteoblast culture mineralization (Figure 2.2), presumably through direct binding to crystal surfaces, consistent with our cell-free, mineral-binding assays. Thus, an apatite-specific peptide may be tailored to control mineralization *in vivo* by the incorporation of phosphoserines. Inhibition of mineralization has likewise been shown for phosphorylated osteopontin peptides in the inhibition of osteoblast mineralization [34], hydroxyapatite [39], calcium oxalate [40], and calcite crystal growth [16].

Interestingly, we observed that scrambling of pVTK reduced its ability to inhibit mineralization (Figure 2.4). These data indicate that amino acid sequence order and not just net charge is important for inhibition of mineralization. The order of amino acids determines any secondary structure the peptide may have which in turn would influence its interaction with the mineral surface. Another explanation could be that although

pVTK and pVTK-scram have equivalent net molecular charges, the phosphoserine residues on pVTK are both concentrated at the C-terminus resulting in concentrated negative charge at one end of the peptide. This indicates the charge distribution of a peptide is also important for mineral binding and inhibition. In order to achieve inhibition of mineralization, the location of the phosphate residues is also a factor to be considered. Although scrambling pVTK inhibited mineralization of osteoblast cultures, scrambling did not decrease binding to mature osteoblast culture mineral (Figure 2.5). It is therefore possible that inhibition of mineralization and mineral binding are controlled by different mechanisms. It is also possible that different apatite crystal faces are exposed during different stages of mineralization and peptides exhibit crystal face specificity in their binding.

The enhanced binding of pVTK (over VTK) to BLM was reflected by the observed inhibition of osteoblast culture mineralization by pVTK. However, scrambling of pVTK reduced the inhibitory potency but did not alter BLM binding. This discrepancy could be attributable to morphological or charge differences between biological mineral and BLM, and further suggests that different mechanisms are important for binding and for inhibition. This observation could permit the design of a peptide that binds strongly to an apatitic substrate but does not prevent osteoblast mineralization.

As a final note, it is important to note that the peptides did not negatively affect cell numbers after 12 days of culture and thus were not cytotoxic. Lack of toxicity supports the potential therapeutic use of peptides such as those examined here. The mineralization inhibitory potential of pVTK could be advantageously used for the management of

ectopic calcifications and hypermineralization pathologies such as kidney stones, arterosclerosis and joint ankylosis.

2.5 Conclusions

Phosphorylation of serine residues on an apatite-binding peptide identified by phage display was used to refine peptide specificity for a variety of apatite-based substrates. We determined that phosphorylation enhances binding to bone-like mineral and to a lesser extent carbonated apatites. Sequence composition appears to be more important than sequence order for binding to synthetic apatite substrates, whereas regulation of osteoblast culture mineralization is determined by both sequence composition and sequence order.

Acknowledgements

I would like to thank my co-authors on this work William Addison, Sharon Miller, Ahmad Mansouri, David Kohn and Marc McKee. I would also like to thank Dr. Henriette Remmer, Peptide Core for assistance with peptide synthesis. These studies were funded by grants from the Canadian Institutes of Health Research (CIHR; MT11360 to MDM) and National Institutes of Health (NIH DE013380 and DE015411 to DHK). MDM is a member of the Jamson T.M. Wong Laboratories for Calcified Tissue Research of the Centre for Bone and Periodontal Research. WNA was the recipient of a studentship from the CIHR Training Grant in Skeletal Health Research. We also thank Dr. Jeffrey J. Gray

and Dr. David L. Masica of Johns Hopkins University for assistance with the RosettaSurface computational simulations.

Peptide	Sequence	Description	Phosphates	Net Charge	pI
VTK	VTKHLNQISQSY	Apatite-specific peptide identified by phage display	0	+1	8.6
pVTK	VTKHLNQI(pS)Q(pS)Y	Phosphorylated VTK	2	-3	4.8
VTK-scram	IYQSKHTLSNQV	Scrambled VTK	0	+1	8.6
pVTK-scram	IYQ(pS)KHTL(pS)NQV	Scrambled phosphorylated VTK	2	-3	4.8

Table 2.1: Amino acid sequences and isoelectric point (pI) of the peptides used in this study

Peptide	Binding Energy (kcal/mol)
VTK	-4.4 ± 2.8
pVTK	-13.6 ± 5.6
VTK-scram	-4.1 ± 2.2
pVTK-scram	-14.0 ± 3.9

Table 2.2: Peptide-hydroxyapatite adsorption energies calculated from RosettaSurface computational modeling. Binding energy is the difference between the mean energies of the 100 lowest energy adsorbed- and solution-state candidate structures (error given is S.D.)

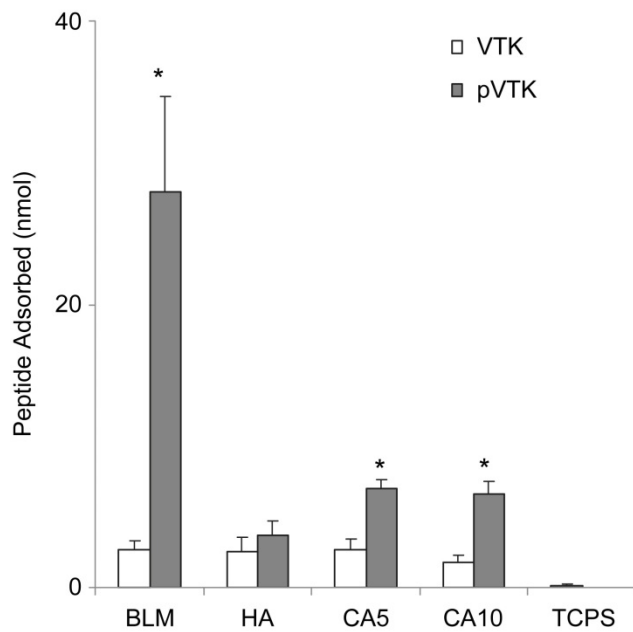


Figure 2.1: Adsorption of VTK and phosphorylated VTK (pVTK) peptides on bone-like mineral (BLM), hydroxyapatite (HA), 5.6% carbonated apatite (CA5), 10.5% carbonated apatite (CA10) and tissue culture polystyrene (TCPS). Phosphorylating serine residues in VTK peptide increased peptide adsorption onto BLM 10-fold in comparison to non-phosphorylated VTK. A similar trend was found on CA5 and CA10 substrates. Data are presented as means \pm S.D. * denotes statistical differences between adsorption of VTK vs. pVTK on a given substrate ($p < 0.05$).

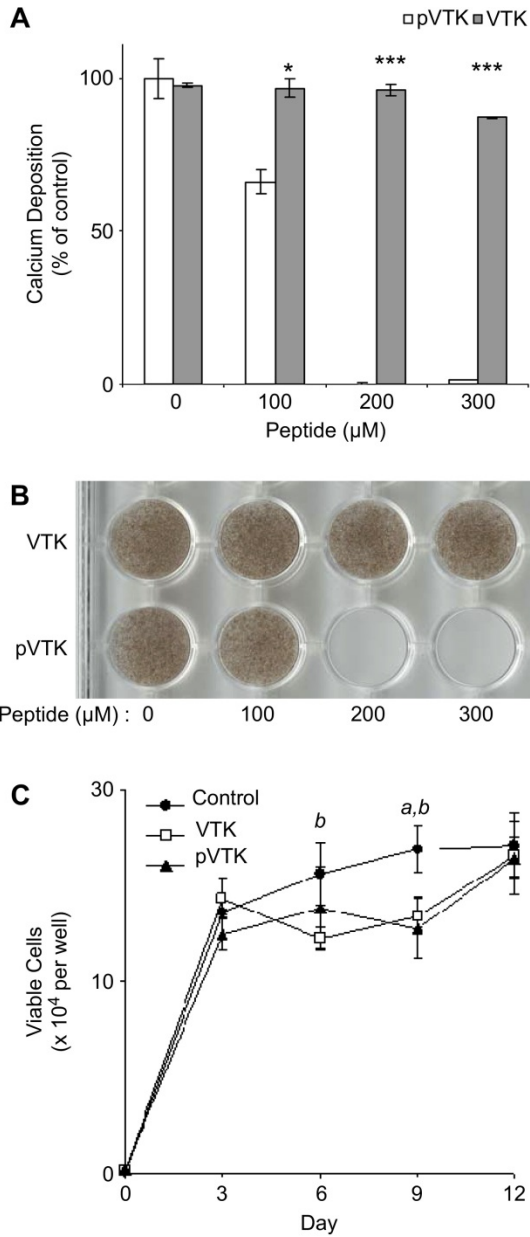


Figure 2.2: Mineralizing MC3T3-E1 osteoblast cultures were incubated with VTK and pVTK at the indicated concentrations for 12 days followed by mineral quantification by (A) calcium content determination expressed as a percentage of untreated control cultures, and (B) von Kossa (silver nitrate) staining for mineral. Data are presented as means \pm S.D. * $p < 0.05$; *** $p < 0.001$ from Student's t -test for statistical differences between the two peptides at a given dose. (C) Cell proliferation in osteoblast cultures treated with, or without, 200 μM pVTK and VTK as measured by MTT assay. a denotes statistical significance between Control and VTK at the given time point. b denotes statistical significance between Control and pVTK at the given time point.

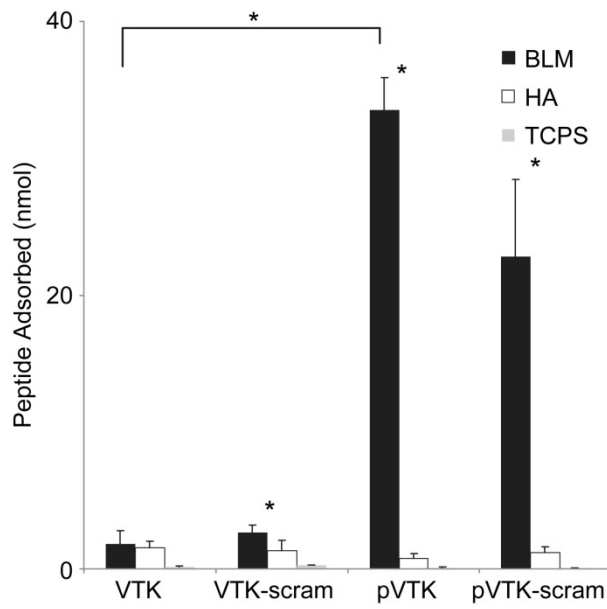


Figure 2.3: Adsorption of fluorescently-labelled VTK, phosphorylated VTK (pVTK), scrambled VTK (VTK-scram) and scrambled phosphorylated VTK (pVTK-scram) on bone-like mineral (BLM), hydroxyapatite (HA) and tissue culture polystyrene (TCPS). pVTK and pVTK-scram showed significantly higher adsorption to BLM than VTK. All peptides except VTK showed significantly higher binding to BLM than HA. Substrate specificity of the peptides was confirmed by absence of binding to TCPS. Bracket denotes a statistical difference between peptides on BLM ($p < 0.05$). Data are presented as means \pm S.D. * denotes statistical differences between adsorption on BLM and HA for a given peptide ($p < 0.01$).

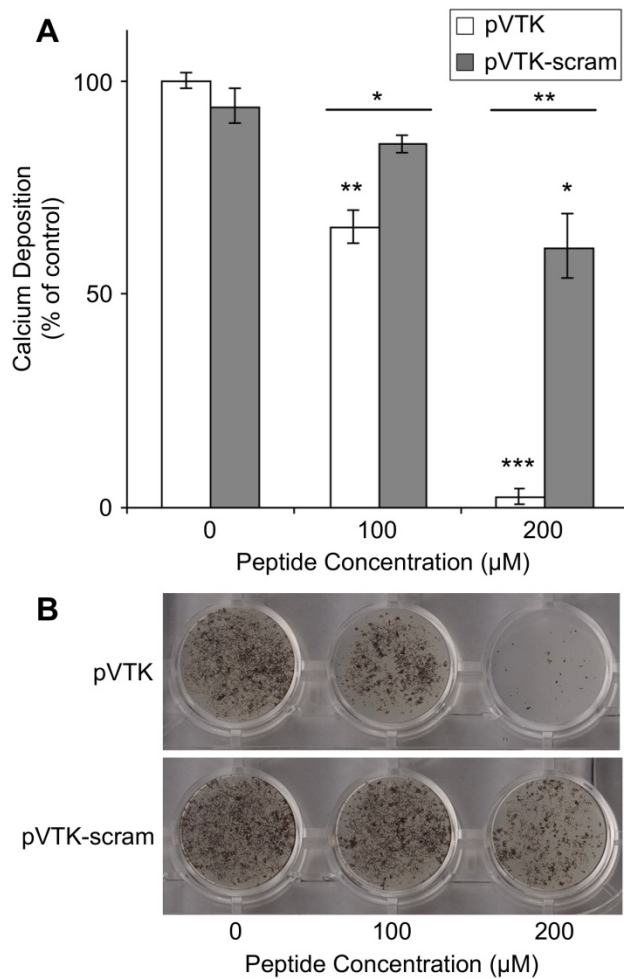


Figure 2.4: Effect of scrambling pVTK on inhibition of osteoblast culture mineralization. MC3T3-E1 osteoblast cultures were treated with the indicated concentrations of pVTK and scrambled pVTK (pVTK-scram) for 12 days followed by (A) quantification of mineralization by calcium content determination expressed as a percentage of untreated control cultures, and (B) von Kossa (silver nitrate) staining for visualization of mineral. Data are presented as means \pm S.D. * $p < 0.05$; ** $p < 0.01$; *** $p < 0.001$ from Student's t -test relative to the untreated control cultures or between the two peptides at a given dose (horizontal bars).

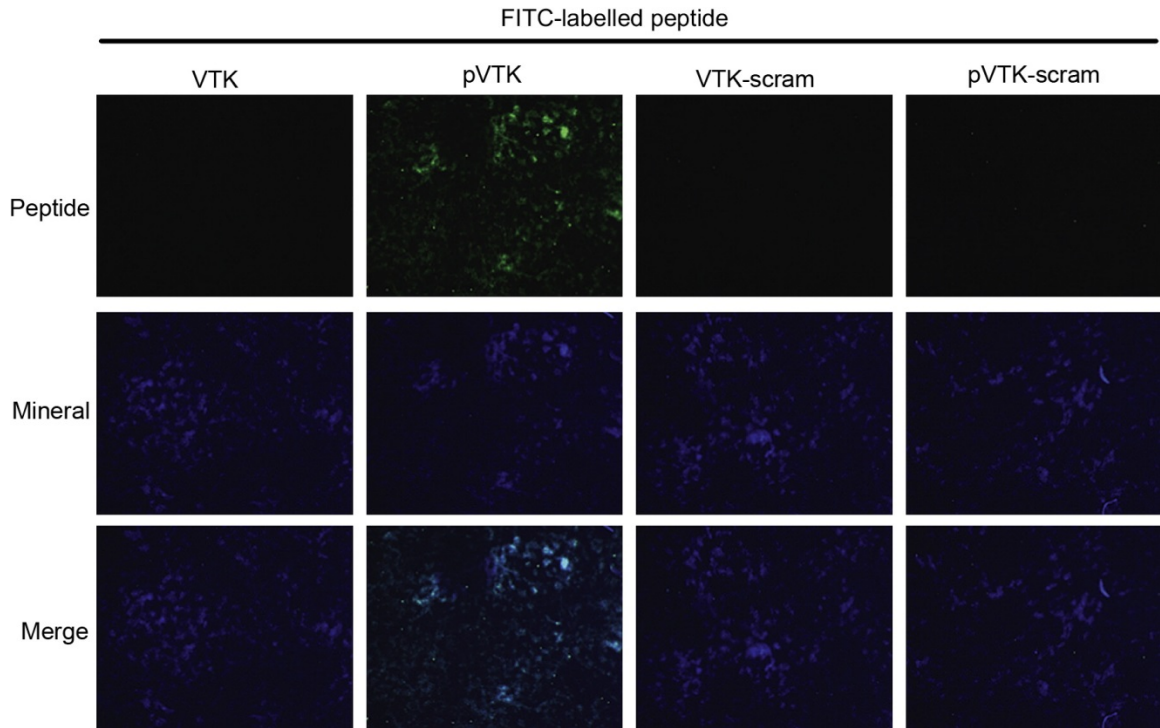


Figure 2.5: Binding of peptides to osteoblast culture mineral. Maximally mineralized MC3T3-E1 osteoblast cultures were incubated with 150 μ M fluorescently tagged peptides for 1 h and examined by fluorescence microscopy for peptides (green) and calcein blue labelled mineral (blue). pVTK co-localized with mineral indicating peptide binding to hydroxyapatite.

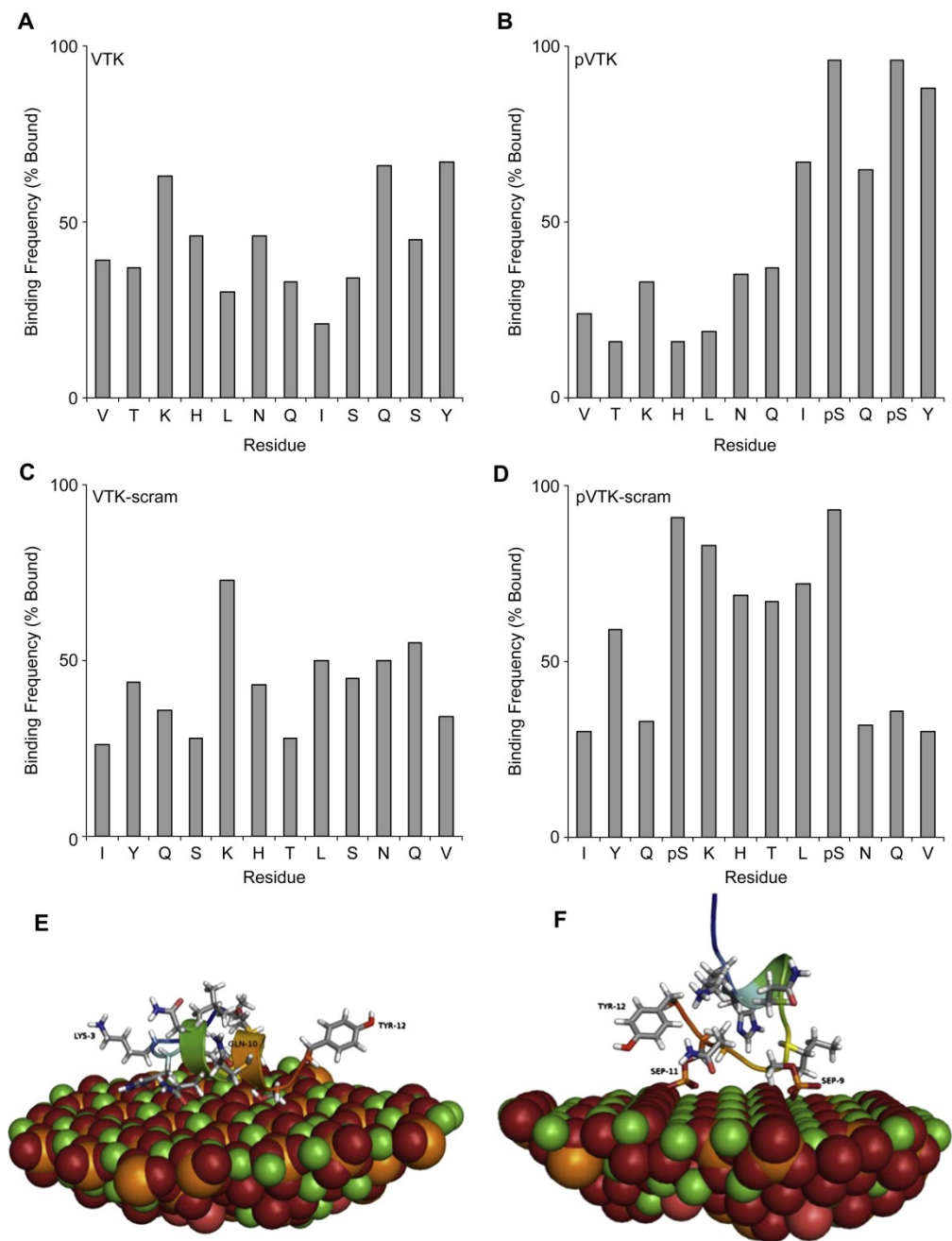


Figure 2.6: Molecular modeling of peptide binding to the {100} crystallographic face of hydroxyapatite. Adsorption frequency of individual residues in the 100 lowest-energy adsorbed state structures. Bound residues are defined as residues closer than 5Å for (A) VTK, (B) pVTK, (C) VTK-scram and (D) pVTK-scram. (E) Structural details of a representative high-scoring VTK model illustrating binding of Lys-3, Gln-10 and Tyr-12. (F) Structural details of pVTK binding illustrating binding of Tyr-12, PSer-9 and PSer-11. (Ca, green; P, orange; O, red; H, white; N, blue).

2.6 References

- [1] Shin H, Jo S, Mikos AG. Biomimetic materials for tissue engineering. *Biomaterials* n.d.;24:4353–64.
- [2] Hubbell JA. Bioactive biomaterials. *Curr Opin Biotechnol* n.d.;10:123–9.
- [3] Geesink RGT. Osteoconductive coatings for total joint arthroplasty. *Clin Orthop Relat Res* n.d.:53–65.
- [4] Alsberg E, Hill EE, Mooney DJ. Craniofacial tissue engineering. *Crit Rev Oral Biol Med* 2001;12:64–75.
- [5] Tanahashi M, Yao T, Kokubo T, Minoda M, Miyamoto T, Nakamuro T, et al. Apatite coated on organic polymers by biomimetic process: Improvement in its adhesion to substrate by glow-discharge treatment. *J Biomed Mater Res* 1995;29:349–57.
- [6] Habibovic P, Blitterswijk CA, Groot K, Layrolle P, Barrère F, Biomimetic Hydroxyapatite Coating on Metal Implants. *J Am Ceram Soc* 2002;85 SRC - :517–22.
- [7] Segvich S, Smith HC, Luong LN, Kohn DH. Uniform Deposition of Protein Incorporated Mineral Layer on Three-Dimensional Porous Polymer Scaffolds. *J Biomed Mater Res B* 2008;84B:340–9.
- [8] Luong LN, Hong SI, Patel RJ, Outslay ME, Kohn DH. Spatial control of protein within biomimetically nucleated mineral. *Biomaterials* 2006;27:1175–86.
- [9] Shin H, Zygourakis K, Farach-Carson MC, Yaszemski MJ, Mikos AG. Attachment, proliferation, and migration of marrow stromal osteoblasts cultured on biomimetic hydrogels modified with an osteopontin-derived peptide. *Biomaterials* n.d.;25:895–906.
- [10] Gilbert M, Shaw WJ, Long JR, Nelson K, Drobny GP, Giachelli CM, et al. Chimeric peptides of statherin and osteopontin that bind hydroxyapatite and mediate cell adhesion. *J Biol Chem* 2000;275:16213–8.
- [11] Fujisawa R, Mizuno M, Nodasaka Y, Kuboki Y. Attachment of Osteoblastic Cells to Hydroxyapatite by a Synthetic Peptide (Glu7-Pro-Arg-Gly-Asp-Thr) Containing Two Functional Sequences of Bone Sialoprotein. *Matrix Biol* 1997;16:21–8.
- [12] Addadi L, Weiner S. Interactions between acidic proteins and crystals: stereochemical requirements in biomineralization. *Proc Natl Acad Sci U S A* n.d.;82:4110–4.

- [13] Gorski JP. Acidic phosphoproteins from bone matrix: a structural rationalization of their role in biomineralization. *Calcif Tissue Int* n.d.;50:391–6.
- [14] Sodek J, Ganss B, McKee MD. Osteopontin. *Crit Rev Oral Biol Med* 2000;11:279–303.
- [15] Chien Y-C, Masica DL, Gray JJ, Nguyen S, Vali H, McKee MD. Modulation of calcium oxalate dihydrate growth by selective crystal-face binding of phosphorylated osteopontin and polyaspartate peptide showing occlusion by sectoral (compositional) zoning. *J Biol Chem* n.d.;284:23491–501.
- [16] Chien Y-C, Hincke MT, Vali H, McKee MD. Ultrastructural matrix-mineral relationships in avian eggshell, and effects of osteopontin on calcite growth in vitro. *J Struct Biol* n.d.;163:84–99.
- [17] Millán JL, Narisawa S, Lemire I, Loisel TP, Boileau G, Leonard P, et al. Enzyme Replacement Therapy for Murine Hypophosphatasia *. *J Bone Miner Res* 2008;23:777–87.
- [18] Segvich SJ, Smith HC, Kohn DH. The adsorption of preferential binding peptides to apatite-based materials. *Biomaterials* 2009;30:1287–98.
- [19] Kriplani U, Kay BK. Selecting peptides for use in nanoscale materials using phage-displayed combinatorial peptide libraries. *Curr Opin Biotechnol* n.d.;16:470–5.
- [20] Adey NB, Mataragnon AH, Rider JE, Carter JM, Kay BK. Characterization of phage that bind plastic from phage-displayed random peptide libraries. *Gene* n.d.;156:27–31.
- [21] Marks C, Marks JD. Phage libraries--a new route to clinically useful antibodies. *N Engl J Med* n.d.;335:730–3.
- [22] Ladner RC, Sato AK, Gorzelany J, de Souza M. Phage display-derived peptides as therapeutic alternatives to antibodies. *Drug Discov Today* n.d.;9:525–9.
- [23] Qin C, Baba O, Butler WT. Post-translational modifications of sibling proteins and their roles in osteogenesis and dentinogenesis. *Crit Rev Oral Biol Med* n.d.;15:126–36.
- [24] Segvich S, Biswas S, Becker U, Kohn DH. Identification of Peptides with Targeted Adhesion to Bone-Like Mineral via Phage Display and Computational Modeling. *Cells Tissues Organs* 2008;189:245–51.

- [25] Obenauer JC, Cantley LC, Yaffe MB. Scansite 2.0: Proteome-wide prediction of cell signaling interactions using short sequence motifs. *Nucleic Acids Res* n.d.;31:3635–41.
- [26] Gasteiger E, Hoogland C, Gattiker A, Duvaud S, Wilkins MR, Appel RD, et al. A. B. Protein Identification and Analysis Tools on the ExPASy Server. vol. 2005 SRC . n.d.
- [27] Wang D, Christensen K, Chawla K, Xiao G, Krebsbach PH, Franceschi RT. Isolation and characterization of MC3T3-E1 preosteoblast subclones with distinct in vitro and in vivo differentiation/mineralization potential. *J Bone Miner Res* 1999;14:893–903.
- [28] Denizot F, Lang R. Rapid colorimetric assay for cell growth and survival. Modifications to the tetrazolium dye procedure giving improved sensitivity and reliability. *J Immunol Methods* n.d.;89:271–7.
- [29] Masica DL, Gray JJ. Solution- and adsorbed-state structural ensembles predicted for the statherin-hydroxyapatite system. *Biophys J* n.d.;96:3082–91.
- [30] Goldberg HA, Warner KJ, Li MC, Hunter GK. Binding of bone sialoprotein, osteopontin and synthetic polypeptides to hydroxyapatite. *Connect Tissue Res* 2001;42:25–37.
- [31] Ryuichi F, Yoshinori K. Preferential adsorption of dentin and bone acidic proteins on the (100) face of hydroxyapatite crystals. *Biochim Biophys Acta BBA Gen Subj* 1991;1075 SRC :56–60.
- [32] Sudo H, Kodama HA, Amagai Y, Yamamoto S, Kasai S. In vitro differentiation and calcification in a new clonal osteogenic cell line derived from newborn mouse calvaria. *J Cell Biol* n.d.;96:191–8.
- [33] Makrodimitris K, Masica DL, Kim ET, Gray JJ. Structure prediction of protein-solid surface interactions reveals a molecular recognition motif of statherin for hydroxyapatite. *J Am Chem Soc* n.d.;129:13713–22.
- [34] Addison W, Masica D, Gray J, McKee MD. Phosphorylation-Dependent Inhibition of Mineralization by Osteopontin ASARM Peptides is Regulated by PHEX Cleavage. *J Bone Miner Res* 2009;25:695–705.
- [35] Goobes G, Goobes R, Schueler-Furman O, Baker D, Stayton PS, Drobny GP. Folding of the C-terminal bacterial binding domain in statherin upon adsorption onto hydroxyapatite crystals. *Proc Natl Acad Sci U S A* n.d.;103:16083–8.

- [36] Aizawa T, Koganesawa N, Kamakura A, Masaki K, Matsuura A, Nagadome H, et al. Adsorption of human lysozyme onto hydroxyapatite. Identification of its adsorbing site using site-directed mutagenesis. *FEBS Lett* n.d.;422:175–8.
- [37] Awonusi A, Morris MD, Tecklenburg MMJ. Carbonate assignment and calibration in the Raman spectrum of apatite. *Calcif Tissue Int* n.d.;81:46–52.
- [38] Astala R, Stott MJ. First Principles Investigation of Mineral Component of Bone: CO₃ Substitutions in Hydroxyapatite. *Chem Mater* 2005;17 SRC - :4125–33.
- [39] Gericke A, Qin C, Spevak L, Fujimoto Y, Butler WT, Sørensen ES, et al. Importance of phosphorylation for osteopontin regulation of biomineralization. *Calcif Tissue Int* 2005;77:45–54.
- [40] Hunter GK, Grohe B, Jeffrey S, O’Young J, Sørensen ES, Goldberg HA. Role of phosphate groups in inhibition of calcium oxalate crystal growth by osteopontin. *Cells Tissues Organs* 2009;189:44–50.

Chapter 3

Inhibition of osteoblast mineralization by phosphorylated phage-derived apatite-specific peptide²

3.1 Introduction

Biomaterials should be able to communicate with their microenvironment, to encourage attachment of specific populations of cells onto their surfaces, and eventually regenerate functional tissue. Surface modification of biomaterials with cell-specific biological factors can provide the signals required to initiate cell adhesion. One approach to controlling biomaterial surface properties is via functionalization with cell- and material-specific peptide sequences, which can serve as anchors between a specific cell population and a specific material chemistry. Short synthetic peptides (9-30 amino acids in length) are advantageous for this application since they can be designed to be non-immunogenic, as well as more specific than full length proteins (containing multifunctional domains). Further, short peptides are easier and less expensive to synthesize, and are less likely to change conformation since they are not as prone to forming secondary/tertiary structures [1].

² Published as Ramaswamy J, Nam HK, Ramaraju H, Hatch NE, Kohn DH.; Biomaterials 2015; 73: 120 - 130

Peptide functionalized apatite-based biomaterials are useful in bone tissue engineering as they mimic aspects of the organic/inorganic hybrid composition of bone (primarily comprised of organic collagen and non-collagenous proteins, and inorganic hydroxyapatite). Traditionally, peptide sequences for bone regeneration have been derived from known bone-binding motifs found in non-collagenous proteins, often containing chains of acidic aspartate and glutamate residues. For example, the peptide EEEEEEEPRGDT (E7PRGDT), derived from bone sialoprotein (BSP), consists of a poly-glutamic hydroxyapatite binding domain and the ubiquitous RGD cell binding domain, and mediates osteoblast attachment to hydroxyapatite and subsequent osteogenesis [2,3]. The fusion peptide N15-PGRGDS, comprising a hydroxyapatite binding sequence (N15) derived from statherin and the RGD cell binding sequence from osteopontin (OPN), facilitates dose-dependent attachment of cells to hydroxyapatite [4]. Modular peptides have also been designed that contain apatite binding sequences derived from osteocalcin (OCN) and growth factor sequences derived from bone morphogenetic protein 2 (BMP2) [5]. These peptides modulate cell binding to apatite, and peptide-coated implants stimulate greater bone formation and ingrowth compared to untreated controls in a sheep bone-implant gap model [6].

A novel way of discovering unique material-specific peptides is through the use of phage display, which involves panning bacteriophage libraries expressing $\sim 10^9$ sequences against a material of interest. Using this approach, along with computational modeling and ELISA, we identified the apatite-specific 12-mer peptide VTKHLNQISQSY (VTK) [7,8]. However, a disadvantage of phage libraries is the inability of bacteriophage to incorporate peptide post translational modifications, such as phosphorylation of serine,

threonine and tyrosine residues, which are particularly important in the regulation of biomineralization [9,10]. To overcome this drawback and further characterize the mineral-binding VTK sequence, we phosphorylated the serine residues on VTK (pVTK) and measured a 10-fold increase in adsorption to synthetic biomimetic apatite, and significantly higher binding affinity of pVTK compared to non-phosphorylated VTK [11].

Additionally, pVTK caused a dose dependent inhibition of mineralization in MC3T3 pre-osteoblastic cells, with minimal cytotoxic effects. Although VTK and pVTK bind to both synthetic and cell-secreted mineral, the relative contribution of peptide sequence and charge is different between the two forms of apatite. Phosphorylation and net charge were more important in peptide binding to synthetic mineral (scrambling the sequence had no effect on binding to biomimetic mineral), whereas peptide sequence and phosphorylation/charge were equally important in inhibiting biological mineralization (scrambling pVTK resulted in 30% less inhibition compared to pVTK) [11]. Understanding how the phosphorylated peptide interacts with mineral and/or cells to inhibit mineralization could enable the application of pVTK in the treatment of pathological mineralization.

Development of therapeutics against pathological calcification is dependent on advancing knowledge of mechanisms of mineralization. Briefly, mineralization is a tightly regulated process determined by the concentrations and properties (including net charge, charge distribution or number of acidic/phosphorylated amino acid residues) of extracellular matrix proteins and other promoter and inhibitor molecules. Inorganic extracellular pyrophosphate (PPi) is a natural inhibitor of mineralization (at micromolar

concentrations) and is formed as a by-product of several metabolic reactions. The concentration of extracellular P_{PPi} is regulated mainly by the action of tissue non-specific alkaline phosphatase (TNAP), ectonucleotide pyrophosphatase/ phosphodiesterase 1 (Enpp1) and the progressive ankylosis protein (Ank). Enpp1 and Ank help inhibit calcification by increasing the concentration of extracellular P_{PPi} – Enpp1 cleaves ATP to release P_{PPi} and Ank transports P_{PPi} from within to outside the cell [12,13]. TNAP decreases P_{PPi} levels by cleaving P_{PPi} to generate phosphate (Pi), thus promoting calcification [14,15]. The actions of TNAP, Enpp1 and Ank maintain the P_{PPi}/Pi ratio, which has a direct consequence on mineralization – high P_{PPi}/Pi ratios inhibit, while low P_{PPi}/Pi ratios promote mineralization. The presence of Enpp1, Ank, TNAP, as well as other osteogenic markers in pathologic mineral deposits [16,17], indicate similarities between physiological (bone) and pathological calcification mechanisms, providing new opportunities for development of therapeutics against pathological calcification.

In this study, we hypothesized that pVTK inhibits MC3T3 mineralization via alteration of the Enpp1-TNAP-Ank axis. We performed assays at the gene and protein-levels to test the effect of peptide treatment on mineralization, collagen deposition, Enpp1 and TNAP enzyme activity, and osteogenic differentiation in MC3T3 cells. The effect of peptide administration on mineralization at various stages of osteogenic differentiation, and the ability to inhibit progression of mineralization in cultures after the initiation of mineralization were also investigated.

3.2 Materials and Methods

3.2.1 Peptide synthesis

The following peptides were used: pVTK (VTKHLNQI(pS)Q(pS)Y; pS = phosphoserine), FITC-pVTK (FITC-VTKHLNQI(pS)Q(pS)Y) and FITC-E7-RGD (FITC-EEEEEEEPRGDT). Peptides were synthesized using Fmoc solid-phase chemistry according to standard peptide synthesis procedures and characterized as having >90 % purity by high-performance liquid chromatography (University of Michigan Proteomics & Peptide Synthesis Core). Phosphorylation at specific serine residues was achieved using preformed, protected phosphoserine amino acids. For experiments involving fluorescence, peptides were labelled on resin before cleavage using 5-(and-6)-carboxyfluorescein succinimidyl ester (Molecular Probes C-1311). The peptides were dissolved in ddH₂O and aliquots were frozen at -20°C until ready to use in experiments.

3.2.2 Cell culture and overview of experimental design

MC3T3-E1 (subclone 14) murine calvarial pre-osteoblasts were maintained in alpha minimum essential medium supplemented with 10% fetal bovine serum and 1% penicillin-streptomycin (growth medium) at 37°C and 5% CO₂ in a humidified incubator. For all experiments, cells were seeded at a density of 10,000 cells/cm² (48 well plates, Corning Costar) and allowed to attach overnight in growth medium. Cells were then differentiated with osteogenic medium (growth medium supplemented with 10mM β-glycerophosphate and 50μg/ml ascorbic acid) with or without 300μM pVTK peptide and cultured for up to 12 days. Media was replaced every 2 days. For analysis of calcium, media was collected every two days during the media change and frozen at -80°C until assayed.

To understand the effect of pVTK on differentiation and mineralization, gene expression of *Enpp1*, TNAP, Runx2, bone sialoprotein, osteocalcin, osteopontin, Ank and Pit-1 was measured at days 3, 7, 10 and 12. The expression of collagen I was also measured after 12 days of peptide treatment. Protein expression (Runx2, OPN) and enzyme activity (*Enpp1*, TNAP) were also measured to confirm the gene-level data. To further determine the inhibitory effects of the peptide at different stages of osteogenic differentiation and mineralization, cells were cultured for 12 days with pVTK added at days 1-6 only (corresponding to cell proliferation and matrix production) or days 6-12 only (corresponding to matrix maturation and mineralization), and compared to untreated controls and cells cultured with the peptide for the entire 12 days. To assess the effect of peptide on mineralizing cell layers, cells were cultured in osteogenic media only until mineralization started on day 10, after which pVTK was added and cells were cultured until day 14.

3.2.3 *Enpp1* and TNAP enzyme activity assays

Cell layers were washed with PBS and harvested in a 10mM Tris-HCl, 2mM PMSF, 0.2% Igepal solution. Samples were frozen at -80°C until assayed, at which time they were thawed, homogenized on ice and centrifuged at 12,600 rpm for 10 min at 4°C. Supernatants were used to assay for TNAP and *Enpp1* activities using substrates p-nitrophenyl phosphate (Sigma Aldrich) and thymidine 5' – monophosphate p-nitrophenyl ester sodium salt (Sigma Aldrich), respectively, and absorbance was measured at 405nm using a microplate reader. A standard curve was used to correlate absorbance units to enzyme concentration, and values were normalized to total protein content (obtained from BCA assays (Pierce) performed with cell lysate supernatants).

3.2.4 Detection and quantification of mineralization

von Kossa staining was used to visualize mineralization of cell layers. Briefly, cells were fixed in zinc buffered formalin for 30 min and rehydrated using a series of graduated ethanol-water mixes. Cells were then exposed to 5% silver nitrate for 30-60 min in bright light. Wells were washed, dried and imaged using a Canon dissecting microscope. Quantification of the area covered by mineral was performed using ImageJ software (NIH). To quantify inorganic calcium levels deposited in cell matrices, cell pellets (obtained from cell lysis and centrifugation described above) were demineralized in 0.6N HCl overnight and calcium content in the supernatants was determined colorimetrically using a Stanbio Total Calcium LiquiColor kit. Calcium content was quantified using a standard curve and normalized to total protein content (obtained from BCA assays (Pierce) performed with cell lysate supernatants). Calcium content in culture media was similarly determined.

3.2.5 Picrosirius Red collagen staining

Cell layers were washed with PBS and fixed in Bouin's fluid for 1h. After washing with water, cells were stained with Sirius Red dye for 1h on a shaker. A standard curve was created by pipetting known concentrations of calf skin collagen (Sigma Aldrich, dissolved in acetic acid) onto microtiter plates, followed by air drying and staining. To quantify the collagen content, wells were destained with 0.1N NaOH for 30 min, absorbance read at 550nm and the collagen content was determined from the standard curve.

3.2.6 Western Blots

Cell layers were harvested in lysis buffer containing 150mM NaCl, 50mM TrisCl, 1mM EDTA, 1% Triton, 1% sodium deoxycholate, 0.1% SDS and protein inhibitor cocktail (Cell Signaling) and frozen at -80°C. Samples were thawed, homogenized on ice and centrifuged at 12,600 rpm for 10 min at 4°C, and protein levels were quantified from the supernatants using the BCA assay (Pierce). 10ug or 25ug of protein (for osteopontin or Runx2 respectively) were mixed with Laemmli loading buffer, boiled and cooled, and separated using SDS-PAGE. Proteins were transferred onto PVDF membranes (Millipore) and blocked in 5% non-fat milk. Membranes were first probed with primary antibodies in 5% non-fat milk or bovine serum albumin and then with horse radish peroxidase (HRP)-conjugated secondary antibodies in 5% non-fat milk. Bands were visualized by chemiluminescence using SuperSignal West Pico substrate (Thermo Scientific). The following primary antibodies and dilutions were used: goat anti-osteopontin (AF808, R&D Systems) at 1:5000, mouse anti-Runx2 (D130-3, MBL International) at 1:500 and rabbit anti-GAPDH (14C10, Cell Signaling Technology) at 1:1000. The following HRP-conjugated secondary antibodies and dilutions were used: anti-goat (A8919, Sigma Aldrich) at 1:20000, anti-mouse (W402B, Promega) at 1:7500 and anti-rabbit (A0545 Sigma Aldrich) at 1:5000.

3.2.7 Quantitative Real Time PCR

Cells were washed with PBS, total RNA was extracted using TRIzol (Invitrogen) and cDNA was synthesized using Taqman cDNA synthesis kit (Applied Biosystems). Real Time PCR was performed using manufacturer protocols (Applied Biosystems) and mRNA levels measured using a standard curve. The following murine genes were

measured using Taqman primer/probes: *Enpp1* Enpp1 (Mm01193752_m1), *Alpl* TNAP (Mm00475834_m1), *Ibsp* BSP (Mm00492555_m1), *Bglap* OCN (Mm03413826_mH), *Ank* Ank (Mm00445050_m1), *Coll1a1* Col1 (Mm00801666_g1), *Runx2* Runx2 (Mm00501578_m1), *Slc20a1* Pit-1 (Mm00489378_m1) and normalized to the housekeeping gene *Hprt* Hprt1 (Mm01545399_m1). Q-RT-PCR studies were repeated at least twice for the majority of genes measured in this study, using different batches of cells and mRNA, and PCR was run on different days to confirm reproducibility of the findings. Data is presented as averages of triplicate or quadruplicate samples from one of the repeated experiments. Peptide effects are shown as fold changes relative to osteogenic treatment without peptide.

3.2.8 Cell internalization of peptide

MC3T3 cells were seeded at a density of 15,000 cells/cm² on tissue culture treated glass coverslips in 24 well plates. Peptides were dissolved in ddH₂O and diluted to 300μM in OPTIMEM (Invitrogen). After media was removed, adherent cells were incubated with 300μM of FITC-pVTK, FITC-E7-RGD, and OPTIMEM control media (no peptide) for 1hr. Cells were subsequently washed in PBS, fixed in 10% neutral buffered formalin, and mounted on glass slides in Vectashield containing the nuclear stain DAPI (Vector Labs). Nikon Ti-Eclipse laser scanning confocal microscope was used to gather images (n=20 per group, across 4 samples). Each fluorescent channel, DAPI and FITC, was imaged individually and merged using Image J.

3.2.9 Statistics

Data is represented as mean ± one standard deviation. SigmaPlot was used to perform all statistical analyses. Sample sizes of n=3-4 per group were used in all experiments. One

way ANOVA or ANOVA on Ranks with Student Neuman Keuls post hoc multiple comparisons tests were used to determine effect of treatment across time (i.e. within osteogenic media or osteogenic media containing peptide). t-tests or Mann Whitney Rank Sum tests were used to determine differences between treatments at specific time points or calcium concentrations. $p < 0.05$ denotes statistical significance.

3.3 Results

3.3.1 Effect of pVTK on mineralization and collagen matrix synthesis

Treatment of MC3T3 cultures with 300 μ M pVTK peptide for 12 days caused inhibition of mineralization compared to non-peptide treated controls cultured in osteogenic medium (Figure 3.1A). To determine if inhibition of mineralization was caused by peptide disruption of collagen matrix deposition, cell layers were stained with PicroSirius Red. pVTK treatment did not inhibit collagen production; rather treatment with peptide resulted in significantly higher amounts of collagen compared to non-peptide controls cultured in osteogenic medium ($p = 0.044$; Figure 3.1B). Similar trends of increased Coll gene expression were seen with peptide treatment compared to osteogenic medium controls (Figure 3.1C).

3.3.2 Effect of pVTK on different stages of cell differentiation

When peptide was added for the first 6 days of culture and then removed, cells were able to mineralize (Figure 3.2). When cells were cultured without peptide from days 1-6 and

peptide added only for the last 6 days of culture, mineralization was significantly inhibited ($p < 0.05$).

3.3.3 Effect of pVTK on Enpp1 and TNAP

Enpp1 enzyme activity and gene expression were significantly inhibited with 12 days of peptide treatment (Figure 3.3A, C; $p = 0.029$ vs. Osteo at both the enzyme and gene-levels). There was a trend of increased TNAP enzyme activity (Figure 3.3B), while gene expression of TNAP was significantly higher with peptide treatment (Figure 3.3D, $p < 0.001$ vs. Osteo).

3.3.4 Effect of pVTK on osteogenic gene expression

Runx2 and BSP levels were also significantly increased with 12 days of peptide treatment, whereas OPN, Pit-1 and Ank were significantly decreased compared to osteogenic medium controls (Figure 3.4, Osteo + Peptide vs. Osteo for Runx2: $p = 0.009$, BSP: $p = 0.004$, OPN and Ank: $p = 0.029$, Pit-1: $p = 0.003$). There was no significant effect of peptide treatment on OCN.

3.3.5 Effect of pVTK on time course of osteogenic expression

To determine the specific times/stages at which the peptide affected osteogenesis and mineralization, gene expression was studied at days 3, 7 and 10 of culture (Figure 3.5). Peptide treatment resulted in significantly lower Runx2 expression at day 3 ($p = 0.003$),

but significantly higher expression at day 10 ($p = 0.029$ vs. Osteo). There was no significant effect of peptide treatment on BSP and TNAP, but a trend of higher expression in peptide treated samples on day 10. Significantly lower expression of OPN and Pit-1, and a trend of lowered expression of Enpp1 and Ank were observed with 10 days of peptide treatment (Osteo + Peptide vs. Osteo for OPN: $p = 0.002$; Pit-1: $p = 0.039$). Similar trends were seen in Runx2 and OPN protein expression; peptide treatment increased Runx2 expression at day 10 and decreased OPN expression at days 10 and 12 (Figure 3.6). Overall, expression levels of genes involved in promoting mineralization (TNAP, Runx2, BSP, OCN) plateaued or declined by d10, whereas genes that inhibit mineralization (Enpp1, Ank, OPN) don't increase until d7-10. Moreover, this latter set of genes do not increase with pVTK. Peptide treatment resulted in a greater reduction (vs. Osteo) in the expression of the inhibitors OPN and Ank compared to the increases in expression of the promoters Runx2 and BSP (vs. Osteo).

3.3.6 Effect of pVTK addition to mineralized cell layers

From a clinical standpoint, it is important to be able to stop the progress of mineralization once it has started. To test if the phosphopeptide was able to stop mineralization after it had initiated, cells were cultured in osteogenic medium until they started to mineralize (by day 10), and peptide was then added for the remaining culture period until day 14. pVTK treatment significantly inhibited the progression of mineralization compared to untreated osteogenic media controls at day 12 (Figure 3.7B, ~ 50% lower, $p = 0.003$ vs. Osteo), and also prevented further increases in mineralization from day 12 to day 14 (Figure 3.7B, Osteo + Peptide: day 12 vs. day 14 not significant; day 14 Osteo vs. day 14

Osteo + Peptide $p = 0.006$). Enpp1 enzyme activity was also significantly decreased with peptide treatment at day 12 (Figure 3.7C, $p < 0.001$ vs. Osteo), while TNAP enzyme activity was significantly higher at day 14 (Figure 3.7D, $p = 0.029$ vs. Osteo), compared to osteogenic media controls.

3.3.7 Cell internalization of peptide

Both FITC-peptides pVTK and E7-RGD were internalized by MC3T3 cells after 1 hr of incubation (Figure 3.8A). However there was more observable translocation of pVTK within MC3T3 cells compared to E7-RGD. The FITC-pVTK signal was co-localized with the cytoskeletal structure of the cells. Additionally, vesicular associations surrounding many cellular nuclei (Figure 3.8B) were also observed, indicating additional intracellular processing of the translocated pVTK peptide. No FITC signal was detected in the no-peptide controls.

3.3.8 Effect of pVTK on calcium chelation

The pVTK peptide has two phosphorylated amino acids and a net negative charge, and hence it is possible for the peptide to sequester calcium in solution, preventing mineralization. To test if this is a mechanism of pVTK-mediated inhibition of mineralization, media was collected at 2 day intervals from cells cultured in the presence or absence of peptide and assayed for soluble calcium levels (Figure 3.9A). For untreated cells cultured in osteogenic media, calcium levels in the media remained constant over time until mineralization started (~ day 10), after which the calcium levels significantly

decreased (Osteo day 10, 12 vs. days 2, 4, 6 and 8, $p < 0.001$). In contrast, media calcium levels remained constant at all times in peptide treated groups and were significantly higher than in untreated osteogenic medium controls on days 10 ($p = 0.003$) and 12 ($p = 0.047$). To determine if mineralization could be achieved by adding supplemental calcium, 0.5 or 1mM additional calcium chloride was added to cells with or without the peptide, and calcium deposition levels measured from demineralized cell layers (Figure 3.9B). Supplementing calcium concentrations in the media resulted in increased calcium deposition in osteogenic medium controls (Osteo 0 mM vs. Osteo 0.5 mM $p = 0.016$, Osteo 0 mM vs. Osteo 1mM $p = 0.003$), but mineralization was still inhibited in peptide treated groups, suggesting that inhibition of mineralization is not due to sequestration of calcium.

3.4 Discussion

Deposition of minerals in soft tissues or the hypermineralization of bones occurs in a number of diseases, yet remains poorly understood. Coronary artery calcification is a strong predictor of cardiovascular mortality and coronary heart disease, which was responsible for approximately 1 in every 6 deaths in the United States in 2007 [18,19]. Craniosynostosis occurs at a frequency of 1 in 2500 live births and, if uncorrected, can cause craniofacial defects, retardation of brain development and death. However, despite the widespread prevalence and morbidity of these and other diseases resulting from pathological calcification, treatment options are often limited to surgery and/or drugs, and are characterized by inconsistent results, adverse side effects on other tissues, and a lack of clear knowledge on mechanisms. The data reported in this paper demonstrate the

ability of a novel peptide, pVTK, to inhibit cellular mineralization *in vitro* and a potential role for peptides in treating abnormal mineralization conditions *in vivo*.

Phosphorylation of serine residues is an important post-translational modification via which mineralization is controlled. For example, the acidic and phosphorylated protein osteopontin loses its mineral inhibition potential when dephosphorylated [20,21]. Similarly, only the phosphorylated form of the VTK peptide (pVTK) inhibits mineralization of MC3T3 cells [11]. Mineralization can be disrupted or delayed by insufficient or aberrant collagen matrix deposition. However, pVTK treatment significantly increased collagen deposition (Figure 3.1B) and Col1 gene expression (Figure 3.1C) in MC3T3 cells. Further, in cells treated with peptide at early stages of culture (days 1-6 only), matrix mineralization was rescued once normal osteogenic culture conditions resumed at later stages of culture (days 7-12) (Figure 3.2), suggesting the organic matrix, which serves as a template for mineralization, was not compromised by pVTK. Collectively, this data indicates that the inhibition of mineralization does not appear to be due to the peptide interfering with collagen deposition.

Clinically, pathological calcification is detected only after significant sized mineral deposits have formed, typically due to presentation of other related symptoms or because of limitations in detection resolution. However, once detected, it is important to be able to stop further progression of mineralization. To test the potential for inhibiting progression of mineralization, peptide was added to MC3T3 cultures that had already started to mineralize. pVTK significantly inhibited further mineralization (Figure 3.7B) compared to osteogenic medium controls. This data is crucial to the application of the peptide to

treat pathological calcification by stopping the progression of mineralization after it has started.

The pVTK peptide has two phosphorylated serine residues and consequently a net negative charge. These negatively charged groups can chelate positively charged calcium ions in solution and prevent mineralization. pVTK treatment resulted in significantly higher media calcium levels compared to non-treated controls starting at day 10, when the osteogenic controls started to mineralize and deplete the media of Ca (Figure 3.9A). However, further supplementation of the medium with CaCl_2 , which would compensate for any ion sequestration, did not result in mineralization (Figure 3.9B), indicating that peptide-calcium sequestration is likely not a mechanism of mineralization inhibition.

The presence of osteochondrogenic markers in pathological mineral deposits and the role of these markers in the progression of pathological calcification indicate similarities in mechanisms between normal bone mineralization and abnormal calcification of soft tissue. For instance, bovine aortic smooth muscle cells mineralize under calcifying conditions, accompanied by loss of smooth muscle specific markers and upregulation of osteogenic markers [16]. *Enpp1* knockout mice have widespread calcification of the coronary artery, aorta, kidneys and joints [17]. Hence, a better understanding of physiologic mineralization and the effect of anti-calcification drugs on mechanisms of mineralization will provide useful information in targeting and treating pathological calcification. In this paper, we studied the effect of pVTK peptide treatment on important regulators of osteoblast mineralization. *Enpp1* and TNAP directly affect the PPi/Pi balance and play critical roles in the regulation of mineralization, along with other osteogenic markers, including OPN and BSP. Peptide treatment inhibited *Enpp1* starting

between day 7 and 10 of culture and this inhibition was sustained until the end of culture (Figure 3.3, Figure 3.5). The primary role of *Enpp1* in osteoblasts is to break down nucleoside triphosphates, such as ATP, to generate PPi, a natural inhibitor of mineralization [12]. Significant decreases were also seen in the expression of OPN and Ank after 10 - 12 days of treatment (Fig. 4, 5). Ank is a membrane transporter protein, responsible for transferring PPi from inside the cell to the extracellular environment [13]. OPN is a negatively charged and highly phosphorylated non-collagenous protein that prevents apatite nucleation and growth [9,22]. Expression of TNAP, Runx2 and BSP was significantly higher with pVTK peptide treatment for 10 - 12 days, compared to non-peptide treated controls cultured in osteogenic medium (Figure 3.3 - Figure 3.5). TNAP promotes mineralization by cleaving PPi (or β -glycerophosphate *in vitro*) to generate Pi [14,15], whereas BSP acts as a nucleator of apatite [23]. Runx2 is an osteoblastic transcription factor and its overexpression enhances mineralization [24].

Collectively, our data show that *Enpp1*, OPN and Ank, which inhibit mineralization (directly or indirectly via PPi), were all significantly lowered with pVTK administration, whereas TNAP, Runx2 and BSP, which are positive regulators of mineralization, were all significantly increased with pVTK treatment. The gene expression data was also confirmed at the protein-level (Figure 3.3 and Figure 3.6). Since this scenario of gene and protein expression might be expected to increase mineralization, our findings of mineral inhibition suggest a possible compensatory mechanism where the peptide treated cells are attempting to rescue the reduced mineralization by downregulating the inhibitors and simultaneously upregulating the promoters (Figure 3.10).

pVTK peptide was internalized by MC3T3 cells and localized to cytoskeletal and vesicular structures (Figure 3.8). However, despite being taken up intracellularly within one hour of incubation, no effect of the peptide treatment was observed at early stages of culture, and most differences in gene and protein expression between peptide treated cells and controls occurred only after mineralization started (around day 10 of culture; Figure 3.2 - Figure 3.6). Additionally, pVTK binds strongly to both biomimetic synthetic mineral and MC3T3 secreted mineral, and computational modeling shows that the phosphoserine residues contribute most to apatite binding [11]. Hence, it is possible that the peptide inhibits mineralization via a combination of physico-chemical and cellular mechanisms, by binding strongly to the initially formed mineral nuclei and preventing further crystal growth. In response to this lack of mineralization and also by direct interaction with pVTK, the cells could be attempting to alter their gene expression towards a more pro-mineralization state (Figure 3.10). Further investigation is necessary to characterize peptide-mineral interactions as well as determine specific cellular compartments involved in peptide internalization.

Measurement of intracellular and extracellular concentrations of Pi and PPI will also provide a better understanding of the effect of peptide on mineralization. In addition to their roles in hydroxyapatite formation, Pi and PPI also act as signaling molecules and directly affect osteogenic gene expression. Pi increases OPN and Pit-1 expression in MC3T3 cells [25,26]; PPI increases TNAP, OPN and Ank expression and also has a concentration-dependent effect on Enpp1 expression in MC3T3 cells [27]. pVTK caused an increase in TNAP and a decrease in Enpp1 and Ank expression (Figure 3.3, Figure 3.4, Figure 3.5). Based on this expression profile, we would expect to find higher

concentrations of extracellular Pi and lowered concentration of extracellular PPI, indicating a shift towards a pro-mineralization state with pVTK administration. However, we also observed lowered expression of Pit-1, a sodium-dependent Pi transporter, which indicates potentially lowered intracellular concentrations of Pi. Pi needs to enter the cell to promote mineralization and influence changes in osteogenic gene expression [25,26,28]. Hence it is possible that lower intracellular Pi levels are also contributing to the lack of mineralization seen in response to peptide treatment, despite a gene expression profile favoring mineralization.

3.5 Conclusions

Phage-derived phosphopeptide pVTK was shown to inhibit mineralization and this inhibition was not due to disruption of collagen deposition or calcium chelation by negatively charged pVTK. The timing of peptide administration was important in inhibiting mineralization – pVTK treatment at later stages of differentiation (days 7-12) was more important in inhibiting mineralization. Further, this peptide could prevent progression of mineralization once it has started. pVTK also decreased the expression of Enpp1, Ank, OPN and Pit-1, while upregulating the expression of TNAP, BSP, OCN, Col1 and Runx2 in MC3T3 cells after 10 - 12 days of treatment. The ability of pVTK to inhibit mineralization can potentially be translated into therapeutics against pathological calcification seen in cardiovascular disease, osteoarthritis or craniosynostosis, or be used to prevent failure of biomaterials due to calcification, such as bioprosthetic heart valves.

Acknowledgements

I would like to thank my co-authors on this work, Hwa Kyung Nam, Harsha Ramaraju, Nan Hatch and David Kohn. I would also like to thank Dr. Henriette Remmer, Peptide Core for assistance with peptide synthesis and Taocong Jin, Molecular Biology Core for assistance with Q-RT-PCR. This work was supported by the National Institutes of Health: NIH DE 013380 and DE 015411 to DHK, JR, and HR, and OVPR grant to HKN and NEH. JR was the recipient of a Rackham Predoctoral Fellowship (2013-2014) from the University of Michigan Ann Arbor.

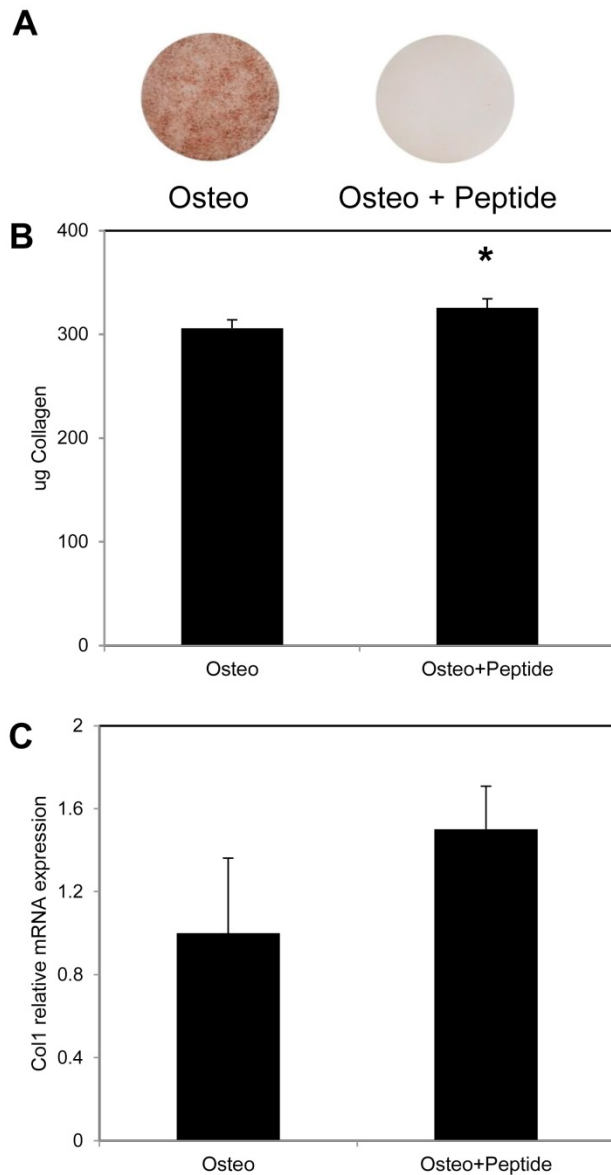


Figure 3.1: Effect of pVTK on mineralization and collagen deposition. MC3T3 cells were cultured for 12 days in osteogenic (Osteo) or osteogenic medium supplemented with 300 μ M pVTK peptide (Osteo + Peptide) for 12 days. (A) von Kossa staining showed that peptide treatment inhibited mineralization compared to osteogenic medium controls; (B) Collagen quantification by PicroSirius Red staining showed that peptide treatment resulted in significantly higher collagen deposition compared to osteogenic medium; (C) Q-RT-PCR for Collagen (Col1) showed a trend of increased gene expression with peptide treatment relative to osteogenic treatment (normalized to Hprt housekeeping gene; * $p < 0.05$, t-test).

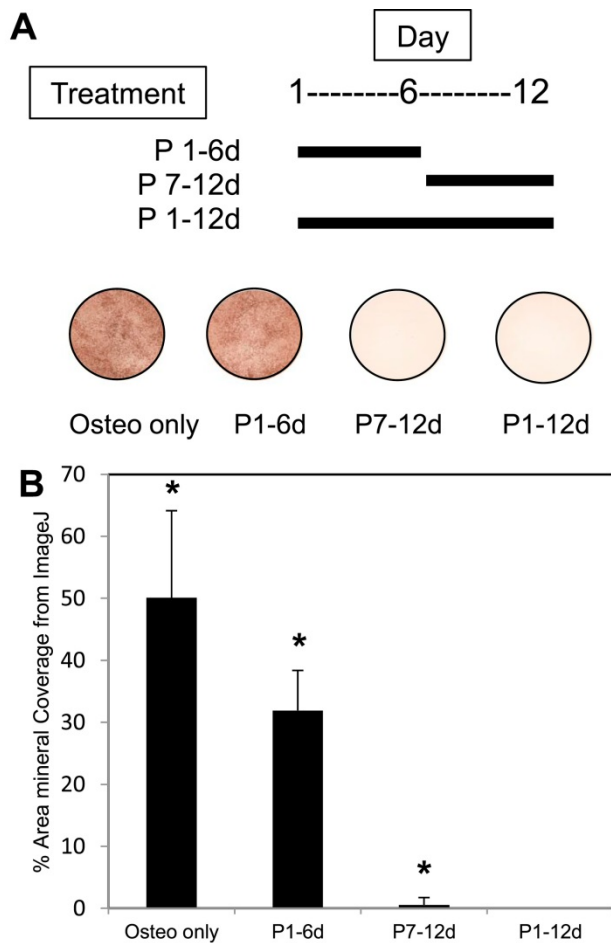


Figure 3.2: Effect of pVTK on different stages of cell culture. MC3T3 cells were cultured for 12 days in osteogenic medium (Osteo) or osteogenic medium supplemented with 300 μ M pVTK peptide (Osteo + Peptide). Peptide was added during early stage culture (days 1-6 only, P1-6d), late stage culture (days 7-12 only, P7-12d) or all 12 days of culture (P1-12d). von Kossa staining and ImageJ analysis of percent area mineralized showed the lack of mineralization in cells treated with pVTK on days 7-12 only and for cells treated for all 12 days. Cells treated with peptide only on days 1-6 were still able to mineralize once peptide was removed. (* $p < 0.05$ compared to all other groups, 1 way ANOVA on Ranks, Student-Newman-Keuls post hoc test).

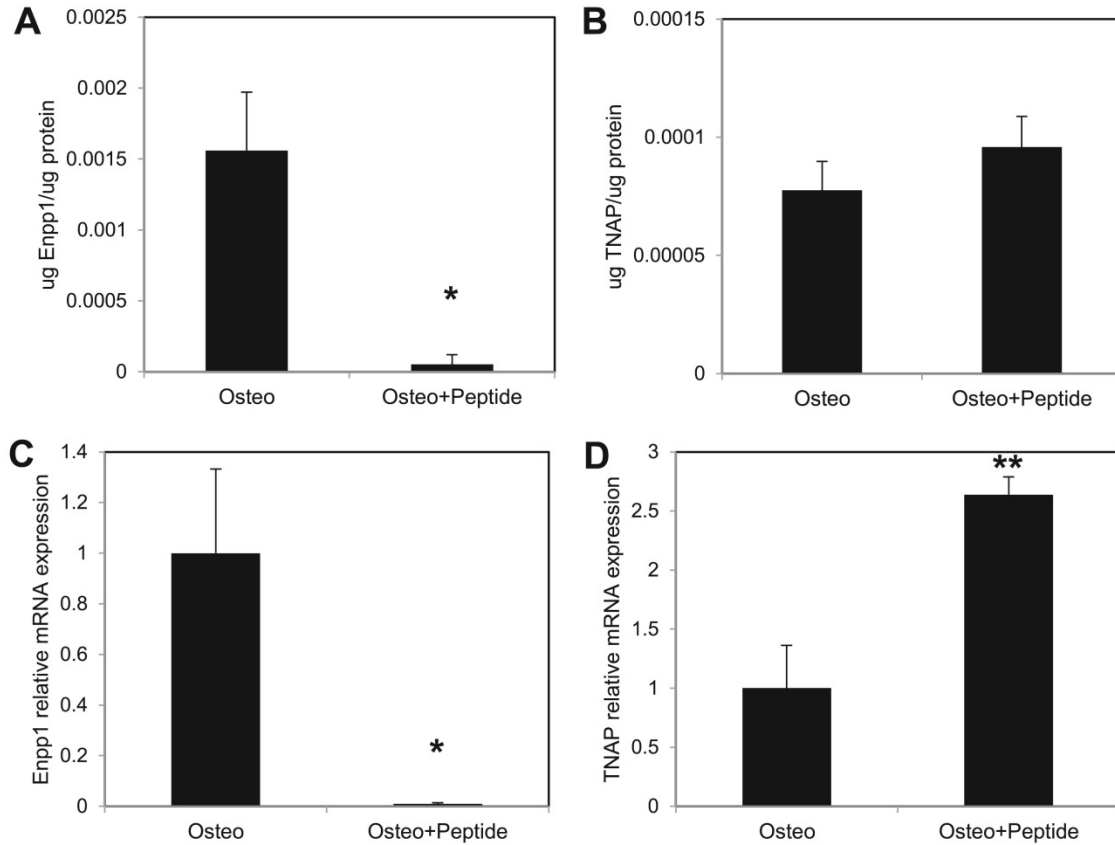


Figure 3.3: Effect of pVTK on Enpp1 and TNAP. MC3T3 cells were cultured in osteogenic medium (Osteo) or osteogenic medium supplemented with 300 μ M pVTK peptide (Osteo + Peptide) for 12 days. (A) Enpp1 enzyme activity was significantly inhibited with pVTK treatment compared to osteogenic medium; (B) TNAP enzyme activity was unaffected by pVTK treatment compared to osteogenic medium; (C) Q-RTPCR showed that gene expression of Enpp1 was significantly inhibited with peptide treatment relative to osteogenic medium; (D) Q-RTPCR showed that gene expression of TNAP was significantly increased with peptide treatment relative to osteogenic medium (normalized to Hprt; * $p < 0.05$, ** $p < 0.001$, t-test or Mann Whitney Rank Sum test).

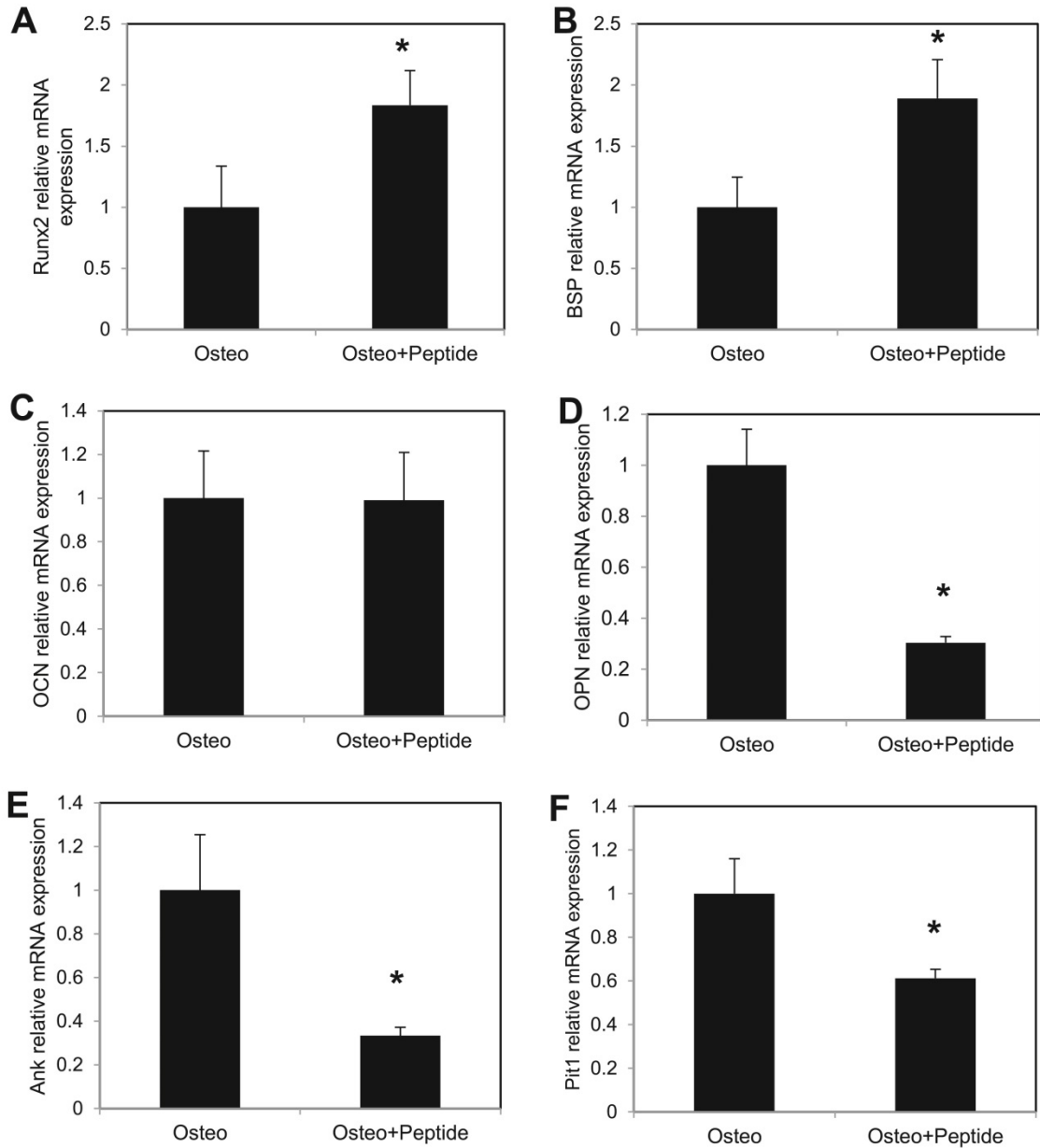


Figure 3.4: Effect of pVTK on osteogenic differentiation. MC3T3 cells were cultured in osteogenic medium (Osteo) or osteogenic medium supplemented with 300μM pVTK peptide (Osteo + Peptide) for 12 days. Q-RT-PCR was used to measure gene expression of (A) Runx2, (B) BSP, (C) OCN, (D) OPN, (E) Ank and (F) Pit-1, all normalized to Hprt. Runx2 and BSP expression were significantly higher with pVTK treatment relative to osteogenic medium. OPN, Ank and Pit-1 expression was significantly lowered with pVTK treatment relative to osteogenic medium (normalized to Hprt housekeeping gene; * $p < 0.05$, t-test or Mann Whitney Rank Sum test).

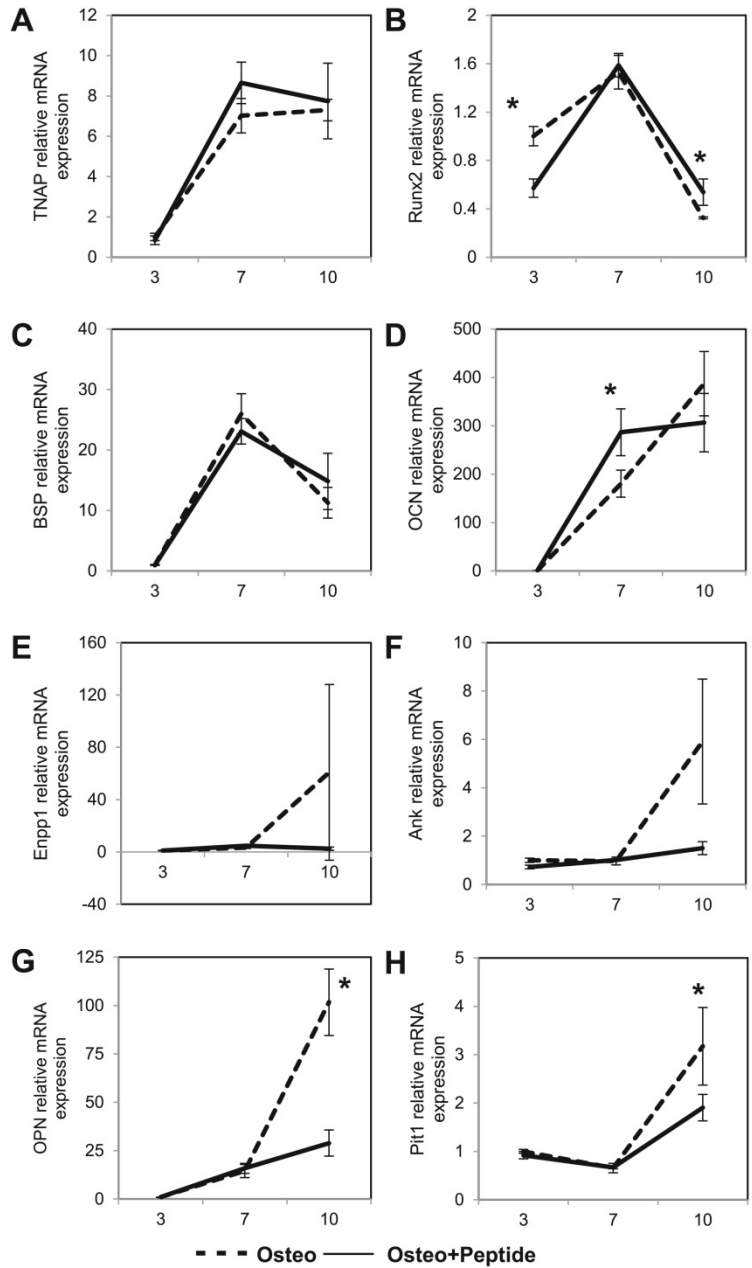


Figure 3.5: Effect of pVTK on time course of gene expression. MC3T3 cells were cultured in osteogenic medium (Osteo) or osteogenic medium supplemented with 300 μ M pVTK peptide (Osteo + Peptide) and gene expression of (A) TNAP, (B) Runx2, (C) BSP, (D) OCN, (E) Enpp1, (F) Ank, (G) OPN and (H) Pit-1, (all normalized to Hprt) was measured at days 3, 7 and 10 of culture via Q-RT-PCR. Peptide treatment resulted in significantly higher Runx2 expression at day 10 and a trend of higher expression of TNAP and BSP on day 10 relative to osteogenic medium. Significantly lowered expression of OPN and Pit-1, and a trend of lowered expression of Enpp1 and Ank were observed with 10 days of peptide treatment relative to osteogenic medium.

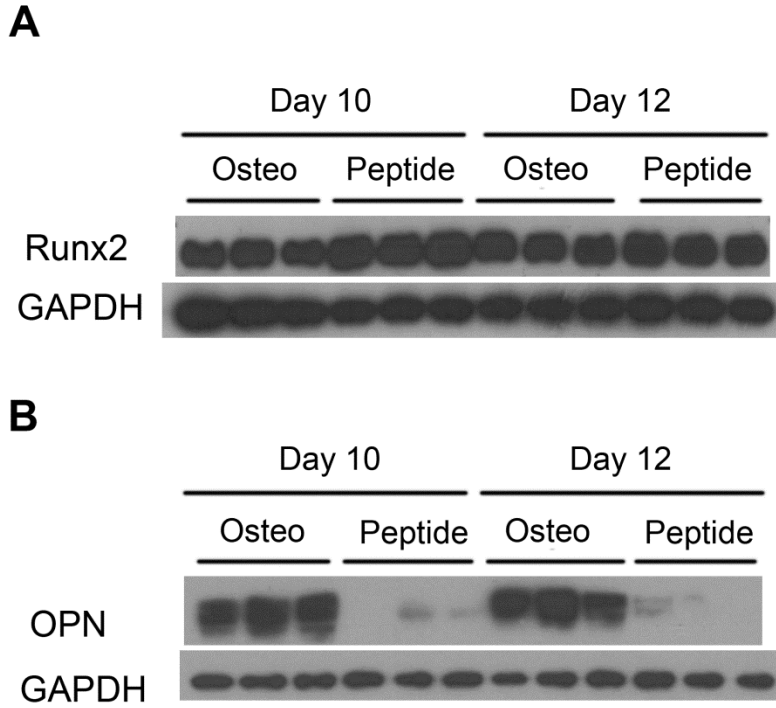


Figure 3.6: Effect of pVTK on Runx2 and OPN protein expression. MC3T3 cells were cultured in osteogenic medium (Osteo) or osteogenic medium supplemented with 300 μ M pVTK peptide (Osteo + Peptide) and protein expression of Runx2 and OPN was measured at days 10 and 12 of culture via Western Blotting. (A) Runx2 expression was increased at day 10 with peptide treatment vs. osteogenic medium; (B) OPN expression was decreased at days 10 and 12 with peptide treatment vs. osteogenic medium.

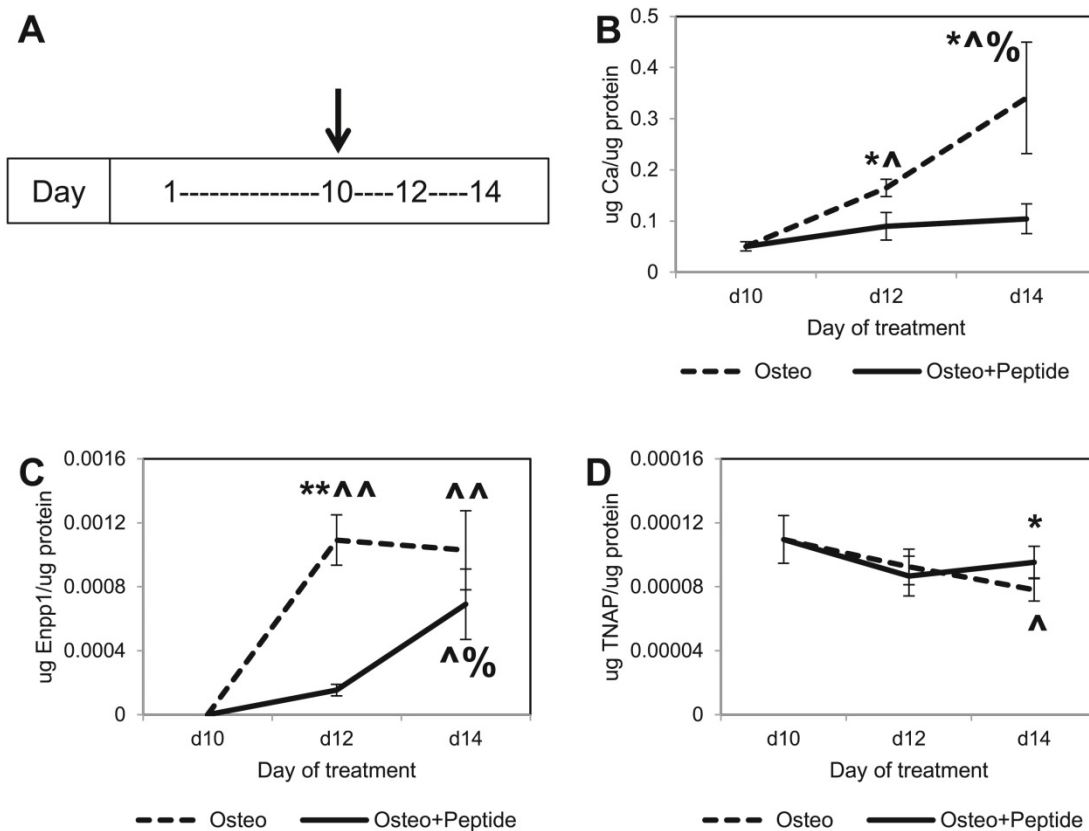


Figure 3.7: Effect of pVTK on progression of mineralization. MC3T3 cells were cultured for 10 days in osteogenic medium until mineralization started, at which time 300 μ M pVTK peptide was added (indicated by arrow on timeline (A)), and cultured for 4 additional days. (B) Calcium levels (quantified from demineralized matrices) and (C) Enpp1 enzyme activity were significantly reduced with peptide treatment (D) TNAP enzyme activity was significantly higher at day 14 with peptide treatment (* $p < 0.05$ Osteo vs. Osteo + Peptide at a specific day, t-test, ** $p < 0.001$ Osteo vs. Osteo + Peptide at a specific day, t-test, ^ $p < 0.05$ compared to day 10 within Osteo or Osteo + Peptide treatment group, ^^ $p < 0.001$ compared to day 10 within Osteo or Osteo + Peptide treatment group, % $p < 0.05$ compared to day 12 within Osteo or Osteo + Peptide treatment group, 1 way ANOVA or 1 way ANOVA on Ranks, Student-Newman-Keuls post hoc test).

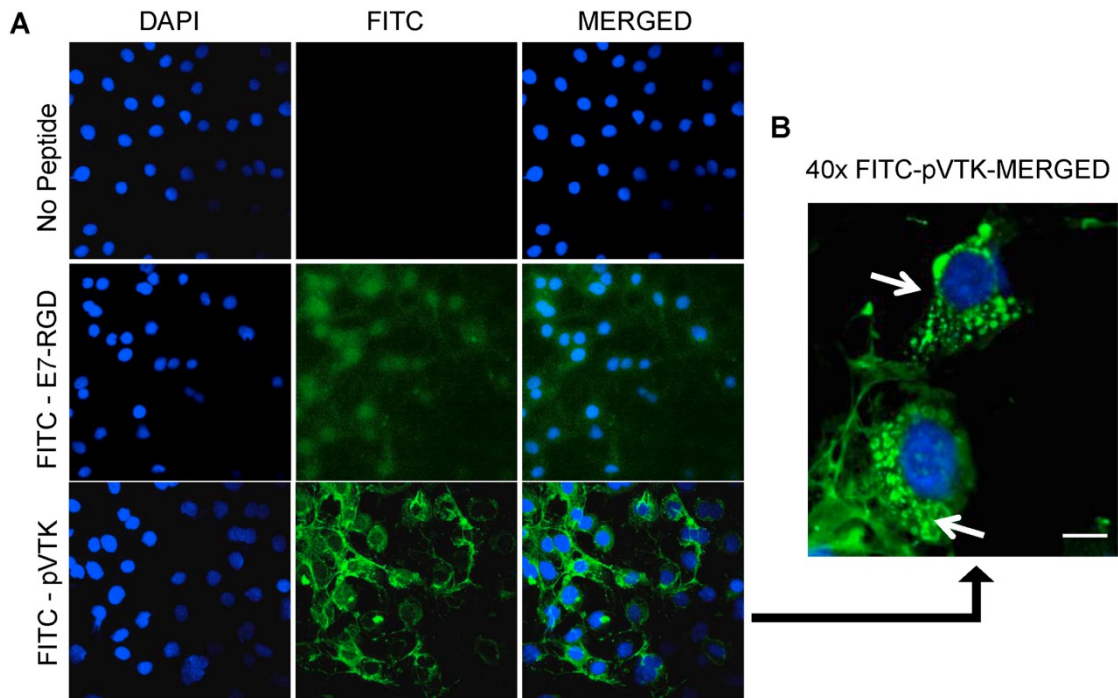


Figure 3.8: Internalization of FITC-tagged pVTK. MC3T3 cells were incubated with or without FITC-tagged pVTK and E7-RGD peptides for 1 hour and their nuclei were stained with DAPI. Representative images of samples were obtained using scanning confocal microscopy and merged using Image J. (A) FITC-pVTK was associated with the cytoskeleton; 20X magnification (B) Magnified image of peptide-treated cells showed vesicular intracellular association of FITC-pVTK; 40X magnification scale bar 100um.

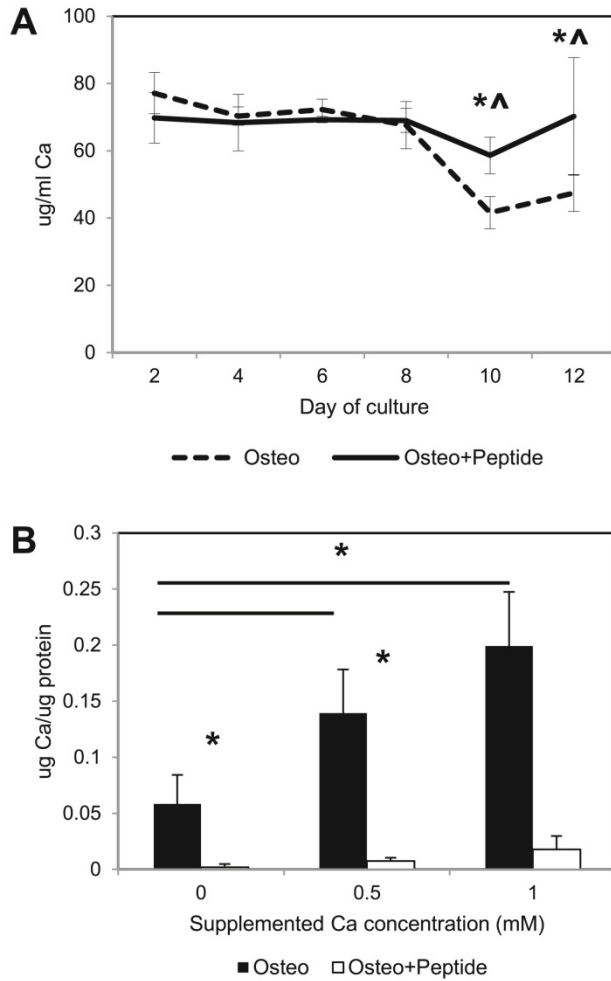


Figure 3.9: Effect of pVTK on media calcium chelation. (A) MC3T3 cells were cultured in osteogenic medium (Osteo) or osteogenic medium supplemented with 300 μ M pVTK peptide (Osteo + Peptide) for 12 days and the media was collected during media changes every 2 days. Quantification of calcium levels in the media showed pVTK treatment resulted in significantly higher calcium levels at days 10 and 12 compared to osteogenic medium controls. [* $p < 0.05$ Osteo vs. Osteo + Peptide at a specific day, t-test , ^ $p < 0.001$ days 2, 4, 6, 8 vs. days 10 and 12 for osteo, 1 way ANOVA on Ranks, Student-Newman-Keuls post hoc test]; (B) MC3T3 cells were cultured in osteogenic medium or osteogenic medium supplemented with 300 μ M pVTK peptide, with or without 0.5 or 1mM of supplemental CaCl_2 for 12 days. Calcium levels (quantified from demineralized cell matrices) were significantly increased with increasing supplemental media calcium levels in osteogenic controls, but no increase in Ca (no mineralization) was seen in peptide treated groups (* $p < 0.05$ compared to groups indicated by bar, or * $p < 0.05$ Osteo vs. Osteo + Peptide at a specific calcium concentration; 1 way ANOVA on Ranks, Student-Newman-Keuls post hoc test within Osteo or Osteo + Peptide treatment across calcium concentration, t-test between Osteo vs. Osteo + Peptide for a specific calcium concentration).

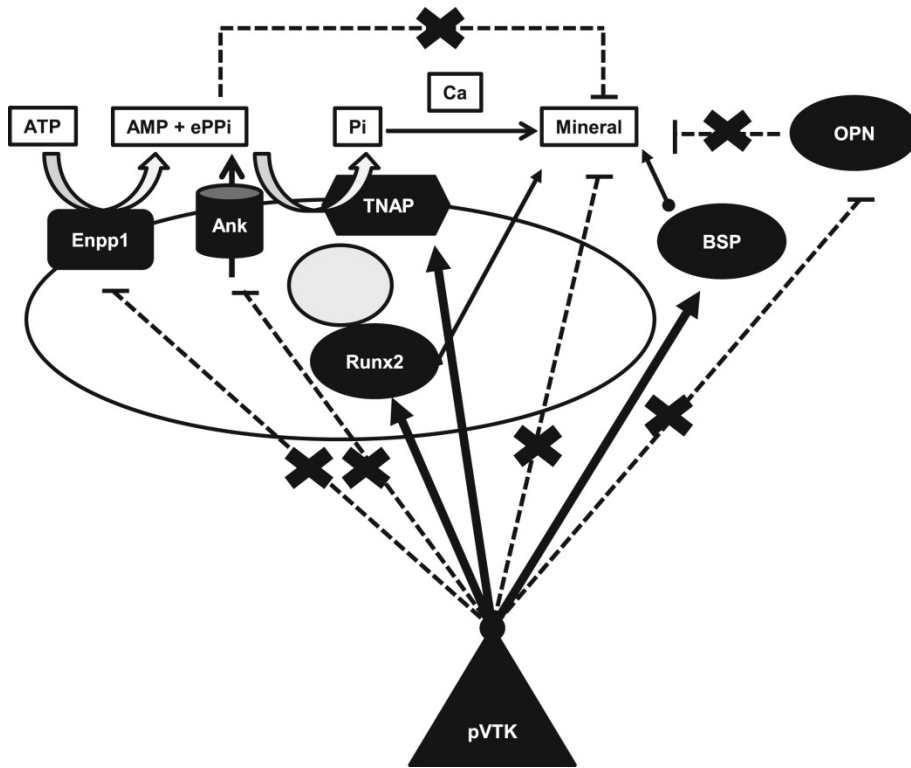


Figure 3.10: Schematic summarizing the effect of pVTK on osteoblastic markers. Enpp1, OPN and Ank inhibit mineralization (directly or indirectly via PPI) and were significantly lowered with pVTK administration (dashed lines), whereas TNAP, Runx2 and BSP are positive regulators of mineralization and were significantly increased with pVTK treatment (thick arrows). This data, in concert with the apatite-binding ability of the peptide and temporal sequence of gene expression, suggest a possible compensatory mechanism where the peptide treated cells are attempting to rescue the abnormal mineralization phenotype by downregulating the inhibitors and simultaneously upregulating the promoters.

3.6 References

- [1] Hersel U, Dahmen C, Kessler H. RGD modified polymers: biomaterials for stimulated cell adhesion and beyond. *Biomaterials* 2003;24:4385–415.
- [2] Fujisawa R, Wada Y, Nodasak Y, Kuboki Y. Acidic amino acid-rich sequences as binding sites of osteonectin to hydroxyapatite crystals. *Biochim Biophys Acta* 1996;1292:53–60.
- [3] Fujisawa R, Mizuno M, Nodasaka Y, Kuboki Y. Attachment of Osteoblastic Cells to Hydroxyapatite by a Synthetic Peptide (Glu7-Pro-Arg-Gly-Asp-Thr) Containing Two Functional Sequences of Bone Sialoprotein. *Matrix Biol* 1997;16:21–8.
- [4] Gilbert M, Shaw WJ, Long JR, Nelson K, Drobny GP, Giachelli CM, et al. Chimeric peptides of statherin and osteopontin that bind hydroxyapatite and mediate cell adhesion. *J Biol Chem* 2000;275:16213–8.
- [5] Lee JS, Lee JS, Murphy WL. Modular peptides promote human mesenchymal stem cell differentiation on biomaterial surfaces. *Acta Biomater* 2010;6:21–8.
- [6] Lu Y, Lee JS, Nemke B, Graf BK, Royalty K, Illgen R, et al. Coating with a modular bone morphogenetic peptide promotes healing of a bone-implant gap in an ovine model. *PLoS One* 2012;7:e50378.
- [7] Segvich S, Biswas S, Becker U, Kohn DH. Identification of Peptides with Targeted Adhesion to Bone-Like Mineral via Phage Display and Computational Modeling. *Cells Tissues Organs* 2008;189:245–51.
- [8] Segvich SJ, Smith HC, Kohn DH. The adsorption of preferential binding peptides to apatite-based materials. *Biomaterials* 2009;30:1287–98.
- [9] Goldberg HA, Hunter GK. The Inhibitory Activity of Osteopontin on Hydroxyapatite Formation In Vitro. *Ann N Y Acad Sci* 1995;760:305–8.
- [10] Addison W, Masica D, Gray J, McKee MD. Phosphorylation-Dependent Inhibition of Mineralization by Osteopontin ASARM Peptides is Regulated by PHEX Cleavage. *J Bone Miner Res* 2009;25:695–705.
- [11] Addison WN, Miller SJ, Ramaswamy J, Mansouri A, Kohn DH, McKee MD. Phosphorylation-dependent mineral-type specificity for apatite-binding peptide sequences. *Biomaterials* 2010;31:9422–30.
- [12] Terkeltaub R, Rosenbach M, Fong F, Goding J. Causal link between nucleotide pyrophosphohydrolase overactivity and increased intracellular inorganic pyrophosphate generation demonstrated by transfection of cultured fibroblasts and

- osteoblasts with plasma cell membrane glycoprotein-1. *Arthritis Rheum* 1994;37:934–41.
- [13] Ho AM. Role of the Mouse ank Gene in Control of Tissue Calcification and Arthritis. *Science* (80-) 2000;289:265–70.
- [14] Moss DW, Eaton RH, Smith JK, Whitby LG. Association of Inorganic-Pyrophosphatase Activity with Human Alkaline Phosphatase Preparations. *Biochem J* 1967;102:53–7.
- [15] Hessle L, Johnson KA, Anderson HC, Narisawa S, Sali A, Goding JW. Tissue-nonspecific alkaline phosphatase and plasma cell membrane glycoprotein-1 are central antagonistic regulators of bone mineralization. *Proc Natl Acad Sci* 2002;99:9445–9.
- [16] Steitz SA, Speer MY, Curinga G, Yang H-Y, Haynes P, Aebersold R, et al. Smooth Muscle Cell Phenotypic Transition Associated With Calcification: Upregulation of Cbfa1 and Downregulation of Smooth Muscle Lineage Markers. *Circ Res* 2001;89:1147–54.
- [17] Mackenzie NCW, Zhu D, Milne EM, van 't Hof R, Martin A, Quarles DL, et al. Altered Bone Development and an Increase in FGF-23 Expression in *Enpp1* Mice. *PLoS One* 2012;7:e32177.
- [18] Vliegenthart R, Oudkerk M, Hofman A, Oei H-HS, van Dijck W, van Rooij FJ a, et al. Coronary calcification improves cardiovascular risk prediction in the elderly. *Circulation* 2005;112:572–7.
- [19] Roger VL, Go AS, Lloyd-Jones DM, Adams RJ, Berry JD, Brown TM, et al. Heart disease and stroke statistics--2011 update: a report from the American Heart Association. *Circulation* 2011;123:e18–209.
- [20] Gericke A, Qin C, Spevak L, Fujimoto Y, Butler WT, Sørensen ES, et al. Importance of phosphorylation for osteopontin regulation of biomineralization. *Calcif Tissue Int* 2005;77:45–54.
- [21] Jono S. Phosphorylation of Osteopontin Is Required for Inhibition of Vascular Smooth Muscle Cell Calcification. *J Biol Chem* 2000;275:20197–203.
- [22] Boskey a L, Maresca M, Ullrich W, Doty SB, Butler WT, Prince CW. Osteopontin-hydroxyapatite interactions in vitro: inhibition of hydroxyapatite formation and growth in a gelatin-gel. *Bone Miner* 1993;22:147–59.
- [23] Hunter GK, Goldberg HA. Nucleation of hydroxyapatite by bone sialoprotein. *Proc Natl Acad Sci* 1993;90:8562–5.

- [24] Byers BA, García AJ. Exogenous Runx2 expression enhances in vitro osteoblastic differentiation and mineralization in primary bone marrow stromal cells. *Tissue Eng* 2004;10:1623–32.
- [25] Beck GR, Zerler B, Moran E. Phosphate is a specific signal for induction of osteopontin gene expression. *Proc Natl Acad Sci U S A* 2000;97:8352–7.
- [26] Beck G. Inorganic phosphate regulates multiple genes during osteoblast differentiation, including Nrf2. *Exp Cell Res* 2003;288:288–300.
- [27] Addison WN, Azari F, Sørensen ES, Kaartinen MT, McKee MD. Pyrophosphate inhibits mineralization of osteoblast cultures by binding to mineral, up-regulating osteopontin, and inhibiting alkaline phosphatase activity. *J Biol Chem* 2007;282:15872–83.
- [28] Beck GR. Inorganic phosphate as a signaling molecule in osteoblast differentiation. *J Cell Biochem* 2003;90:234–43.

Chapter 4

Evaluation of animal models of pathological calcification

Several mouse models of pathological calcification were tested to identify a suitable model to assess efficacy of peptide treatment. A brief discussion of animal models currently available to study each condition is provided, followed by specific models that were tested.

4.1 Vascular calcification

Calcification of cardiovascular tissues is seen in coronary heart disease, diabetes and chronic kidney disease. Stiffening of blood vessels and heart valves increases blood pressure, requires more cardiac work, and increases the potential for heart failure. The development of animal models of cardiovascular calcification has advanced our understanding of the underlying mechanisms. Mutant mice in which the genes encoding for *Enpp1* and *Ank* have been knocked out undergo vessel calcification due to lowered extracellular P_{PPi} levels [1,2]. Matrix Gla Protein (MGP) knockout mice also possess highly calcified arteries and valves and die at the age of 2 months from aortic rupture [3]. Mice deficient in osteoprotegerin (OPG) develop mineralized arteries, but to lesser extents than MGP knockout mice [4]. It is also possible to induce vessel calcification by

using diets high in fat, cholesterol or calcium/phosphate, or using stimulants such as nicotine/vitamin D, adenine, warfarin and calcitriol.

In a first set of experiments, an *Enpp1* knockout mouse model (in collaboration with Dr. Nan Hatch, University of Michigan and Dr. Jose Millan, Sanford Burnham Institute) was characterized for the presence of a vascular calcification phenotype *in vitro* and *in vivo*.

4.1.1 Materials and methods

4.1.1.1 Animals

All animal procedures were approved by the University Committee on Use and Care of Animals (UCUCA) at the University of Michigan. *Enpp1*^{+/-} heterozygous mice were bred to generate homozygous knockout *Enpp1*^{-/-} and wild type mice. Genotypes were determined using tail or ear biopsy samples.

4.1.1.2 Isolation of primary vascular smooth muscle cells (VSMCs)

Primary VSMCs were harvested from the aortas of 6-7 and 11-12 week old *Enpp1* knockouts using enzymatic digestions. CO₂ was used to sacrifice the animals and aortas were dissected from the thoracic region to diaphragmatic insertion and placed in dishes containing sterile HBSS with 1% antibiotic-antimycotic solution. The adventitia was gently removed using a cotton swab, the vessels were cut open longitudinally and the endothelium and blood clots were gently scraped off using a cotton swab. The vessels from 6-8 animals were then cut into 3-5mm pieces and digested with collagenase type II for 20 min at 37°C, and then completely digested in collagenase type II/elastase type III

solution for 45 min – 1h at 37°C. The cells were centrifuged at 1000rpm for 5 min, supernatant discarded and cells were plated in a T-25 flask in DMEM supplemented with 20% FBS and 1% antibiotic-antimycotic. Primary VSMCs were characterized using immunocytochemistry for positive staining with mouse anti-human α -smooth muscle actin and negative staining with rabbit anti-human von Willebrand factor, an endothelial cell marker. 100% of harvested cells stained positively for VSMC-specific markers and no endothelial cell contamination was observed (data not shown).

4.1.1.3 VSMC mineralization

Primary VSMCs were cultured in DMEM or modified alpha-MEM supplemented with 20% FBS and 1% antibiotic-antimycotic (growth media) at 37°C in a humidified atmosphere containing 5% CO₂. A7r5 cells (rat VSMC line) and MOVAS cells (mouse VSMC line) were cultured in DMEM and modified alpha-MEM, respectively, supplemented with 10% FBS and 1% penicillin/streptomycin (growth media) under the same conditions as primary cells. For mineralization assays, cells were seeded in 24-well plates at a density of 20,000 - 30,000 cells/cm² and allowed to attach for 24h. Growth media was then supplemented with either 10mM β -glycerophosphate/50 μ g/ml ascorbic acid or 2mM inorganic phosphate (4:1 ratio of Na₂HPO₄:NaH₂PO₄) and cells were cultured for up to 4 weeks with media changes every other day. To assess mineralization, cultures were fixed, stained with 5% silver nitrate solution (von Kossa staining) or Alizarin Red and imaged using a dissecting microscope.

4.1.1.4 Histology

Aortas were harvested from two 23 week old Enpp1 knockout mice and blood was flushed from the lumens. Tissues were rinsed with PBS, fixed in 10% neutral buffered formalin for 24 hours and transferred to 70% ethanol for storage. 5µm sections were stained with von Kossa (counterstained with fast nuclear red) or Alizarin Red to observe vessel calcification.

4.1.2 Results

Aortic calcification has been reported in 3 – 5 month old Enpp1 knockout mice and in vascular smooth muscle cells (VSMCs) isolated from these mice [1,2]. Mice with an aortic calcification phenotype had a mixed genetic background (C57BL6/Sv 129). The mice used in the current experiment had been backcrossed until they were on a pure C57BL6 background. No vessel calcification was seen through von Kossa staining (Figure 4.1). Only a few scattered spots of positive staining were observed with Alizarin red (Figure 4.2). VSMCs isolated from the aortas of Enpp1 knockouts also did not mineralize when cultured in osteogenic medium (not shown). Hence, the Enpp1 knockout model was unsuitable as it failed to develop pathological vessel calcification. It was hypothesized that this difference in phenotype from published reports arose from differences in genetic background – aortic calcification occurs when the mice are maintained on a mixed genetic background, but this phenotype is possibly lost or lower in severity when mice are bred onto a pure C57BL6 background. Differences in genetic background among in-bred mouse strains fed an atherogenic diet cause variations in the

degree and frequency of arterial wall calcification [5]. Genetic background also plays a role in skeletal mineralization, and affects bone shape, density, microstructure and mechanical properties [6–9]. However, bone phenotype of *Enpp1* knockouts bred on a C57BL6 background was unchanged compared to knockouts bred on a mixed background (unpublished observations Hatch lab, not shown). Thus, although we are aware of the effect of genetic background on phenotype, we did not suspect the differences to have an effect on vascular mineralization.

VSMCs derived from wild type mice or immortalized VSMC cell lines also failed to mineralize in osteogenic medium containing β -glycerophosphate as a phosphate source (Table 4.1). Some mineralization was observed when Pi was used as a phosphate source to mineralize VSMCs (Figure 4.3). For our experiments, we required VSMCs to mineralize using β -glycerophosphate as a phosphate source, as we intended to test the effect of peptide on tissue non-specific alkaline phosphatase (TNAP) which cleaves β -glycerophosphate for mineralization (while the use of Pi does not involve TNAP activity for mineralization). Hence, the effect of peptide treatment could not be tested using *Enpp1* knockout cardiovascular calcification experimental models.

4.2 Heterotopic ossification in fibrodysplasia ossificans progressiva

In a percutaneous induction model of fibrodysplasia ossificans progressiva (FOP), a Matrigel carrier mixed with rhBMP4 is injected into the abdominal musculature of mice, inducing HO formation within 2 weeks of implantation [10]. A transgenic mouse model of BMP4 overexpression (under the neuron-specific enolase promoter) exhibits

progressive HO formation characteristic of FOP, eventually leading to immobilization [11]. A transgenic mouse model of FOP has been created, where the mice develop HO in their joints due to a mesodermal tissue-specific mutation resulting in constitutively active BMP signaling [12].

For our experiments, an inducible transgenic model of FOP was used (in collaboration with Dr. Yuji Mishina, University of Michigan), where mice carrying a mutation in the gene encoding BMP receptor 1 developed site-specific HO in their hind limb musculature [13]. Affected muscles were characterized by inflammatory cell infiltration and edema. Progressive loss of mobility and impaired range of motion were observed in hip, knee and ankle joints. HO formation was initiated around the tibia and fibula, eventually fusing with the pelvis and femur, rendering hip, knee and ankle joints immobile.

4.2.1 Materials and methods

4.2.1.1 Animals

All animal procedures were approved by the University Committee on Use and Care of Animals (UCUCA) at the University of Michigan. The development of transgenic mice carrying the Cre-inducible mutation ALK^{Q207D} has been described [14]. HO was induced in the hind limbs of 9-10 day old transgenic mice by retro-popliteal injections of adenovirus expressing Cre (0.3×10^9 or 0.7×10^9 plaque forming units) and cardiotoxin, an inflammatory toxin that induces muscle degeneration [13].

4.2.1.2 Treatment and semi-quantitative analysis of HO formed

Induced mice were treated with 10 μ l of PBS or 3mM pVTK peptide in one or both legs, or left untreated for 10 days (19-20 days of age). Range of motion (ROM) scoring was performed by scruffing mice and scoring the angle between the ankle and tibia on a scale of 0-3 (Figure 4.4). A score of 0 indicated an angle of less than 20 $^{\circ}$ (normal) while a score of 3 indicated an abnormal angle of greater than 135 $^{\circ}$, caused by maximum HO formation. Mice were then sacrificed by CO₂ overdose and radiographed with a Faxitron machine (90s exposure, 35kV, 3X magnification). The amount of HO visually observed on the X-rays was scored on a scale of 0-3, with 0 indicating no HO formation and 3 indicating maximum HO formation among all animals compared (Figure 4.4). Legs were then dissected out from the hip, fixed in 10% neutral buffered formalin and transferred to 70% ethanol for storage.

4.2.1.3 Micro-computed tomography

Pairs of legs were embedded in 1% agarose, placed in a 34 mm diameter tube and scanned using a microCT system (μ CT100 Scanco Medical, Bassersdorf, Switzerland). Scan settings were: voxel size 18 μ m, 70 kVp, 114 μ A, 0.5 mm AL filter, and integration time 500 ms. Three dimensional rendering of scanned legs were used to visualize ectopic HO formation.

4.2.2 Results

Since the phenotype of FOP progression and severity had been documented [13], the animal model was not characterized further. The effect of pVTK delivery on inhibition of HO was tested. For the first experiment, induced mice (n=11) received PBS and peptide in the left and right legs respectively. Four out of 11 mice did not show any differences in their range of motion in either leg (score of 0), and the remaining 7 mice mostly scored between 0 and 1 (Table 4.2). Median and total ROM scores were higher in right legs compared to left legs. Scoring of the X-ray images also showed higher formation of HO in the right legs compared to left legs, with μ CT images following the same trend (Figure 4.5).

To determine if increased HO formation in right legs was truly an effect of treatment, a second experiment was conducted where only left legs were treated with PBS (n=7) or peptide (n=8), and right legs left untreated. Similar trends were observed as in the first experiment – ROM and X-ray scores were higher in right legs compared to left legs (Table 4.3) and μ CT images also reflected this trend (Figure 4.6). Four more experiments were conducted (data not shown), testing various combinations of treatments/no treatment in one or both legs as well as different techniques of adenovirus HO induction (total of 6 experiments and 60 mice). In the majority of experiments, higher ROM and X-ray scores were seen in right legs vs. left legs, irrespective of treatment. Additionally, a high variability in HO formation was observed both within and across experiments, despite being induced with the same amount of virus at the same time. As a result, this mouse model of FOP was considered unsuitable to test effects of peptide treatment.

4.3 Craniosynostosis

Mouse models serve as excellent systems to understand craniosynostosis in humans, for the following reasons: a) analogous sets of cranial sutures are found between humans and mice differing only slightly in nomenclature (metopic suture in humans is referred to as interfrontal or frontal suture in mice, all other sutures are named similarly), b) fusion of only the posterior frontal suture in mice with all other sutures remaining patent provides the opportunity to study mechanisms underlying suture patency and fusion within the same model, c) mutations found in syndromic craniosynostosis patients can be replicated in murine models, providing invaluable information on the effects of gain or loss of function of various signaling molecules on craniofacial development. Additionally, the calvarial model is attractive for testing the efficacy of peptide treatment *in vivo* as the skull experiences minimal mechanical load (compared to load bearing bones) and does not involve inflammatory cell infiltration (seen in some models of vascular calcification as well as heterotopic ossification), which could complicate the interpretation of treatment effects.

Mice carrying C342Y and S252W mutations in FGFR2 mimic aspects of Crouzon and Apert syndrome respectively, characterized by fusion of the coronal suture and other craniofacial abnormalities [15–17]. Mutations in FGFR1 simulate conditions seen in Pfeiffer syndrome patients, and mutant mice exhibit fusion of frontal, coronal and sagittal sutures [18]. Mutations causing constitutively active BMP signaling in cranial neural crest cells result in fusion of the anterior frontal (AF) suture [19]. TNAP knockout models of hypophosphatasia develop partially fused coronal sutures by three weeks after birth [20].

For our experiments, three different models of craniosynostosis were characterized (2 Crouzon-FGFR2 mutations and 1 BMP mutation) in collaboration with Dr. Nan Hatch and Dr. Yuji Mishina (University of Michigan). Methods and results are presented below for Crouzon mice experiments. The BMP animal model data is presented in Chapter 5. Dr. Hatch has developed two mouse models of craniosynostosis on different genetic backgrounds – BALB/c and C57BL6. Both models carry mutations in FGFR2 and mimic the Crouzon syndrome of craniosynostosis, characterized by fusion of the coronal suture, bulging wide-set eyes and maxillary hypoplasia in humans [21]. The BALB/c model shares features with the less severe and more common form of Crouzon syndrome [16].

4.3.1 Materials and methods

4.3.1.1 Animals

All animal procedures were approved by the University Committee on Use and Care of Animals (UCUCA) at the University of Michigan. FGFR2-C342Y transgenic mice were back-crossed onto BALB/c or C57BL6 genetic backgrounds for at least eight generations before breeding for experimental use. Heterozygous transgenic and wild type mice genotypes were determined using tail or ear biopsy samples [16].

4.3.1.2 *Ex vivo* calvarial organ culture

1-2 day old mice pups were sacrificed by decapitation and skulls dissected out, cleared of soft tissue and trimmed to include only the calvaria. Tissues were rinsed in PBS and alpha-MEM before being placed in 12-well dishes. Calvaria were cultured in alpha MEM

supplemented with non-essential amino acids, gentamicin, insulin-transferrin-selenite, sodium phosphate and ascorbic acid for up to two weeks (media change every 3 days).

4.3.1.3 Alizarin Red whole skull staining

Freshly isolated calvaria or cultured samples were fixed in 100% ethanol and stained with 10ug/ml Alizarin Red S for 1.5 hours on a shaker. Tissues were rinsed with PBS, stored in 70% ethanol and imaged using a dissecting microscope.

4.3.1.4 Histology

Fixed calvaria were dehydrated using a series of alcohol and xylene washes and embedded in methyl methacrylate. Plastic blocks were trimmed parallel to the sagittal suture to within 1-2mm from the sagittal suture and polished with 320 grit paper. 10 μ m sections were prepared using a microtome equipped with a tungsten carbide knife, transferred to slides and dried. Mineralization was visualized by staining sections with von Kossa (counterstained with toluidine blue).

4.3.2 Results

μ CT scans of 4 and 12 week old BALB/c mice indicated only a few point fusions along the coronal sutures. Additionally, suture fusion was not clearly observed in all mice and was inconsistent from animal to animal (visual observations, data not shown).

The C57BL6 model was thought to be more severe – preliminary experiments were carried out to characterize the craniosynostosis phenotype. Alizarin Red whole mount staining of skulls dissected from one/two day old C57BL6 mice showed coronal sutures

that appeared to be fused or close to fusion. Skulls of the same age were also cultured *ex vivo* for 1-2 weeks and stained to better understand the progression of suture fusion in these mice; however from visual observation of stained skulls, no clear change in coronal suture fusion was determined (Figure 4.7). Cultured calvarial sections stained with von Kossa showed coronal suture bones closer to each other, compared to wild type mice (Figure 4.8). From these observations, irreversible suture fusion in the C57BL6 model is initiated early, possibly even in-utero, making it difficult to treat. Additionally, we faced several challenges with mouse breeding – times between litters were long (up to two months), and litter yields were small, resulting in small sample sizes. Hence, these models of craniosynostosis were also determined to be unsuitable to study the effects of peptide treatment on mineral inhibition.

4.4 Conclusions

Several models of pathological calcification, spanning 3 different clinical disorders (cardiovascular calcification, FOP and craniosynostosis), were evaluated as potential candidates to test peptide efficacy *in vivo*. Altering genetic background changed the occurrence of pathological calcification phenotypes. Additionally, while breeding mice on mixed genetic backgrounds mimics aspects of disease heterogeneity observed in humans, large variations in mouse phenotype severity may be introduced, which can muddle the interpretation of treatment effects. Therefore detailed evaluation of the effects of altering genetic background on the degree and severity of calcification must be

completed before pursuing more experiments studying efficacies of anti-calcification treatments.

Acknowledgements

I would like to thank Dr. Nan Hatch, Dr. Jin Liu, Hwa Kyung Nam, Dr. Yuji Mishina and Haichun Pan for providing the animal models and assisting with all aspects of experiments and troubleshooting. I also want to thank Dr. Jose Millan and Dr. Sonoko Narisawa (Sanford Burnham Institute) for providing MOVAS cells as well as sharing protocols and other resources regarding cardiovascular calcification studies. Finally, I also wish to thank Dr. Rupak Rajachar (Michigan Technological University) for providing hands-on training on cardiovascular cell isolation procedures.

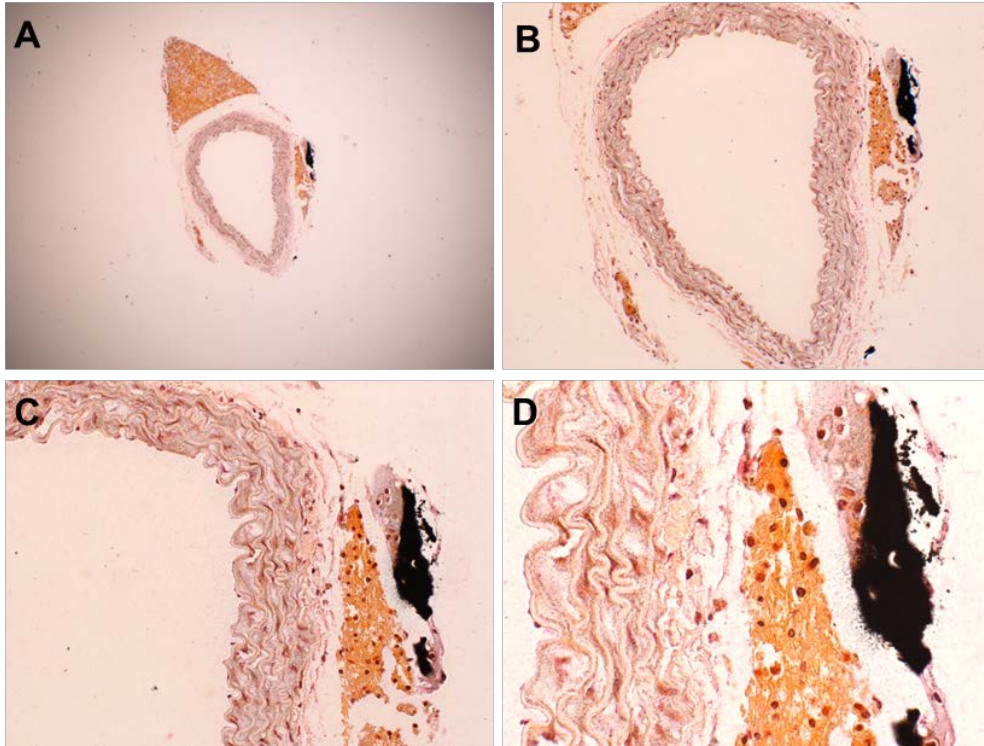


Figure 4.1: Aortas from 23 week old *Enpp1* knockout mice were sectioned and stained with von Kossa (counter stained with fast nuclear red) to detect arterial calcification. (A) 4X magnification, (B) 10X magnification, (C) 20X magnification, (D) 40X magnification. No calcification was detected within the vessels.

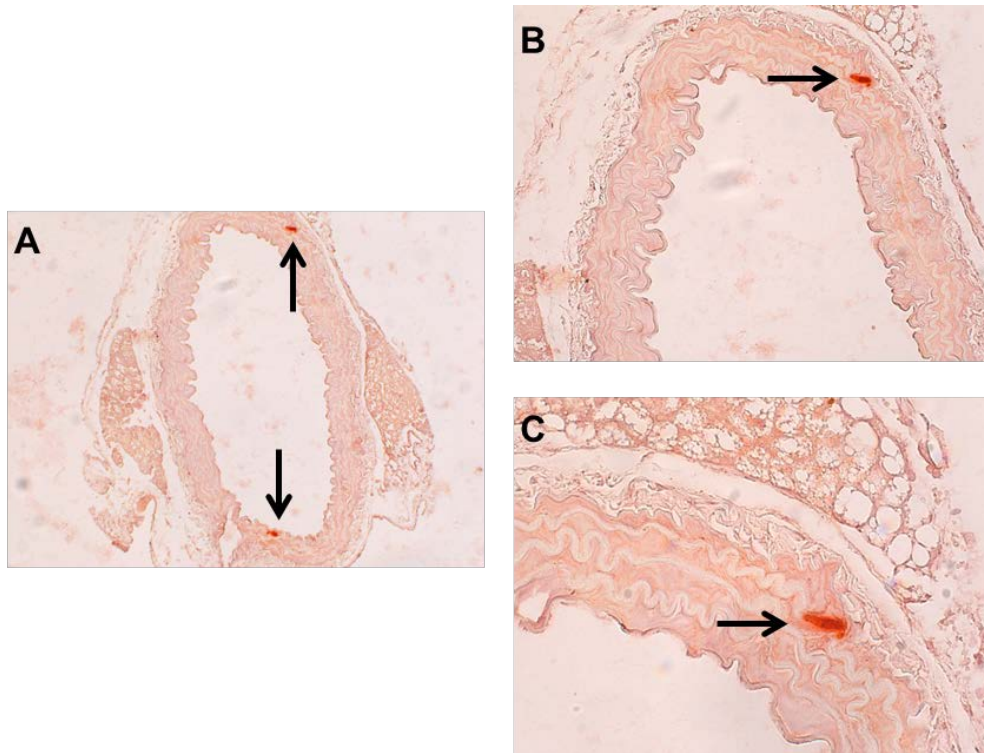


Figure 4.2: Aortas from 23 week old *Enpp1* knockout mice were sectioned and stained with Alizarin Red to detect arterial calcification. (A) 10X magnification, (B) 20X magnification and (C) 40X magnification of top portion of (A). A few sites of positively stained calcification were observed, indicated by arrows.



Figure 4.3: Mineral formation by vascular smooth muscle cells (VSMCs) cultured with 2mM Pi for 4 weeks and stained by von Kossa. (A) primary murine VSMCs isolated from wild type mice, (B) A7r5 rat VSMC line.

Timeline	VSMC source	Culture conditions	Result
2010 - 2012	5 week old wild type male BALB/c mice	DMEM, FBS, β -GP/ascorbic acid for 4 weeks	No mineral seen by von Kossa staining
	8 week old wild type male BALB/c mice	DMEM, FBS, β -GP/ascorbic acid or Pi for 4 weeks	VSMCs cultured with Pi showed some diffuse dots, no mineral seen with β -GP/ascorbic acid group (von Kossa staining)
	A7r5 rat VSMC cell line	DMEM, FBS, β -GP/ascorbic acid or Pi for 4 weeks	VSMCs cultured with Pi showed had some mineralization, no mineral seen with β -GP/ascorbic acid group (von Kossa staining)
	A7r5 rat VSMC cell line	DMEM, FBS, β -GP/ascorbic acid/insulin for 4 weeks	No mineral seen
	6-7 week old Enpp1 knockouts, mixed genders	DMEM, FBS, β -GP/ascorbic acid for 4 weeks	No mineral seen (von Kossa)
	11-12 week old Enpp1 knockouts, mixed genders	Passaged in ascorbate-free medium; mineralization experiment with β -GP/ascorbic acid in modified alpha-MEM and lot tested FBS for upto 4 weeks	No calcium deposition seen (demineralized and quantified calcium using o-cresolphthalein complexone method)
	MOVAS mouse VSMC cell line	β -GP/ascorbic acid in modified alpha-MEM and lot tested FBS for upto 3 weeks	No mineral seen (von Kossa, Alizarin Red or calcium quantification)

Table 4.1: Summary of experiments conducted to test for vascular smooth muscle cell (VSMC) calcification in culture. Primary cells and cell lines were tested with several different combinations of culture conditions and mineralization detection techniques, but failed to mineralize.

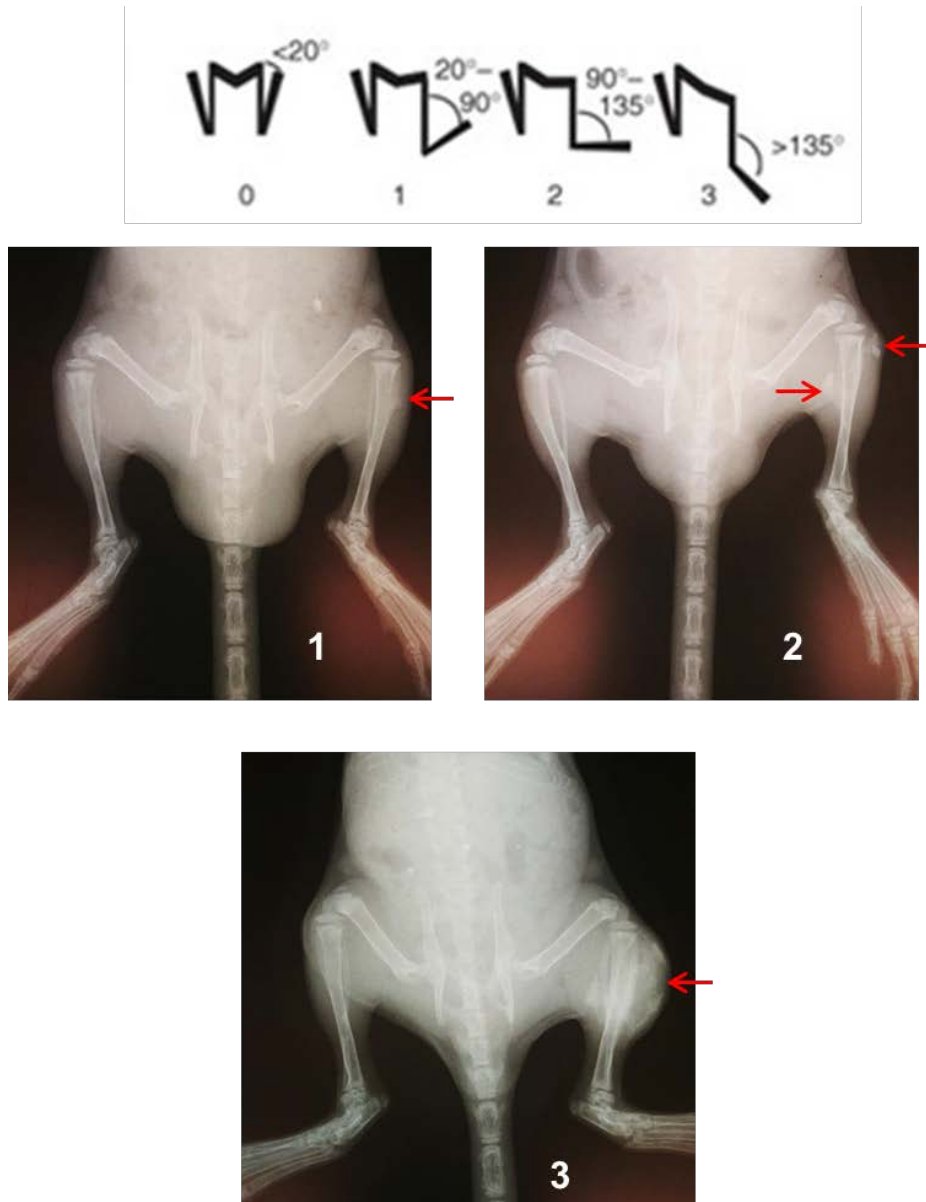


Figure 4.4: Schematics demonstrating scoring for range of motion (ROM) and X-ray analysis of heterotopic ossification (HO). Upper panel – scoring for ROM analysis based on angles formed between tibia and ankle (adapted from [13]). A score of 0 indicated an angle of less than 20° (normal) while a score of 3 indicated an abnormal angle of greater than 135° , caused by excessive heterotopic ossification (HO). Lower panels – Radiographs demonstrating scoring scheme for X-ray analysis of HO formed in hind limb musculature (indicated by arrows). The amount of HO visually observed on the X-rays was scored on a scale of 0-3, with 0 indicating no HO formation and 3 indicating maximum HO formation among all animals compared.

Treatment	Range of Motion (ROM)		X-ray	
	Left	Right	Left	Right
Left leg: PBS, right leg: peptide	1	0	0	2
	0	0	1	0
	0	1	1	1
	1	1	0	2
	1	2	0	3
	0	1	2	3
	1	1	2	3
	1	1	0	0
	0	0	0	2
	0	0	1	2
	0	0	0	2
Median	0	1	0	2
Total	5	7	7	20

Table 4.2: Range of motion (ROM) and X-ray scoring of mice induced with HO and treated with PBS (left leg) and peptide (right leg). Median and total scores were higher in right legs than left legs.

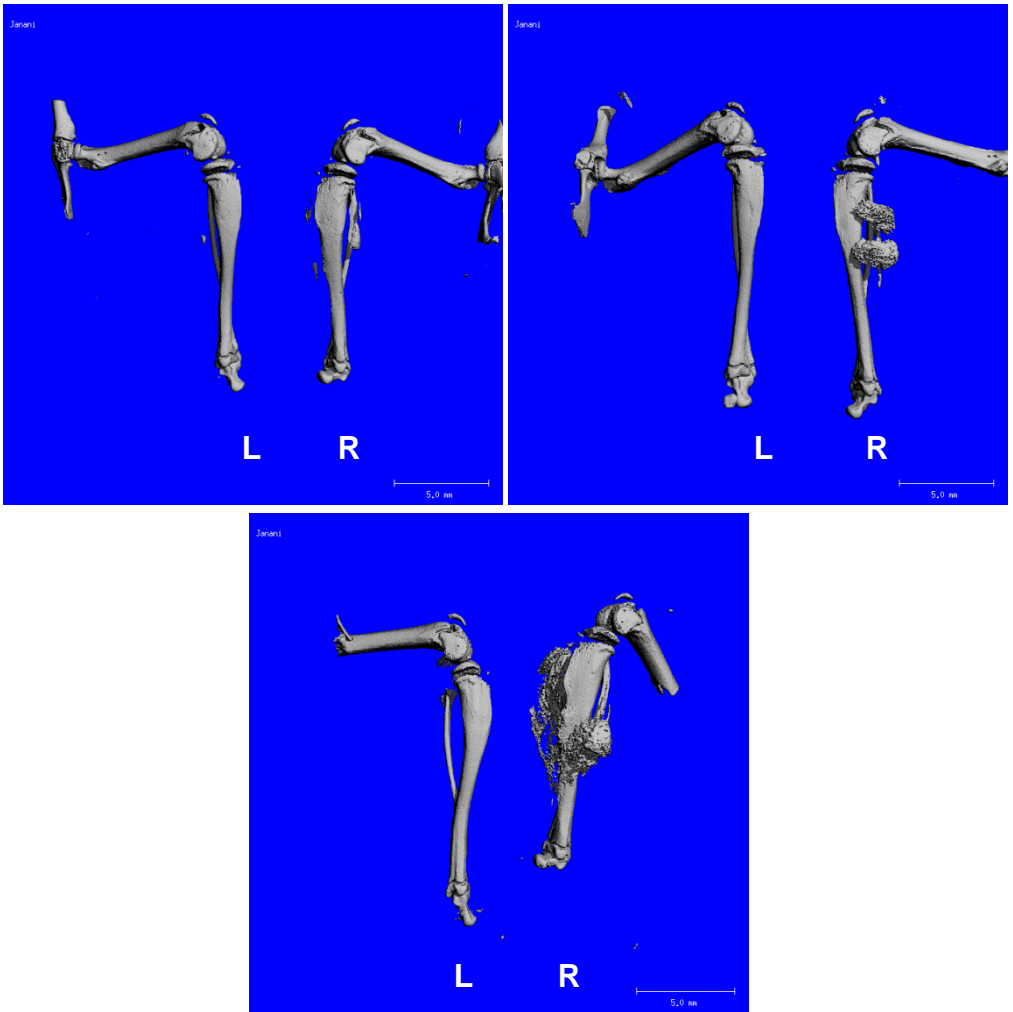


Figure 4.5: μ CT images of legs dissected from HO-induced mice treated with PBS (left leg, L) and peptide (right leg, R). More HO was observed in right legs compared to left, and there was high variability in phenotype from mouse to mouse.

	Range of Motion (ROM)		X-ray	
	L	R	L	R
Left leg: peptide, right leg: no treatment	1	2	2	2
	0	2	0	3
	1	2	1	2
	1	2	0	3
	1	3	1	2
	2	1	2	2
	2	3	2	3
	2	3	0	3
Median	1	2	1	2.5
Total	10	18	8	20
Left leg: PBS, right leg: no treatment	0	3	1	3
	2	1	2	1
	0	0	0	1
	1	2	3	3
	1	2	0	3
	0	1	0	3
	0	2	0	2
Median	0	2	0	3
Total	4	11	6	16

Table 4.3: Range of motion (ROM) and X-ray scoring of mice induced with HO and treated with either PBS or peptide (left leg), leaving the right leg untreated. Median and total scores were higher in right legs than left legs.

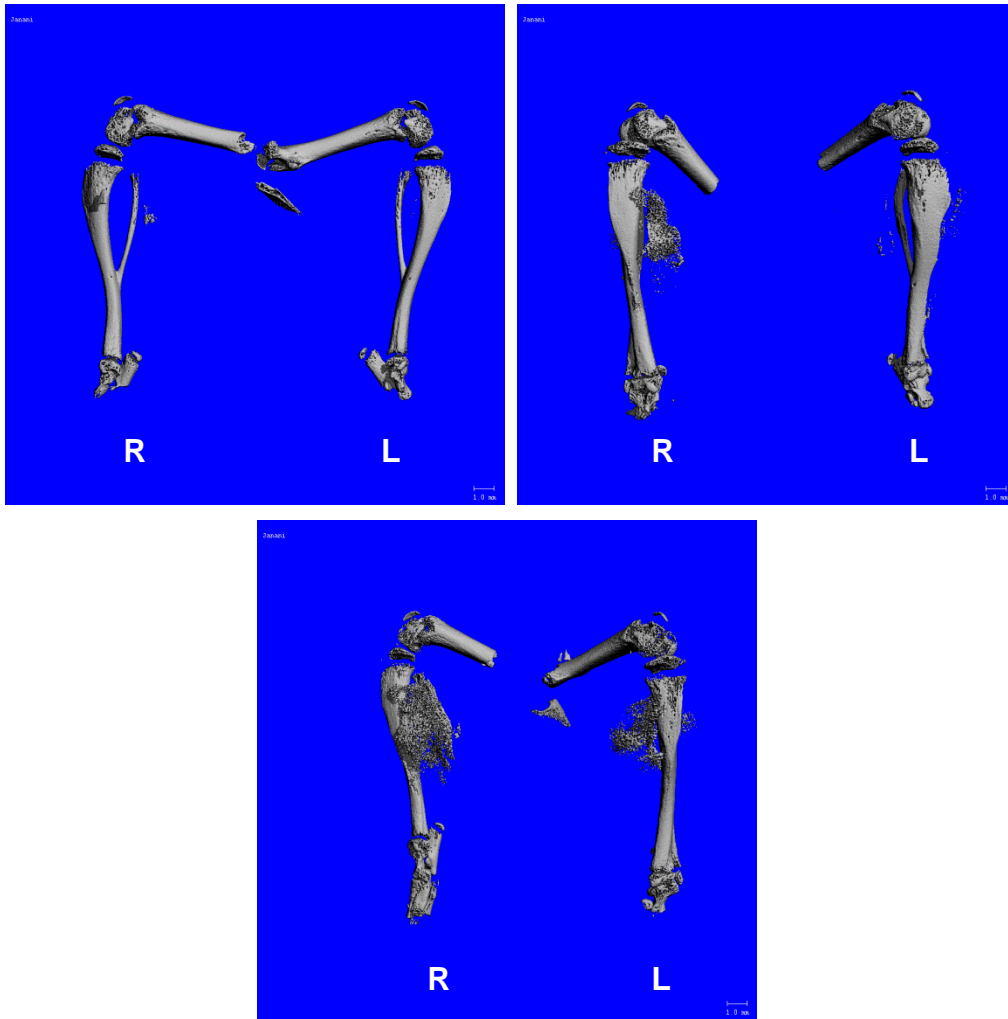


Figure 4.6: μ CT images of legs dissected from HO-induced mice treated with PBS (left leg, L; right leg, R was untreated). More HO was observed in right legs compared to left, and there was high variability in phenotype from mouse to mouse.

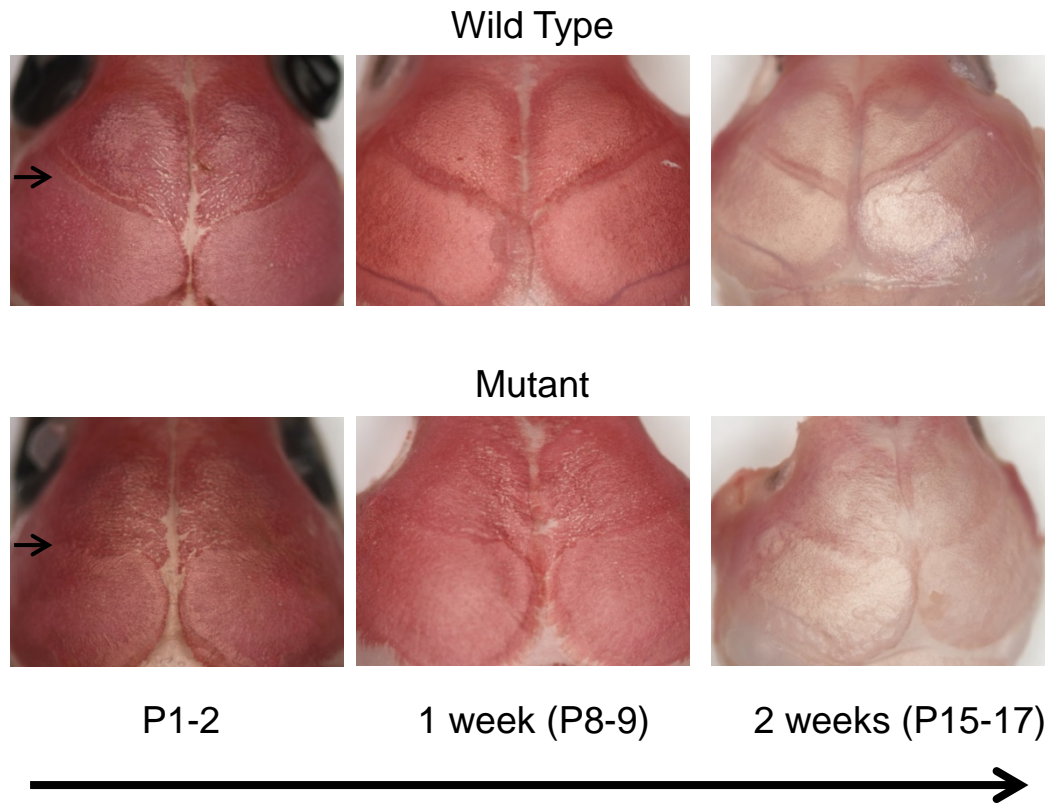


Figure 4.7: Whole mount Alizarin Red staining of calvaria harvested from 1-2 day old (P1-2) C57BL6 Crouzon mice (left panels) and calvaria cultured *ex vivo* for 1 (middle panels) and 2 weeks (right panels). Small black arrows point to the coronal suture which remains patent in wild type mice (upper panel) and appears to be fused or close to fusion in mutant mice (lower panel).

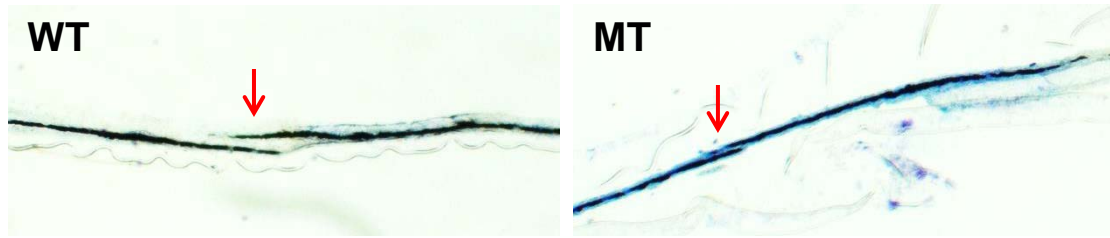


Figure 4.8: Calvaria of *ex vivo* cultured C57BL6 *Crouzon* mice were sectioned and stained with von Kossa (counterstained with Toluidine blue) to visualize coronal sutures (red arrows). Sutures were patent in wild type mice, and close to fusion in mutant mice.

4.5 References

- [1] Narisawa S, Harmey D, Yadav MC, O'Neill CW, Hoylaerts MF, Millan JL. Novel Inhibitors of Alkaline Phosphatase Suppress Vascular Smooth Muscle Cell Calcification. *J Bone Miner Res* 2007;22:1700–10.
- [2] Mackenzie NCW, Zhu D, Milne EM, van 't Hof R, Martin A, Quarles DL, et al. Altered Bone Development and an Increase in FGF-23 Expression in *Enpp1* Mice. *PLoS One* 2012;7:e32177.
- [3] Luo G, Ducy P, McKee MD, Pinero GJ, Loyer E, Behringer RR, et al. Spontaneous calcification of arteries and cartilage in mice lacking matrix GLA protein. *Nature* 1997;386:78–81.
- [4] Bucay N, Sarosi I, Dunstan CR, Morony S, Tarpley J, Capparelli C, et al. osteoprotegerin-deficient mice develop early onset osteoporosis and arterial calcification. *Genes Dev* 1998;12:1260–8.
- [5] Qiao JH, Xie PZ, Fishbein MC, Kreuzer J, Drake TA, Demer LL, et al. Pathology of atheromatous lesions in inbred and genetically engineered mice. Genetic determination of arterial calcification. *Arterioscler Thromb Vasc Biol* 1994;14:1480–97.
- [6] Lovell DP, Johnson FM. Quantitative genetic variation in the skeleton of the mouse: I. Variation between inbred strains. *Genet Res* 2009;42:169.
- [7] Beamer WG, Donahue LR, Rosen CJ, Baylink DJ. Genetic variability in adult bone density among inbred strains of mice. *Bone* 1996;18:397–403.
- [8] Turner CH, Hsieh YF, Müller R, Bouxsein ML, Baylink DJ, Rosen CJ, et al. Genetic regulation of cortical and trabecular bone strength and microstructure in inbred strains of mice. *J Bone Miner Res* 2000;15:1126–31.
- [9] Jepsen KJ, Pennington DE, Lee YL, Warman M, Nadeau J. Bone brittleness varies with genetic background in A/J and C57BL/6J inbred mice. *J Bone Miner Res* 2001;16:1854–62.
- [10] Glaser DL, Economides AN, Wang L, Liu X, Kimble RD, Fandl JP, et al. In vivo

somatic cell gene transfer of an engineered Noggin mutein prevents BMP4-induced heterotopic ossification. *J Bone Joint Surg Am* 2003;85-A:2332–42.

- [11] Kan L, Hu M, Gomes WA, Kessler JA. Transgenic Mice Overexpressing BMP4 Develop a Fibrodysplasia Ossificans Progressiva (FOP)-Like Phenotype. *Am J Pathol* 2004;165:1107–15.
- [12] Agarwal S, Loder SJ, Brownley C, Eboda O, Peterson JR, Hayano S, et al. BMP signaling mediated by constitutively active Activin type 1 receptor (ACVR1) results in ectopic bone formation localized to distal extremity joints. *Dev Biol* 2015;400:202–9.
- [13] Yu PB, Deng DY, Lai CS, Hong CC, Cuny GD, Buxsein ML, et al. BMP type I receptor inhibition reduces heterotopic ossification. *Nat Med* 2008;14:1363–9.
- [14] Fukuda T, Scott G, Komatsu Y, Araya R, Kawano M, Ray MK, et al. Generation of a mouse with conditionally activated signaling through the BMP receptor, ALK2. *Genesis* 2006;44:159–67.
- [15] Eswarakumar VP, Horowitz MC, Locklin R, Morriss-Kay GM, Lonai P. A gain-of-function mutation of Fgfr2c demonstrates the roles of this receptor variant in osteogenesis. *Proc Natl Acad Sci U S A* 2004;101:12555–60.
- [16] Liu J, Nam HK, Wang E, Hatch NE. Further analysis of the Crouzon mouse: effects of the FGFR2(C342Y) mutation are cranial bone-dependent. *Calcif Tissue Int* 2013;92:451–66.
- [17] Chen L, Li D, Li C, Engel A, Deng C-X. A Ser250Trp substitution in mouse fibroblast growth factor receptor 2 (Fgfr2) results in craniosynostosis. *Bone* 2003;33:169–78.
- [18] Zhou YX, Xu X, Chen L, Li C, Brodie SG, Deng CX. A Pro250Arg substitution in mouse Fgfr1 causes increased expression of Cbfa1 and premature fusion of calvarial sutures. *Hum Mol Genet* 2000;9:2001–8.
- [19] Komatsu Y, Yu PB, Kamiya N, Pan H, Fukuda T, Scott GJ, et al. Augmentation of Smad-dependent BMP signaling in neural crest cells causes craniosynostosis in mice. *J Bone Miner Res* 2013;28:1422–33.

- [20] Liu J, Nam HK, Campbell C, Gasque KC da S, Millán JL, Hatch NE. Tissue-nonspecific alkaline phosphatase deficiency causes abnormal craniofacial bone development in the *Alpl*(^{-/-}) mouse model of infantile hypophosphatasia. *Bone* 2014;67:81–94.
- [21] Cunningham ML, Seto ML, Ratisoontorn C, Heike CL, Hing A V. Syndromic craniosynostosis: from history to hydrogen bonds. *Orthod Craniofac Res* 2007;10:67–81.

Chapter 5

In vivo delivery of peptide in a mouse model of craniosynostosis

5.1 Introduction

Craniosynostosis, a condition affecting ~ 1 in 2500 live births, is caused by premature fusion of cranial sutures, leading to craniofacial abnormalities, increased intracranial pressure, abnormal brain development and auditory and visual defects [1,2]. Genetically altered mouse models are useful in replicating and understanding different aspects of craniosynostosis, as well as for testing efficacies of new drug treatments. In this Chapter, the phenotype of a transgenic craniosynostosis mouse model with constitutively active bone morphogenetic protein (BMP) receptor type 1 was characterized, and the effects of pVTK on inhibiting pathological suture calcification *in vivo* were tested. Mutant mice were reported to have enhanced BMP signaling in nasal and frontal bones (derived from cranial neural crest (CNC) cells) and developed premature fusion of the anterior-frontal (AF) suture starting 8 days after birth [3]. Mutant mice also had craniofacial abnormalities such as shorter snouts, wide-set bulging eyes, and lowered bone volume fractions in nasal and frontal bones [3]. For our experiments, further characterization of this craniosynostosis model was conducted, by analyzing craniofacial bone lengths, as well as bone volume and tissue mineral density. Additionally, pVTK peptide was locally delivered to the AF suture, and skulls were analyzed for changes in craniofacial morphology, suture fusion and bone quality.

5.2 Materials and Methods

5.2.1 Animals

All animal procedures were approved by the University Committee on Use and Care of Animals (UCUCA) at the University of Michigan. Mice were maintained on a mixed genetic background – C57Bl6/J and 129S6. Mice with a mutation in BMP receptor *Bmpr1a* were bred with *P0-Cre* mice, which express the enzyme Cre-recombinase under the control of the CNC-specific P0 promoter. Mutant (MT) mice had constitutively active BMP receptors and enhanced BMP signaling in CNC-derived frontal and nasal bones. Mice expressing only *P0-Cre* transgene, but not the *Bmpr1a* transgene, were designated as control mice (CT). Mouse genotypes were determined by performing PCR with tail/ear tissues biopsies. The following primers were used: Cre-Gamma CGAACATCTTCAGGTTCTGCGG, Cre-Omega GTCGATGCAACGAGTGATGAGG, TF41:GTGCTGGTTATTGTGCTGTCTC, TF61:ACGACAGTATCGGCCTCAGGAA (TF 41/61 used to check for *Bmpr1a* transgene).

5.2.2 Subcutaneous calvarial injections

To determine the optimal age to treat mice with peptide, a time course experiment was conducted to characterize mutant phenotype across different ages. Newborn mice were injected with 2 μ l of PBS over the AF cranial suture once a day starting postnatal day 1 (P1), or left untreated until they were sacrificed at P7, P10, P13 or P17 of age. Skulls were dissected out and cleared of soft tissue. Samples were fixed in 10% neutral buffered formalin, transferred to 70% ethanol and scanned via μ CT. No negative effects were observed due to injections (not shown). Based on observations of phenotype progression,

P10 was chosen as the end-point for all subsequent experiments. At ten days of age, the mutant phenotype (suture fusion, craniofacial defects) had progressed sufficiently to be measurable, allowing improvement or continued progression of the phenotype to be detected post treatment. pVTK peptide was dissolved in sterile PBS at 3mM concentration and aliquots frozen at -20°C. P1 mice were subcutaneously injected with 2µl of peptide, PBS or left untreated until P10, at which time they were sacrificed and samples processed as described above.

5.2.3 Micro-computed Tomography (µCT)

Skulls were embedded in 1% agarose and placed in a 34 mm diameter tube and scanned over the entire length of the skull using a microCT system (µCT100 Scanco Medical, Bassersdorf, Switzerland). Scan settings were: voxel size 18 µm, 55 kVp, 109 µA, 0.5 mm AL filter, and integration time 500 ms. A 140 slice region of interest was defined around the AF suture, and used for the quantification of bone volume (BV) and tissue mineral density (TMD).

5.2.4 Digital caliper measurements

Digital calipers were used to measure cranial morphology. The following lengths and widths were measured (Figure 5.1): lengths of nasal bone (N), frontal bone (F) and parietal bone (P); width between the eyes, and at the widest part of skull (near the lambdoid suture). Ratios of the nasal, frontal and combined nasal + frontal bone lengths relative to the parietal bone lengths were calculated.

5.2.5 Categorization of phenotype severity

Large variability in the severity of the mutant phenotype was observed. To overcome this inconsistency, mutants were separated into three categories based on the following phenotypes: Category 1/mild - genotypically identified as mutant but phenotype resembled controls with normal bone shape and patent sutures, Category 2/medium - mutant phenotype clearly observed with shorter triangular shaped snouts, wider skulls and fused sutures, and Category 3/severe – mutants with severely undermineralized and fragile skulls which were undetectable in μ CT scans (excluded from all analysis) (Figure 5.2). Body weight, digital caliper measurements and μ CT data are presented from all mutants combined, as well as classified by categories 1 and 2.

5.2.6 Histology

Fixed skulls were decalcified in 10% EDTA (pH 7.4) for 10-14 days, rinsed with water and transferred to 70% ethanol. Samples were dehydrated using a series of ethanol mixtures and embedded in paraffin. Serial 5 μ m coronal sections were taken at 150 μ m intervals along the length of the AF suture, starting anterior to the eyes. Sections were stained with hematoxylin/eosin and imaged with an Olympus light microscope.

5.2.7 Primary osteoblast cell culture

Cranial pre-osteoblasts were isolated from nasal and frontal bones of 1-3 day old transgenic mice using a series of enzymatic digestions, as described [4]. Cells were maintained in alpha minimum essential media supplemented with 10% fetal bovine serum and 1% penicillin-streptomycin (growth medium) at 37°C and 5% CO₂ in a humidified incubator. Cells were seeded at a density of 10,000 cells/cm² (24 well plates,

Corning Costar) and allowed to attach overnight in growth medium. Cells were then differentiated with osteogenic medium (growth medium supplemented with 10mM β -glycerophosphate and 50 μ g/ml ascorbic acid) with or without 300 μ M pVTK peptide and cultured for 20 days. Media was replaced every 2 days.

5.2.8 von Kossa staining

Cells were fixed in zinc buffered formalin for 30 min and rehydrated using a series of graduated ethanol-water mixes. Cells were then exposed to 5% silver nitrate for 30-60 min in bright light. Wells were washed, dried and imaged.

5.2.9 Statistics

Data is presented as mean \pm standard deviation. SigmaPlot was used to perform all statistical analyses. T-tests or Two way ANOVA with Student Newman Keuls (SNK) post hoc comparisons were used to determine the effect of genotype (control vs. mutant) and treatment (PBS vs. peptide) on body weight, craniofacial and μ CT measurements. If data was non-parametric, Mann Whitney Rank Sum tests were used to determine significance. * $p < 0.05$ and ** $p < 0.001$ denote statistical significance.

5.3 Results

5.3.1 Effect of pVTK on body weight

PBS treated mutants had trends of lowered body weights than controls (Figure 5.3A). Similarly, peptide treated mutants had significantly lowered body weights than controls

($p = 0.01$). Trends of lowered body weight with peptide treatment were observed in categorized mutants (Figure 5.3C, D).

5.3.2 Effect of pVTK on AF suture fusion

AF sutures in category 1 mutants (tissue sections at the eye-level) were patent (Figure 5.4A, B), and sutures in category 2 mutants were fused (Figure 5.4C, D), within both PBS and peptide treatment types. Sutures remained patent in control mice, as expected (Figure 5.4E, F).

5.3.3 Effect of pVTK on craniofacial morphology

Length ratios of nasal, frontal and nasal + frontal bones relative to parietal bones were all significantly lowered in PBS treated mutant mice compared to controls (Figure 5.5A; $p < 0.001$). PBS treated mutants had significantly wider skulls at the eye-level than controls (Figure 5.5B; $p < 0.001$). Peptide treated mutants had significantly lowered length ratios compared to controls (Figure 5.5A; N/P peptide $p = 0.029$ F/P, N+F/P, $p < 0.001$). Peptide treatment reduced skull width at the eye-level compared to PBS treated mutants (Figure 5.5B; $p = 0.022$).

Within category 1 mutants, trends of higher N/P, lowered F/P, N+F/P and eye width were measured following peptide treatment, relative to PBS (Figure 5.6A, B). Within category 2 mutants, trends of higher length ratios with peptide treatment were measured (Figure

5.6C). Skull width at the eye-level of category 2 mutants was significantly lowered with peptide treatment (Figure 5.6D; $p = 0.016$).

5.3.4 Effect of pVTK on bone volume and tissue mineral density

BV was significantly lowered in PBS treated mutants compared to controls (Figure 5.7A; PBS $p = 0.002$). TMD was also significantly lower in PBS treated mutants compared to controls (Figure 5.7B; $p = 0.001$). With peptide treatment, BV was significantly lower in mutants compared to controls (Figure 5.7A; $p < 0.001$). pVTK peptide also lowered BV in mutants compared to PBS treatment ($p = 0.046$). Peptide treatment resulted in significantly decreased TMD in control mice compared to PBS treated controls (Figure 5.7B; $p = 0.021$).

Within category 1 mutants, trends of lowered BV and TMD were measured following peptide treatment (Figure 5.8A, B). Within category 2 mutants, significantly lowered BV was measured following peptide treatment compared to PBS (Figure 5.8C; $p = 0.047$). Category 2 mutants displayed trends of increased TMD following peptide treatment (Figure 5.8D).

5.3.5 Effect of pVTK on primary osteoblast culture

pVTK treatment did not inhibit primary pre-osteoblast mineralization after three weeks of culture. Cells treated with peptide mineralized similar to cells cultured in osteogenic medium only (Figure 5.9).

5.4 Discussion

We used a transgenic mouse model of conditionally enhanced BMP signaling in bones derived from CNC cells, leading to synostosis of the AF suture (Figure 5.4) [3]. Large variation in phenotype severity was observed qualitatively and quantitatively in this mouse model of craniosynostosis. The reason for this variability is unknown; we hypothesize that mixed genetic backgrounds or differences in the levels of Cre expression in breeder pairs could be contributing to the inconsistencies. While variability in phenotype is reflective of the heterogeneity seen in craniosynostosis patients, it becomes difficult to detect differences arising from treatment.

To reduce the variance in the data, mice were categorized into mild, medium and severe phenotypes (categories 1-3) based on observations of μ CT 3D rendered images (Figure 5.2). Severely affected mutants (category 3) often did not survive beyond the first few days after birth; those that survived the duration of the experiment had small skulls that were highly undermineralized, lacked structural integrity, and were therefore excluded from analysis. Category 2 mutants had wide-set eyes, shorter triangular snouts and areas of undermineralized bones. Additionally, AF sutures in category 2 mutants fused prematurely. Category 1 “mutants” were identified as mutants by genotyping, but phenotypically resembled control mice. Category 1 mice did not have craniofacial defects such as shorter noses, wider skulls or large undermineralized areas in the nasal or posterior frontal bones (Figure 5.8). The AF sutures in Category 1 mutants did not undergo premature fusion, but remained patent (Figure 5.4). Hence, these mice had no abnormal craniofacial conditions.

Mutant mice exhibited craniofacial abnormalities such as wider set eyes and shorter nasal and frontal bones length ratios (Figure 5.5). Peptide treatment corrected the wide set eyes, by significantly lowering the skull width at the eye level compared to PBS treated mutants (Figure 5.5, Figure 5.6). Further, trends of higher nasal and frontal bone length ratios were observed in peptide treated category 2 mutants (Figure 5.6), suggesting beneficial effects of peptide treatment on craniofacial morphologies. However, AF sutures continued to undergo premature fusion irrespective of peptide treatment (Figure 5.4), suggesting that higher peptide doses or longer administration periods may be necessary to prevent suture fusion. Alternatively, the underlying mechanisms contributing to craniofacial abnormalities may be distinct from those involved in suture fusion in this model of craniosynostosis.

Mutant mice had significantly lowered BV and TMD around the AF suture, compared to control mice (Figure 5.7). pVTK treatment further lowered BV in mutants, and also lowered TMD in control mice, compared to PBS treatment (Figure 5.7). Hence it is possible that pVTK has negative effects on bone mineralization. Studying bone growth and turnover using fluorochrome injections and histomorphometric analysis will provide more clarity on the effects of peptide on mineralization *in vivo*.

pVTK peptide inhibits the mineralization of MC3T3 pre-osteoblasts [5]. However, no inhibition of mineralization was observed with peptide treated primary pre-osteoblasts that were isolated from mutant mice (Figure 5.9). We hypothesize that this lack of inhibition arises from differences in cytokine signaling in mutant cells compared to MC3T3 cells. Pre-osteoblasts isolated from mutant mice exhibit enhanced Smad-dependent BMP signaling and FGF signaling pathways (and unaltered proliferation,

differentiation or mineralization profiles compared to cells from control skulls) [3]. While we have demonstrated altered expression levels of various promoters and inhibitors of mineralization in peptide-treated MC3T3 cells [6], we did not examine the effect of pVTK on BMP or FGF signaling pathways. Further evaluation of peptide effects on these cytokine signaling pathways, as well as their interactions with different regulators of mineralization, will help understand better the mechanisms behind pVTK-mediated inhibition of mineralization. It is also possible that the scenario of increased BMP signaling overrides the effects of pVTK, or that higher peptide concentrations or more sustained delivery profiles are required to inhibit mineralization.

pVTK treatment in a BMP-linked craniosynostosis model had positive effects on some aspects of craniofacial morphology, no effect on suture fusion and negative effects on BV and TMD. Further reduction in variance of the phenotype severity may provide more definitive outcomes following peptide treatment. Evaluation of BMP signaling to confirm constitutively active BMP type 1 receptors and enhanced downstream signaling in category 1 mice, may provide further insight into understanding the discrepancies between genotype and phenotype seen in these mice. Despite the categorization of mice based on severities, high variability in the μ CT data within category 2 was still observed (Figure 5.8), potentially contributing to the lack of statistically significant differences (in TMD) observed between treatments. Further sub-categorization within category 2 based on BV or body weight measurements, combined with appropriate increases in sample size within sub-categories may help to further reduce the inconsistencies and observe clear effects of peptide treatment. Measurement of Cre expression levels will also identify if variation among breeder pairs is contributing to the high variance in severity.

5.5 Conclusions

Peptide treatment resulted in a partial correction of craniofacial morphology defects, in a mouse model of BMP-linked craniosynostosis. pVTK did not prevent fusion of the AF suture and did not inhibit primary mutant-derived pre-osteoblast mineralization in culture. Additionally, treatment with peptide lowered bone volume and tissue mineral density, indicating negative effects on bone growth and turnover. Studies exploring the effects of peptide treatment on BMP and FGF cytokine signaling pathways will provide invaluable insight into the mechanisms of peptide-mediated inhibition of mineralization.

Acknowledgements

I am deeply grateful to Dr. Yuji Mishina (YM) for providing the animal model as well as for his guidance and assistance with facilitating all aspects of experiments conducted in this chapter. I also thank Haichun Pan for her help with genotyping and Satoru Hayano for training me on subcutaneous calvarial injection techniques. Thank you to Michelle Lynch and Chris Strayhorn, for their assistance with μ CT (School of Dentistry μ CT Core) and histology (School of Dentistry Histology Core) respectively. This work was funded by: NIH/NCRR S10RR026475-01 (μ CT), NIDCR/NIH R01DE020843 (YM), NIH DE 013380 and DE 015411.

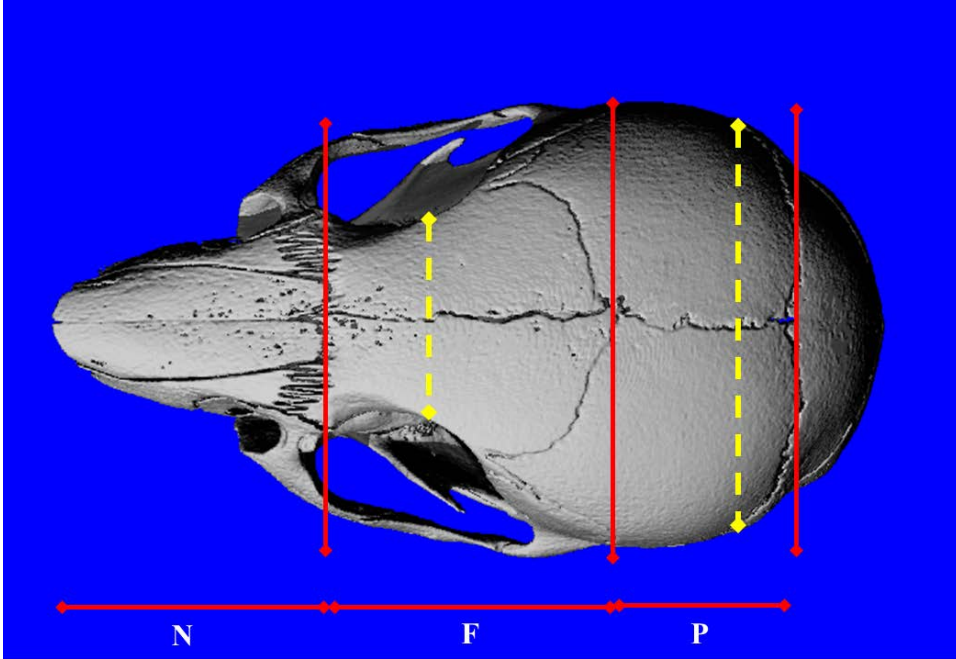


Figure 5.1: Schematic depicting locations on mouse skull where craniofacial measurements were acquired using digital calipers. Lengths of nasal (N), frontal (F) and parietal (P) bones were measured, indicated by distances between solid red lines. Skull width was measured at the eye-level and at the widest point of the skull (near lambdoid suture), indicated by dotted lines.

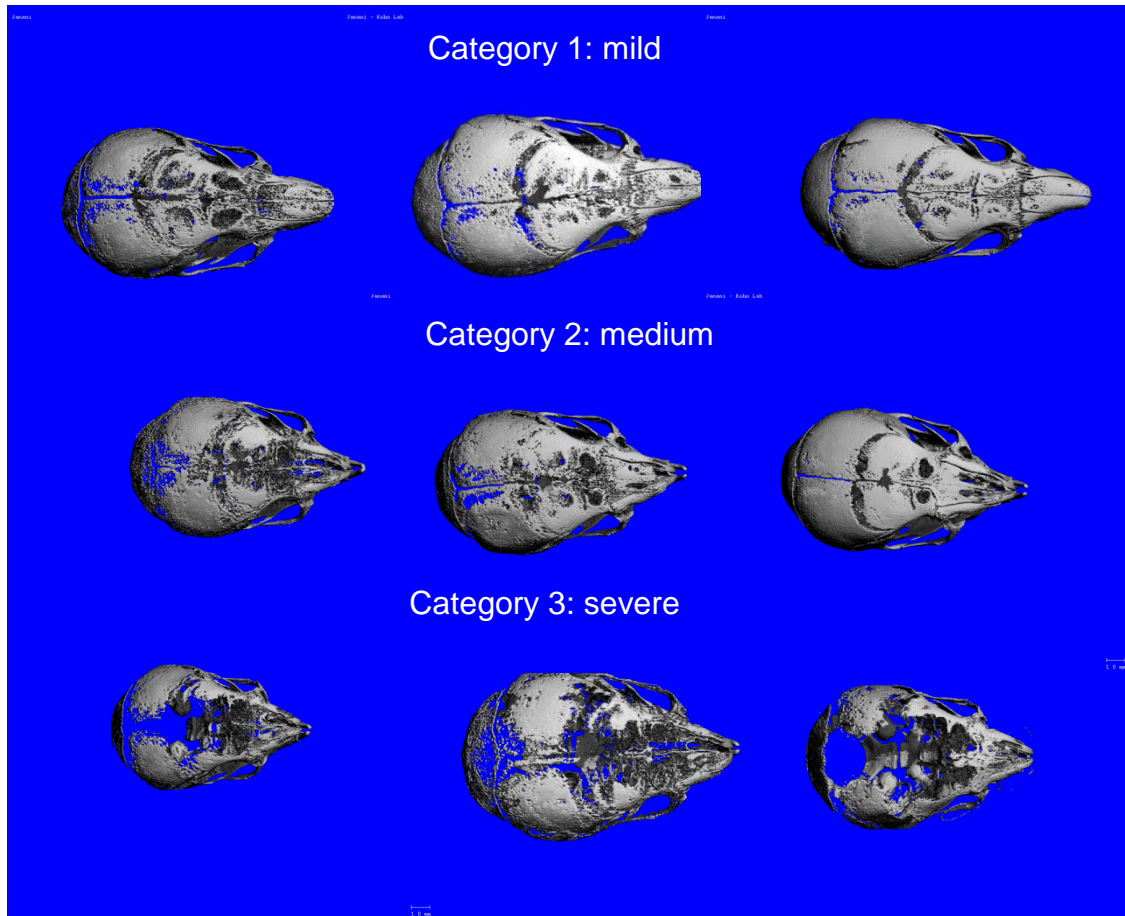


Figure 5.2: Categorization of P10 mutants based on phenotype severity as observed in μ CT 3D rendered images of skulls. Category 1/mild mice included animals genotypically identified as mutants, but phenotypically resembled control mice (no obvious craniofacial abnormalities). Category 2/medium mutants had shorter and triangular snouts and wide-set eyes. Category 3/severe mutants had large areas of undermineralized bones, and were excluded from analysis. Images of skulls are not on same scale.

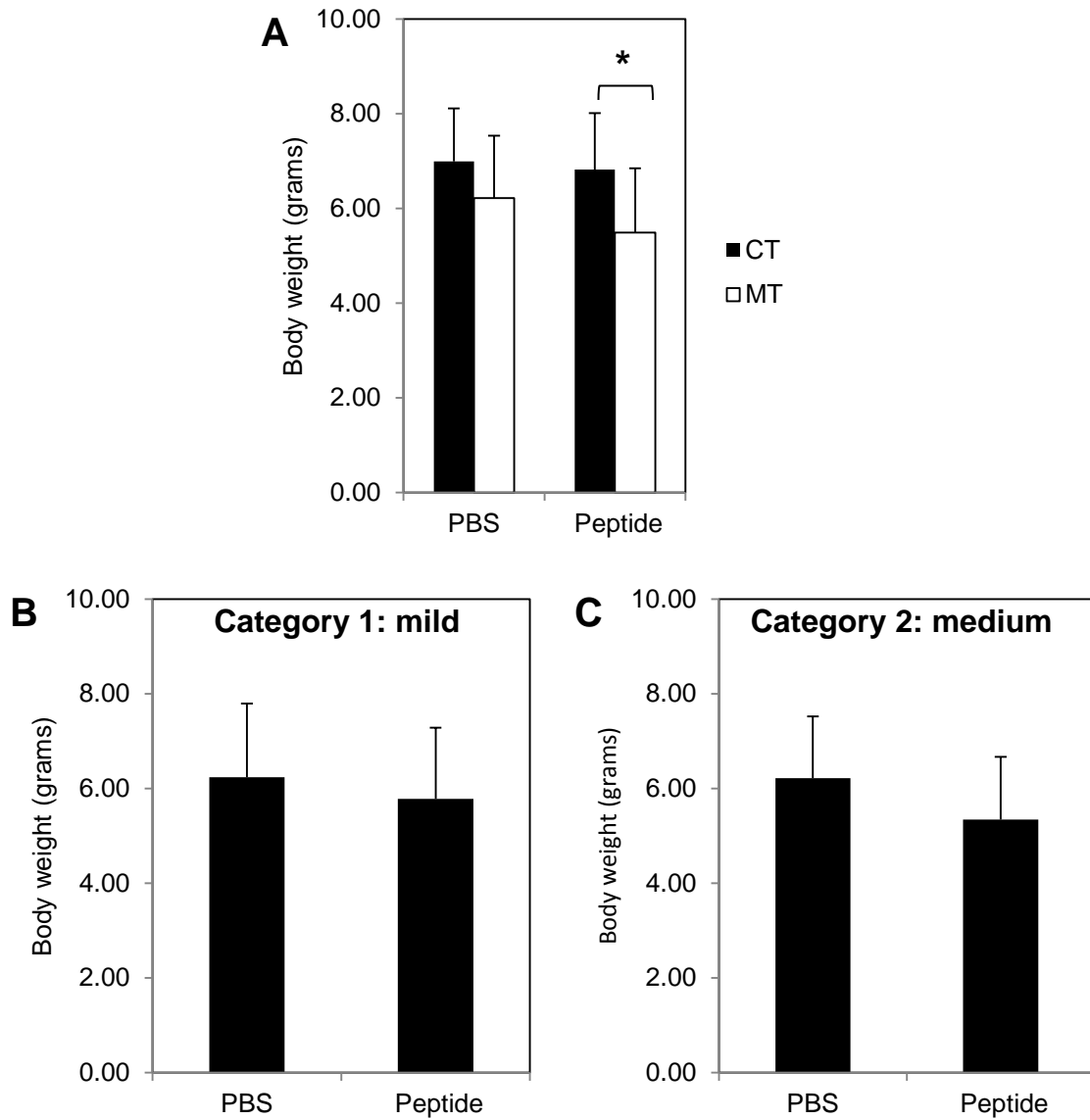


Figure 5.3: Body weights (A) Mutants pooled across categories 1 and 2 (MT) treated with PBS/peptide had lower body weights than their corresponding controls (CT). No differences were detected between mutants in mild or severe categories (B - C). * $p < 0.05$ Mann-Whitney Rank Sum test). Sample sizes: $n = 10$ for CT-PBS and CT-Peptide; $n = 17$ for MT-PBS; $n = 18$ for MT-Peptide.

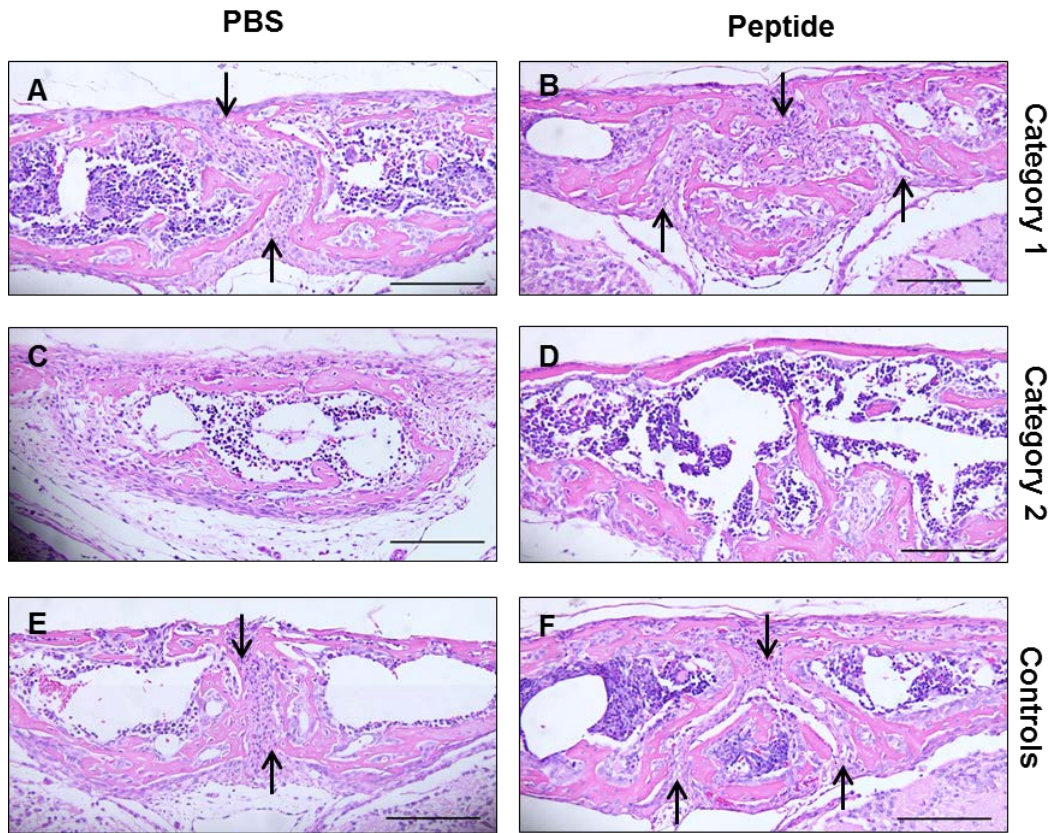


Figure 5.4: Histological assessment of anterior-frontal (AF) suture fusion. AF sutures remained patent in Category 1 mutants (A, B) and in controls (E, F), indicated by black arrows. Category 2 mutant mice had fused AF sutures (C, D). Scale bar 200 μ m.

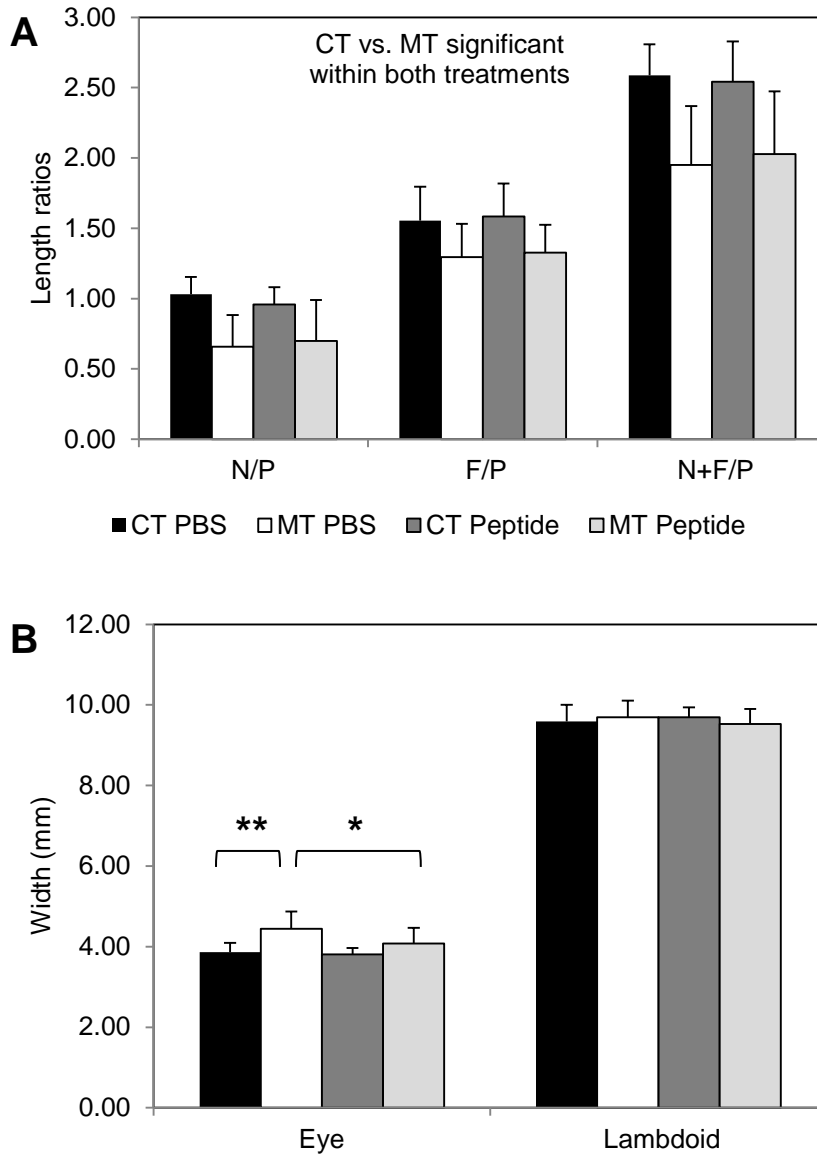


Figure 5.5: Digital caliper measurements of nasal (N), frontal (F) and parietal (P) bone lengths and skull widths at the eye and lambdoid sutures. (A) Length ratios were calculated relative to the parietal bone, and were significantly higher in controls (CT) compared to mutants (MT) irrespective of treatment. (B) MT-PBS mice had significantly wider skulls at the eye-level compared to CT-PBS and MT-Peptide mice. * $p < 0.05$; ** $p < 0.001$. *t* – tests/Mann Whitney Rank Sum tests were used for N/P and Eye measurements, Student Newman Keuls (after two way ANOVA) post multiple comparisons for all other measurements. Sample sizes: $n = 10$ for CT-PBS and CT-Peptide; $n = 14$ for MT-PBS; $n = 16$ for MT-Peptide.

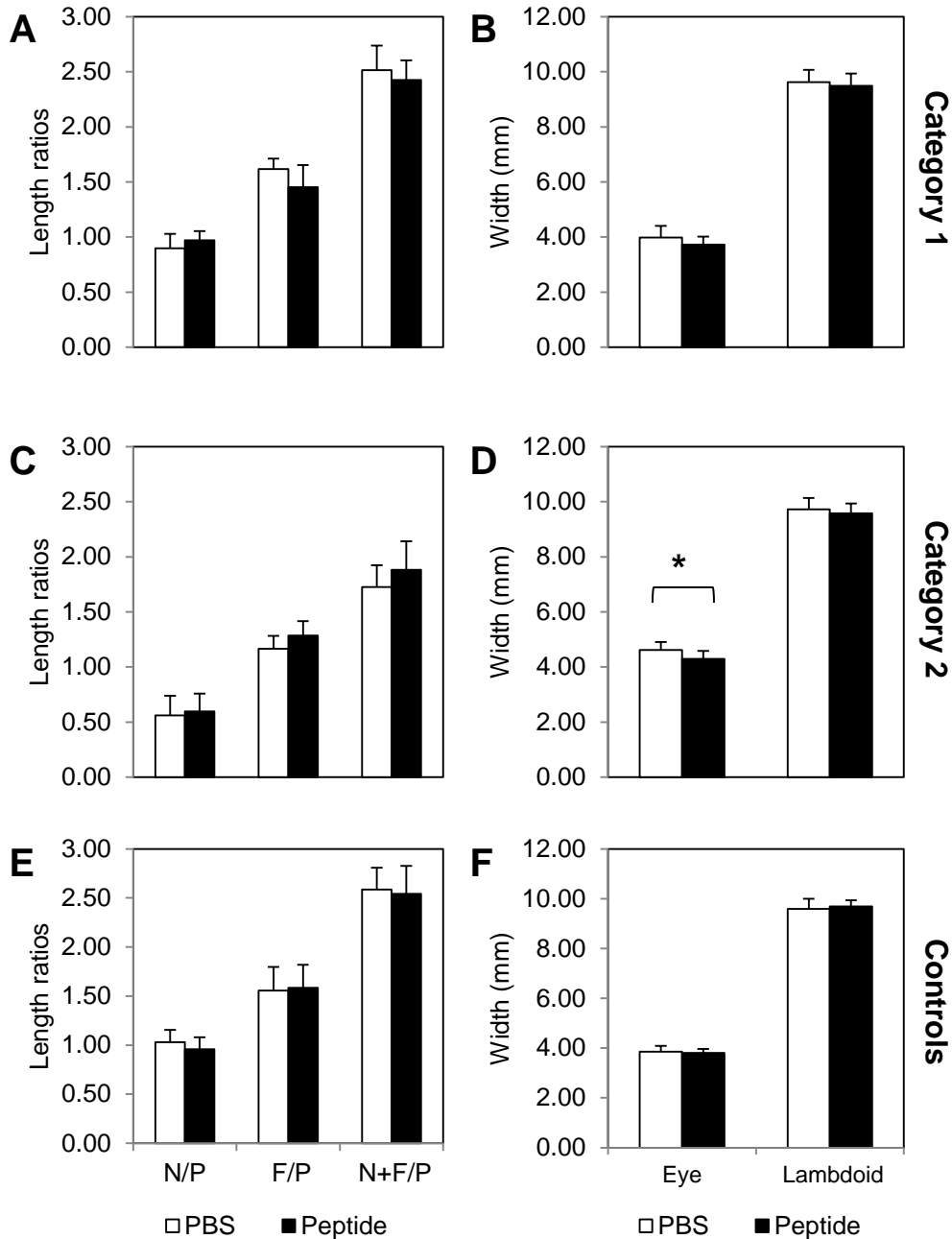


Figure 5.6: Digital caliper measurements of categorized mutant nasal (N), frontal (F) and parietal (P) bone lengths and skull widths at the eye and lambdoid sutures. Length ratios were calculated relative to the parietal bone. (A) Category 1: mild – trends of higher N/P and lower F/P and N+F/P length ratios, and (B) lowered widths were measured following peptide treatment; (C) Category 2: medium – trends of higher length ratios were measured following peptide treatment; (D) Width at the eye-level was significantly lowered with peptide treatment; (E) and (F) No effect of treatment on control mice. * $p < 0.05$, t - test. Sample sizes: Category 1 PBS $n = 4$, peptide $n = 6$; Category 2 PBS and peptide $n = 10$; controls PBS and peptide $n = 10$.

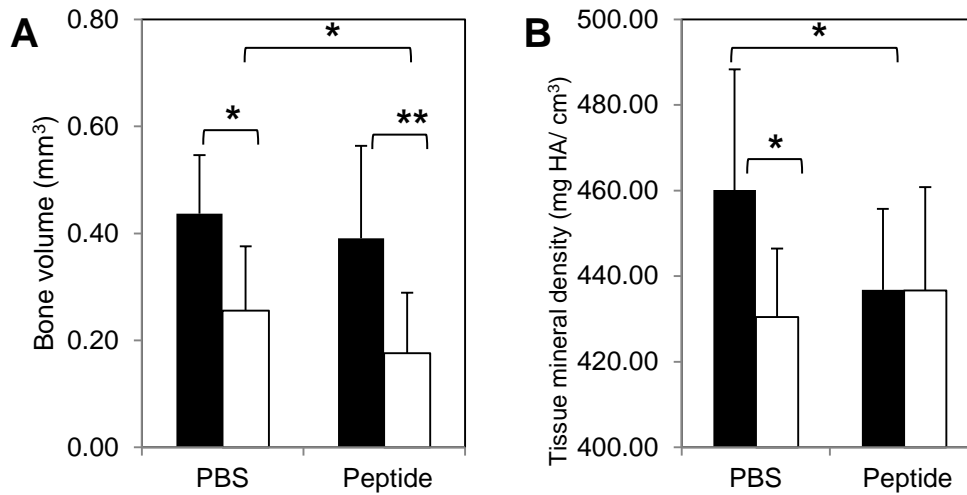


Figure 5.7: μ CT measurements of bone volume (BV) and tissue mineral density (TMD) around the anterior-frontal (AF) suture in pooled mutants (MT). (A) MT had significantly lowered BV than controls (CT) within each treatment. Peptide treated MT had significantly lowered BV than PBS treated MT (t – test /Mann Whitney Rank Sum tests). (B) Within PBS treatment, MT had significantly lowered TMD than CT. Peptide treated CT had significantly lowered TMD than PBS treated CT (Student Newman Keuls post hoc comparisons after two way ANOVA). * $p < 0.05$, ** $p < 0.001$. Sample sizes MT-PBS $n = 17$, MT-Peptide $n = 16$; CT-PBS and CT-Peptide $n = 10$.

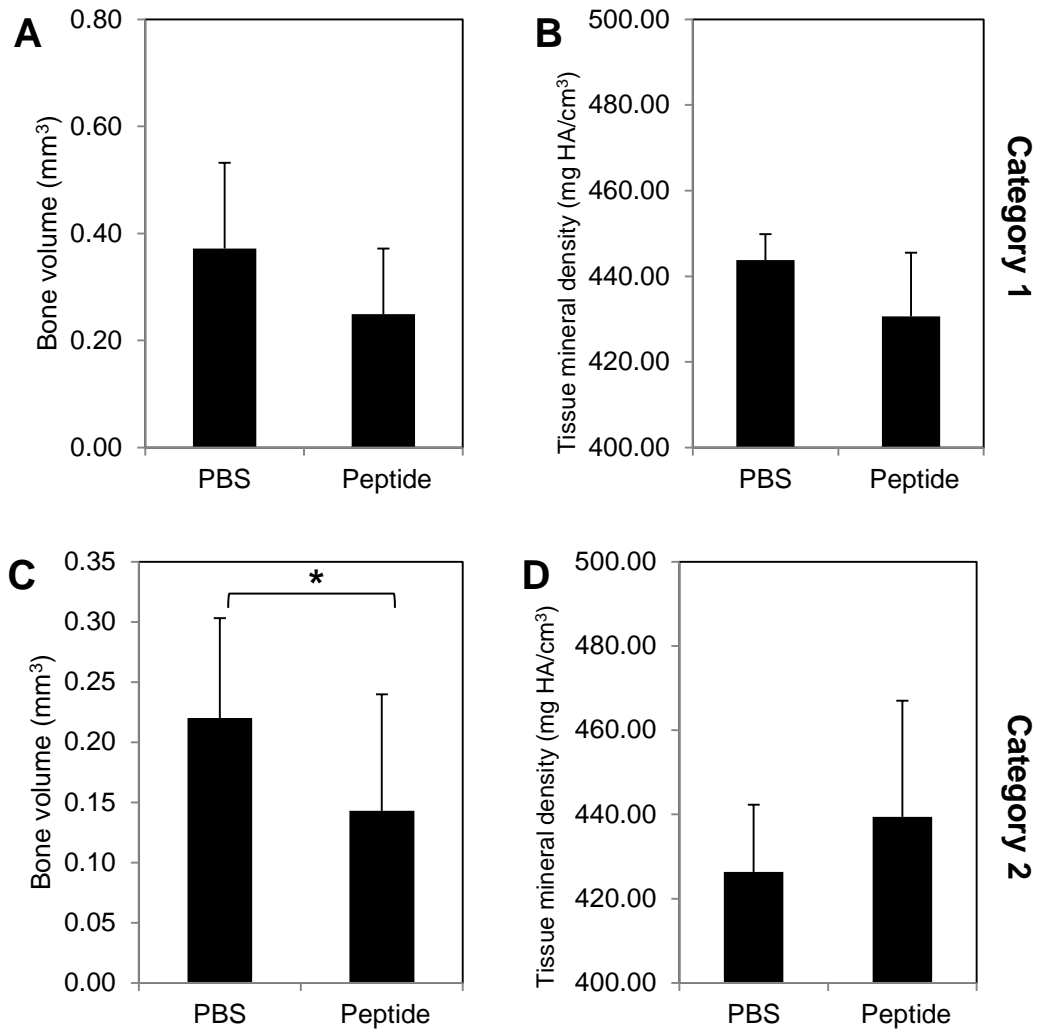


Figure 5.8: μ CT measurements of bone volume (BV) and tissue mineral density (TMD) around the anterior-frontal (AF) suture in categorized mutants. Category 1 (mild) mutants had trends of (A) lowered BV and (B) lowered TMD with peptide treatment. Category 2 (medium) mutants had significantly lowered BV and trends of higher TMD with peptide treatment; * $p < 0.05$ t-test. Sample size: Category 1: MT-PBS $n = 4$, MT-Peptide $n = 5$; Category 2: MT-PBS $n = 13$, MT-Pep $n = 11$.

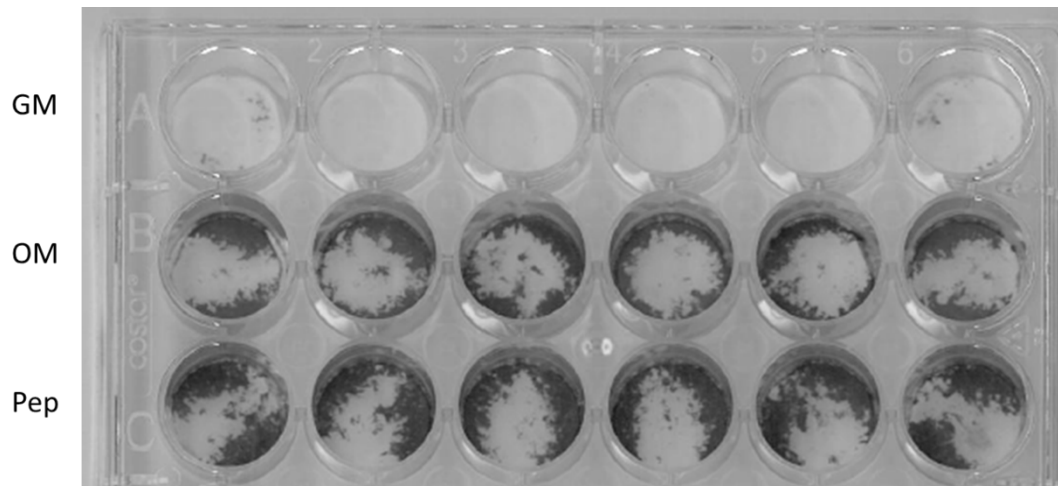


Figure 5.9: Pre-osteoblasts isolated from mutant mice were cultured in growth medium (GM), osteogenic medium (OM) or osteogenic medium supplemented with 300 μ m of pVTK peptide (Pep) for 20 days. von Kossa staining showed that peptide treatment did not inhibit mineralization in these cells.

5.6 References

- [1] Renier D, Lajeunie E, Arnaud E, Marchac D. Management of craniosynostoses. *Child's Nerv Syst* 2000;16:645–58.
- [2] Goldin JH, Wake MJC, Stavrou P, Sgouros S, Willshaw HE, Hockley a. D. Visual failure caused by raised intracranial pressure in craniosynostosis. *Child's Nerv Syst* 1997;13:64–7.
- [3] Komatsu Y, Yu PB, Kamiya N, Pan H, Fukuda T, Scott GJ, et al. Augmentation of Smad-dependent BMP signaling in neural crest cells causes craniosynostosis in mice. *J Bone Miner Res* 2013;28:1422–33.
- [4] Liu F, Fang F, Yuan H, Yang D, Chen Y, Williams L, et al. Suppression of Autophagy by FIP200 Deletion Leads to Osteopenia in Mice Through the Inhibition of Osteoblast Terminal Differentiation. *J Bone Miner Res* 2013;28:2414–30.
- [5] Addison WN, Miller SJ, Ramaswamy J, Mansouri A, Kohn DH, McKee MD. Phosphorylation-dependent mineral-type specificity for apatite-binding peptide sequences. *Biomaterials* 2010;31:9422–30.
- [6] Ramaswamy J, Nam HK, Ramaraju H, Hatch NE, Kohn DH. Inhibition of osteoblast mineralization by phosphorylated phage-derived apatite-specific peptide. *Biomaterials* 2015;73:120–30.

Chapter 6

Summary and Future Work

6.1 Effect of peptide phosphorylation on apatite binding and mineralization

In Chapter 2, phosphorylation and amino acid sequence were used as tools to control both peptide-mediated binding to synthetic and biological apatite, and inhibition of mineralization *in vitro*. Phosphorylation resulted in increased pVTK binding and specificity to carbonated forms of synthetic apatite, compared to non-phosphorylated peptide. Altering amino acid order and charge distribution had no effect on phosphopeptide binding to synthetic apatite. Hence, phosphorylation provides a significant benefit in tailoring and refining peptide binding to biomaterials, and this advantage of increased affinity and specificity overrides any effects of altered charge distribution and sequence.

When applied *in vitro* to osteoblast cultures, pVTK dose-dependently inhibited mineralization, whereas non-phosphorylated peptide had no effect on mineralization. Altering amino acid order and charge distribution reduced pVTK's ability to inhibit mineralization, but had no effect on peptide binding to cell-secreted mineral. Therefore, phosphorylation of VTK is required to inhibit mineralization. Additionally, peptide sequence and charge distribution play different roles in pVTK binding to mineral vs. inhibition of mineralization – peptide composition and overall charge were more

important in binding to apatite, while amino acid sequence and peptide charge distribution were more important in inhibiting mineralization.

The use of phosphorylation as a means to modulate protein properties is relevant in a broad range of biomaterial and tissue engineering applications. The number and relative spacing of phosphorylated residues can be optimized to modulate protein binding, specificity and affinity to any substrate, allowing easy engineering of surface properties. Modification of material surface characteristics will in turn provide control over recruitment and interactions with specific biomolecules and/or cells *in vitro* and *in vivo*. Further, the role of phosphorylation in inhibiting bone can be exploited to create smart biomaterials with patterned peptides at different concentrations, which will be able to inhibit calcification in a gradient manner. These materials can then be used to spatially control and restrict bone regeneration within desired regions and prevent calcification of adjoining cartilage/soft tissue.

6.2 Mechanisms of mineralization inhibition *in vitro*

In Chapters 3 and 5, we advanced our understanding of the mechanisms of pVTK-mediated inhibition of mineralization. The effects of peptide on key regulators of osteoblast mineralization were studied. pVTK was internalized by MC3T3s within one hour of incubation, but had maximal effects on gene and protein expression only at day 10 following induction of osteoblast differentiation and later, when mineralization usually begins. Peptide treatment caused MC3T3 cells to upregulate the expression of positive regulators of mineralization such as bone sialoprotein (BSP), Runx2 and tissue

non-specific alkaline phosphatase (TNAP), and downregulate the negative regulators such as ectonucleotide pyrophosphatase phosphodiesterase 1 (Enpp1), ankylosis protein (Ank) and osteopontin (OPN). Additionally, phosphopeptide bound strongly to both synthetic and cell-secreted apatite (Chapter 2). Hence it was hypothesized that pVTK binds to initially formed mineral nuclei and prevents their growth, and the cells alter their expression profile to a pro-mineralization state in an attempt to compensate and overcome the lack of mineralization. However, pVTK treatment in primary pre-osteoblasts with enhanced BMP signaling did not inhibit mineralization (Chapter 5), implying that peptide-mediated physico-chemical prevention of mineral crystal growth is not the primary mechanism underlying mineral inhibition. Altered extracellular and intracellular concentrations of inorganic phosphate (Pi) or pyrophosphate (PPi) with peptide treatment may be contributing to mineral inhibition and should be analyzed (discussed in Future Work). Finally, it was demonstrated that peptide cytotoxicity, calcium chelation or negative effects of peptide on cellular collagen matrix production were not mechanisms of mineral inhibition.

Understanding the mechanisms underlying peptide-mediated inhibition of mineralization will allow the development of a novel class of peptide drugs designed to treat undesired calcification, which is associated with a large number of clinical conditions (including but not limited to cardiovascular disease, craniosynostosis, osteoarthritis, chronic kidney disease, diabetes, kidney stones and dental plaque). Furthermore, calcification of bioprosthetic heart valves is a leading cause of valve failure and can also be potentially prevented using mineral inhibitory drugs. In addition to its effects on cell differentiation, pVTK was also able to completely prevent the progression of mineralization once it had

started. This finding is advantageous in the development of pVTK as a drug, as it fulfills the key requirement of a therapeutic to be able to stop further disease progression before pursuing subsequent clinical strategies for disease management. Peptide treatments can also be potentially supplemented with simultaneous delivery of growth factors or other biologics promoting the regeneration of healthy tissue.

6.3 Animal model characterization and *in vivo* delivery of peptide

Several animal models of pathological calcification were evaluated as potential candidates to test peptide efficacy *in vivo* (Chapter 4). Phenotype and severity of pathological calcification was dependent on mouse genetic background. Enpp1 knockouts bred on a pure C57BL6 background did not develop robust vascular calcification when compared to knockouts maintained on a mixed background. Crouzon mice with FGF2R mutations developed more severe craniosynostosis when bred on a C57BL6 background vs. a BALB/c background. Hence, it is important to characterize the contributions of genetic factors on occurrence and severity of pathological calcification disorders.

In Chapter 5, pVTK was locally delivered to prematurely mineralizing anterior-frontal (AF) sutures in a mouse model of bone morphogenetic protein (BMP)-mediated craniosynostosis. Large variability in phenotype severity was observed, possibly due to mice being maintained on a mixed genetic background, or due to differences in Cre recombinase expression. To reduce the variation observed, mutants were separated into mild, medium and severe categories based on severity. Peptide treatment partially corrected craniofacial morphologies in medium category mutants, but did not prevent

suture fusion, indicating the need for higher/longer dosing of peptide, or differences in mechanisms involved in suture fusion vs. morphological abnormalities. pVTK also lowered bone volume (BV) in mutants and lowered tissue mineral density (TMD) in controls, suggesting potentially negative effects on bone growth and/or turnover.

Characterization of peptide efficacy and demonstration of inhibition of pathological calcification *in vivo* are key steps in the drug development process. With this information, suitable drug delivery vehicles can be developed and tested to tailor peptide release based on the specific disease etiology and progression for different types of pathological calcification conditions.

6.4 Future work

The work in this thesis describes the characterization and understanding of the newly discovered VTK and pVTK peptides. The knowledge gained from this body of work on designing phosphopeptide therapeutics, evaluating mechanisms of action and characterizing animal disease models can be utilized to derive the next generation of anti-calcification drugs. Future studies should continue to dig deeper into the mechanisms of peptide-mediated inhibition of mineralization, which will in turn provide valuable insight into the types of pathological calcification disorders that can be potentially treated with pVTK.

Based on findings of pVTK inhibiting mineralization, our studies focused on molecules that have vital roles in osteoblast mineralization. Peptide treatment significantly altered Enpp1, Ank, Pit-1 and TNAP expression, all of which are directly involved in Pi and/or

PPi regulation. Direct quantification of any changes in Pi and PPi levels with peptide treatment, will provide a better understanding of how lowered Enpp1, Ank, Pit-1 and increased TNAP expression levels are contributing to mineral inhibition. In addition to their roles as Pi and PPi regulators at the osteoblast membrane, TNAP and Enpp1 also have ATPase, ADPase and pyrophosphatase activities in matrix vesicles (membranous structures where mineralization is thought to be initiated), which can contribute to changes in localized Pi and PPi concentrations [1,2]. Analysis of Enpp1, TNAP and Pi/PPi levels in matrix vesicles derived from pVTK-treated matrix vesicles would provide further clarity in understanding the effect of peptide on the initiation of mineralization.

Incubation of MC3T3 cells with fluorescently labeled pVTK showed peptide uptake and internalization within 1 hour, with fluorescent signal observed in association with cytoskeletal structures as well as in perinuclear intracellular compartments. Identification of the specific vesicular structures involved in peptide internalization will help understand cellular processing of pVTK and subsequent downstream gene expression changes observed with peptide treatment. Additionally, it is important to determine if pVTK enters the nucleus of treated cells before use in any therapeutic applications.

Altering charge distribution and phosphorylated amino acid spacing by scrambling peptide sequence lowered pVTK's ability to inhibit mineralization. Changes in amino acid order could be affecting the conformation and secondary structure of the peptide, and altering the way it is presented to the cells and should be characterized. Repeating the mechanistic studies described in this thesis with the scrambled phosphopeptide, will

elucidate the effects of charge distribution on cellular uptake, differentiation and mineralization, when compared to non-scrambled pVTK.

pVTK failed to inhibit mineralization of primary mutant osteoblasts derived from mice with enhanced BMP signaling, opening up new avenues to explore in elucidating mechanisms of inhibition. Mutant osteoblasts had upregulated BMP and FGF signaling pathways (increased phosphorylated Smad and ERK levels), but no changes in proliferation, TNAP activity or mineralization were observed [3]. Studying the expression levels of other regulators of mineralization such as Enpp1, Ank, OPN, BSP and Runx2 will help understand their interactions with BMP and FGF signaling, both in the absence and presence of pVTK. Additionally, testing the ability of pVTK to inhibit mineralization in a variety of normal and genetically modified osteoblasts will help narrow down potential mechanisms to explore, as well as determine what genetic mouse models are appropriate to demonstrate inhibition of pathological calcification *in vivo*.

pVTK delivery to the AF suture in a BMP-mediated mouse model of craniosynostosis resulted in a correction of the wide-set eyes observed in mutants, but did not prevent suture fusion. When premature suture fusion occurs in craniosynostosis patients, bone growth is unable to proceed normally in the affected areas, while the remaining skull bones continue to grow parallel to the fused sutures, resulting in abnormal skull shape and eye placement. Our observations of normal eye width, as well as trends of increased bone length ratios despite suture fusion in peptide-treated mutants, suggest potentially different mechanisms contributing to suture fusion vs. craniofacial abnormalities in this model of craniosynostosis. Further investigation into craniofacial morphological changes vs. suture fusion will help advance our understanding of craniosynostosis, and possibly

aid the development of new treatments. Alternatively, the use of higher peptide dosage or longer treatment times than the parameters used in our studies, may prevent premature suture fusion.

Peptide treatment resulted in lowered BV in mutants and lowered TMD in control mice. Histomorphometric measurements of bone growth and turnover using calcein or Alizarin red fluorochrome injections can identify the reasons for lowered BV and TMD in peptide-treated mice.

As an intermediate step before further testing pVTK in genetically modified animal models of pathological calcification, the effect of peptide on bone regeneration or healing defects in wild type mice can also be tested. For example, the healing of non-critical sized defects created in mouse calvaria can be studied with or without peptide treatment. Similarly, the ability of pVTK to prevent bone formation in ectopically implanted osteoconductive biomaterials can also be tested. However, in using wound healing models, the presence of inflammatory cells and cytokines may affect peptide properties or stability. Development and characterization of delivery vehicles to provide gradual and sustained release of peptide over the time period of bone formation will be beneficial. It is also important to characterize the stability and clearance rates of the peptide *in vitro* and *in vivo*, to tailor dosage and release characteristics from delivery vehicles.

6.5 References

- [1] Ciancaglini P, Yadav MC, Simão AMS, Narisawa S, Pizauro JM, Farquharson C, et al. Kinetic analysis of substrate utilization by native and TNAP-, NPP1-, or PHOSPHO1-deficient matrix vesicles. *J Bone Miner Res* 2010;25:716–23.
- [2] Millán JL. The role of phosphatases in the initiation of skeletal mineralization. *Calcif Tissue Int* 2013;93:299–306.
- [3] Komatsu Y, Yu PB, Kamiya N, Pan H, Fukuda T, Scott GJ, et al. Augmentation of Smad-dependent BMP signaling in neural crest cells causes craniosynostosis in mice. *J Bone Miner Res* 2013;28:1422–33.